The Pennsylvania State University

The Graduate School

UTILIZATION OF THE SQUARE ARRAY EARTH RESISTIVITY METHOD FOR CHARACTERIZING ANISOTROPY IN FRACTURED SEDIMENTARY ROCK

A Dissertation in

Geosciences

by

David A. Yoxtheimer

Submitted in Partial Fulfillment
of the Requirements
for the Degree of
Doctor of Philosophy

December 2019

The dissertation of David A. Yoxtheimer was reviewed and approved* by the following:

Andrew Nyblade
Professor of Geosciences
Dissertation Adviser
Chair of Committee

Derek Elsworth
Professor of Geo-Environmental Engineering

Peter LaFemina
Professor of Geosciences

Anthony Buda
USDA Research Hydrologist

Mark Patzkowsky
Professor of Geosciences
Associate Head for Graduate Programs and Research

*Signatures are on file in the Graduate School

ABSTRACT

Fractured bedrock aquifers are key sources of potable groundwater globally. Therefore it is important to characterize the presence and orientations of subsurface fractures that impact groundwater flow in order to develop, manage and protect these critical water resources. A significant challenge in characterizing groundwater flow in a fractured bedrock aquifer is determining if anisotropic conditions exist. The square array method provides a means to estimate geo-electrical anisotropy, which can be useful when conducting hydrogeologic investigations including mapping fracture orientations, siting water supply wells, conducting source water protection programs, or mapping contaminant plumes. However, this method has not been previously tested to characterize the hydrogeology of folded and fractured carbonate bedrock overlain by conductive layers of soil and epikarst, nor for characterizing shale formations. In this study, the square array method is used to measure the change in electrical resistivity of the subsurface with respect to azimuth at six locations in the Cambrio-Ordovician carbonate bedrock aquifer of Spring Creek watershed and the shale formation underlying the Susquehanna Shale Hills Critical Zone Observatory (SSHCZO), both located within the Appalachian Valley and Ridge Province of central Pennsylvania.

The carbonate bedrock aquifer is mantled with residual soils consisting primarily of silt and clay loams of variable thickness (0 to greater than 10 meters) below which occurs an epikarst system that plays a significant role in shallow groundwater flow. The square array is used to characterize the carbonate aquifer's bedrock strike- and fracture-related anisotropy and provide estimates of secondary porosity. The results show that the square array apparent resistivity data correlates well with known bedrock structure, in particular the resistivity minima for the deeper measurements (40- and 50-meter a-spacings) are coincident with the northeast-southwest

orientation of bedrock strike and/or mapped fractures, where present. In addition, estimates of secondary porosity from the square array's 40- and 50-meter a-spacings (range of 0.7-4.4% with a mean of 3.1%) generally compare favorably to independent estimates of bedrock structure and secondary porosity from outcrop measurements and groundwater level/streamflow recession data (1-5%). The results of this study demonstrate that the square array method can be used effectively in complex, fractured carbonate bedrock settings to characterize bedrock anisotropy and secondary porosity, which were field-validated based on bedrock outcrop structure and fracture geometry measurements. Previous square array studies have detected anisotropy and estimated secondary porosity in both carbonate and crystalline bedrock, however this research further validates the method by comparing field measurements to the square array data, and thus advances the method's application.

Geo-electrical anisotropy associated with inclined bedding planes and fractures in bedrock is often not factored into apparent resistivity results, much less data inversion, which can lead to misleading model results. In particular, the "paradox of anisotropy" occurs where collinear resistivity data are collected in areas with inclined bedding planes or fractures and longitudinal apparent resistivity is greater than transverse apparent resistivity, which is the converse of when true resistivity values are considered. The SSHCZO study expands critical zone research by evaluating the effects of anisotropy on earth resistivity measurements in a fractured shale bedrock setting using both square and Wenner arrays. The square array can be used to determine the magnitude and orientation of anisotropy, as it is not subject to the paradox of anisotropy, whereas collinear arrays are, including the Wenner array. In fractured shale bedrock the anisotropy effects can be significant, including the paradox of anisotropy, which can lead to significantly inaccurate models if not factored into the input data. In this study the square array

was used to evaluate site anisotropy at variable depths, including through the soils and bedrock profile, including fractured, weathered and unweathered bedrock intervals. The square array's anisotropy coefficient was then factored into apparent resistivity data from strike parallel and perpendicular 2-D Wenner arrays to correct for the paradox of anisotropy. The corrected 2-D resistivity data were then inverted to obtain model results where longitudinal resistivity values were lower than transverse resistivity values, as would be expected. In addition, a series of ten parallel 2-D Wenner arrays were run and used to create "pseudo" 3-D models of the site's resistivity distribution using anisotropy corrections from the square array data for comparison to 3-D models without this correction. This sequence of steps resulted in a 3-D resistivity model that provided useful insights into shallow groundwater interflow at the SSHCZO site. Ultimately this study provides a method that can be applied to geophysically characterize the groundwater flow mechanisms in the critical zone and allow investigators to design subsurface monitoring programs to further advance hydrologic and hydrogeologic research.

The combined results of these studies show the square array can be utilized in fractured carbonate and shale bedrock settings to ascertain geo-electrical anisotropy, which correlates well to bedrock and fracture strike. For the fractured carbonate aquifer the square array was validated to provide reasonable estimates of secondary porosity based on both outcrop fracture measurements and groundwater level recession analysis. In the shale bedrock setting, the square array provided a useful correction factor for the coefficient of anisotropy in 2-D collinear resistivity arrays, which then yielded useful insights into shallow groundwater flow conditions via 3-D modeling developed from the corrected 2-D resistivity arrays. It should be noted that this thesis has been written as two stand-alone papers for journal submission, therefore some degree of repetition exists in the background and methods sections of Chapters 2 and 3.

TABLE OF CONTENTS

LIST OF FIGURES

LISTS OF TABLES

ACKNOWLEDGMENTS

I owe a great deal of gratitude to many people who have enabled me to finish my doctorate. I sincerely thank my dissertation committee for their thoughtful guidance including my advisor Andy Nyblade for persevering with me along this geophysical journey, Derek Elsworth for his keen insights and keeping me on his graduate student list for a very long time, and Peter LaFemina and Tony Buda for their willingness to join my committee deep in the process to help me complete my long-awaited goal. Additionally I'd like to thank former committee members Kamini Singha and Richard Parizek for their guidance and enthusiastic support as well as Mark Patzkowsky for his administrative assistance. Some of this work was financially supported by the National Science Foundation for the Susquehanna Shale Hills Critical Zone Observatory to SLB (EAR 13-31726). Shale Hills research was conducted in Penn State's Stone Valley Forest, which is funded by the Penn State College of Agriculture Sciences, Department of Ecosystem Science and Management and managed by the staff of the Forestlands Management Office. I'd like to thank Sue Brantley, Brandon Forsythe, Jeremy Harper, David Oakley and Greg Mount for the opportunity to collaborate during the Shale Hills data collection. I will be forever grateful to Mike Arthur for the opportunity to work with him at Penn State and encouraging me to finish my doctorate. Last but not least I'd like to thank my wife Carrie for her love and support, my kids for providing inspiration, and my parents for putting me on this planet and being there through life's many twists and turns.

Chapter 1

Introduction

This dissertation investigates the application of square array earth resistivity measurements to characterize shallow bedrock in two different sedimentary bedrock settings, including a fractured, karstified carbonate formation and a fractured shale formation. The objectives of this research include the following:

- Determining the geo-electrical anisotropy of fractured carbonate and shale bedrock aquifers,
- Correlating bedrock geo-electrical anisotropy with existing and new geological and hydrogeological data,
- Estimating the secondary porosity of the carbonate bedrock aquifer with the square array data for comparison to field data for method validation,
- Characterizing the anisotropy of fractured shale using the square and Wenner arrays,
- Evaluating the utility of the square array in shale bedrock for resolving the "paradox of anisotropy" associated with 2-D collinear resistivity arrays,
- Identifying groundwater "interflow" zones with 2-D Wenner array modeling, and
- Inverting parallel 2-D collinear arrays into a 3-dimensional earth resistivity model in a fractured shale bedrock setting using a series of steps that account for the paradox of anisotropy to characterize shallow groundwater interflow in the critical zone.

Characterizing fractured bedrock aquifers is especially challenging for hydrogeologists since properties such as hydraulic conductivity can change by orders of magnitude over meter scale

distances due to the presence of discrete fracture zones. Structural features such as bedrock strike, joints, fractures and faults can strongly influence groundwater flow direction, velocity, and volumes, especially in karstified carbonate aquifers. Either direct or indirect methods that estimate the influence these types of geologic features have on groundwater flow can be useful for groundwater supply and contaminant investigations in fractured bedrock aquifers. Indirect measurements of an aquifer's characteristics through use of earth resistivity surveys such as the square array are relatively simple, non-invasive, rapid, and inexpensive.

The results of this research demonstrate the significant utility of the square array earth resistivity method, especially in combination with geologic mapping and collinear resistivity surveys, to refine the hydrogeologic characterization of bedrock aquifer settings. In addition, the ability to characterize 3-dimensional properties in a fractured shale bedrock setting using the square array highlights its ability for use in a variety of fractured bedrock aquifer settings.

The purpose of conducting earth resistivity surveys is to determine the subsurface resistivity distribution by making resistance measurements at the ground surface. From these resistance measurements, the distribution of the subsurface resistivity within the sampled rock volume can be estimated. Near surface resistivity is related to various geological parameters including soil type, lithology, geologic structure, fracture density, fracture orientation, porosity, pore fluid content, degree of pore saturation, and pore fluid conductivity. Geologic structure of a bedrock aquifer including strike, dip, and the presence of one or multiple sets of subsurface joints or fractures collectively form the geologic "fabric" of a hydrostratigraphic unit. Collectively, these geologic features can determine preferred groundwater and contaminant flow paths. In the same way the geologic structure and fracture sets can influence groundwater flow they can also control

the transmission of an electrical current through the subsurface, especially where relatively conductive clays or formation waters occur.

The presence of fractures or bedding plane partings can change earth resistivity by orders of magnitude within the sampled rock volume, for example between unfractured carbonate bedrock having high resistivity and an adjacent water-filled fracture with low resistivity. These large resistivity contrasts are useful for earth scientists to identify fractured zones, which may be a path of preferred groundwater flow, and assist with developing conceptual models of the earth's subsurface conditions.

Electrical resistivity surveys have been applied to hydrogeological, geotechnical, environmental, and archeological investigations for multiple decades. The resistivity measurements are normally made by introducing an electrical current into the ground through two current electrodes (designated as C1 and C2), and measuring the resulting voltage difference at two potential electrodes (designated as P1 and P2). The earth's resistance can be calculated from Ohm's law, where: $R=V/I$

where

R= Resistance (ohms)

V=Voltage difference (volts)

I=Current (amps)

This resistance measurement is spatially meaningless until the geometric factor (K), which includes the distance between each of the electrodes, is added into the equation to yield an apparent resistivity (ρ_a), where $\rho_a=K*V/I$.

The calculated resistivity value is not the true resistivity of the subsurface, but an “apparent” value which is the resistivity of a homogeneous ground which will give the same resistance value for the same electrode arrangement (Habberjam, 1972). The relationship between the “apparent” resistivity and the “true” resistivity is a complex relationship requiring a modeled inversion of the measured apparent resistivity values.

Typically, collinear arrays are expanded outward from a central point by increasing the a-spacing between the electrodes for a series of measurements. By increasing the electrode a-spacing the penetration depth of the current and therefore the resistivity measurement’s depth increases for that point location resulting in a 1-D resistivity survey, commonly known as a vertical electrical sounding. For example, the Wenner array’s depth of measurement is approximately one half of the a-spacing (Bristoll, 1997). Therefore, increasing the a-spacing around a central point using a collinear array increases each measurement’s depth and produces a vertical electrical sounding of resistivity versus depth. Another commonly used approach is to conduct a lateral profile of the earth’s resistivity by collecting measurements at incremental distances using a fixed a-spacing along a given transect to determine how resistivity changes in any lateral direction, known as a constant-spacing traverse. A significant limitation of the resistivity sounding method is that both horizontal and lateral changes in the subsurface resistivity commonly occur and will influence the apparent resistivity values which may be misinterpreted as changes with depth in the subsurface resistivity. Therefore, caution should be taken with profiling and sounding measurements in very complex geologic settings.

To be able to generate a 2-D or 3-D resistivity model, a series of measurements need to be collected at various a-spacings and locations along a survey line or a planar grid. In addition, azimuthal measurement surveys can be collected by rotating the collinear survey around a fixed

center point in relatively small increments (e.g., 15 degrees) to determine the variation of earth resistivity with orientation. Where the earth resistivity values from each orientation of the rotated azimuthal arrays plot as an ellipse, this is indicative of a homogeneous but anisotropic medium (Taylor, 1982; Taylor and Fleming, 1988). For resistivity values from rotated collinear arrays that plot as an ellipse, the highest apparent resistivity value indicates the direction of the prevailing joint/fracture trend while the lowest apparent resistivity is perpendicular to the joint/fracture trend, a phenomena known as the paradox of apparent resistivity (Taylor and Fleming, 1988). Wenner arrays utilized for azimuthal studies can falsely indicate apparent anisoptropy when a dipping surface exists between materials that are homogeneous and isotropic, and when a lateral increase or decrease in resistivity exists (Watson and Barker, 1999; Massoud et al., 2009).

Standard collinear electrical resistivity surveying methods have been demonstrated to be useful for hydrogeologic characterization, including the presence of voids, caves, and other karst features in carbonate bedrock. Applying these methods in carbonate bedrock provides insight into a karst aquifer's anisotropy. Furthermore, electrical resistivity methods have been utilized to estimate aquifer hydraulic properties, such as hydraulic conductivity and transmissivity, based on the corollary relationships between Ohm's Law and Darcy's Law that describe electrical current and groundwater flow, respectively. The correlation between subsurface electrical current flow and groundwater flow is founded on the principal that each follows the path of least resistance from high to low potential.

The square array technique was originally developed by Habberjam and Watkins (1967) as an alternative to conventional Wenner or Schlumberger arrays when dipping subsurface bedding or foliation was present. Habberjam (1972) showed that a square array is more sensitive to

anisotropy in the subsurface and requires less surface area than collinear arrays. Additional studies conducted by Matias and Habberjam (1984), Lane et al., (1995), Matias (2002) and Boadu, et al., (2005), have successfully used the square array technique for identifying crystalline bedrock fracture orientation. In addition, the square array has been used to detect productive fracture zones in crystalline bedrock for groundwater supply (Darboux-Afouda and Louis, 1989; Sehli, 1990). These studies verified Habberjam's earlier work, showing that the square array has a greater sensitivity to a given bedrock anisotropy and requires less surface area than collinear arrays.

The research presented herein will build on the foundation of this previous work by using the square array technique to characterize a fractured, karst, carbonate bedrock aquifer to estimate preferred geo-electrical anisotropy orientation, correlate this information to known geologic and hydrogeologic data, and ultimately estimate the karst aquifer's secondary porosity at each site. The hydraulic gradient and direction of groundwater flow in karst aquifers is often times locally or regionally controlled by bedrock fracturing, bedding planes, and other structural features, thus lending a preferred anisotropy to the aquifer's hydraulic conductivity. In addition, this research includes characterizing a shale formation's anisotropy using the Wenner array, in particular for resolving the paradox of anisotropy with the square array for more representative data inversion. Once the 2-D Wenner array apparent resistivity data has been adjusted for anisotropy more representative 3-D earth resistivity models can be developed.

Chapter 2

An Assessment of the Square Array Resistivity Method's Ability to Geo-Electrically Characterize the Cambrio-Ordovician Karst Aquifers of the Appalachian Valley and Ridge Physiographic Province

Abstract

Carbonate bedrock aquifers are a key source of potable groundwater globally, and constitute a primary drinking water source for many regions of central Pennsylvania. A significant challenge in characterizing groundwater flow in a fractured, karst aquifer is determining if anisotropic conditions exist, the associated primary fracture set orientation, and how this relates to groundwater flow. The square array method may provide a means to estimate geo-electrical anisotropy, which can be useful when conducting hydrogeologic investigations, including siting water supply wells, conducting source water protection programs, or mapping contaminant plumes. However, this method has not been previously tested in folded and fractured carbonate bedrock overlain by conductive layers of soil and epikarst. In this study, the square array method is used to measure the change in electrical resistivity of the subsurface with respect to azimuth at six locations in the Cambrio-Ordovician carbonate bedrock aquifer of Spring Creek watershed within the Appalachian Valley and Ridge Province of central Pennsylvania. This carbonate bedrock aquifer is mantled with residual soils consisting primarily of silt and clay loams of variable thickness (0 to greater than 10 m) below which an epikarst (highly-weathered carbonate bedrock interval) system occurs that can play a significant role in shallow groundwater flow. The carbonate aquifer's secondary porosity is also estimated using the square array data. The results show that the square array apparent resistivity data correlate well with known bedrock structure. In particular the resistivity minima for the deeper measurements (40- and 50-m a-

spacings) at each site paralleled the northeast-southwest orientation of bedrock strike or mapped fractures, where present. In addition, estimates of secondary porosity from the 40- and 50- meter a-spacings (range of 0.7-4.4% with a mean of 3.1%) of the square array generally compared favorably to independent estimates of bedrock structure and secondary porosity from outcrop measurements and groundwater level/streamflow recession data (1-5%). The results of this study demonstrate that the square array method can be used effectively in complex karst settings to characterize bedrock anisotropy and secondary porosity, and validates the method by direct comparison of bedrock anisotropy and porosity estimates obtained from square array data to field measurements of anisotropy and porosity.

Introduction

Approximately 14% of the Earth's land surface consists of carbonate bedrock (Chen et al., 2017), from which karst landforms and aquifers can form. Karst aquifers currently supply about 25% of the global population with drinking water (Bakalowicz, 2005; Ford and Williams, 2007), therefore providing a necessary water resource for human health, ecology, agriculture, food, energy, and industry. Karst aquifers are characterized by having rapid infiltration (both diffuse and concentrated), high heterogeneity with significant anisotropy, and fast transport from recharge inputs to the springs, often controlled by the presence and orientation of conduits (Jones and White, 2012). The water recharged into karst aquifers moves down-gradient through the bedrock using some combination of highly anisotropic pathways, often encompassing three levels of permeability including matrix (intergranular), fracture (joints and bedding plane partings), and conduit (openings >1 cm) permeability in the bedrock (White, 2002). As a result of these varying scales of permeability in karst aquifers, properties such as hydraulic conductivity can change by orders of magnitude over meter scale distances, which can strongly

influence groundwater flow direction, velocity, and volumes. Utilizing direct methods such as aquifer tests or indirect methods such as earth resistivity surveying to estimate the influence these types of geologic features can have on groundwater flow aids in the investigation of groundwater supply, wellhead protection, and contaminant transport in karst aquifers. As a result of these hydrogeologic complexities, characterizing and managing karst groundwater resources can be more complex than other aquifers (Parise et al., 2018) and thus can be especially challenging for hydrogeologists. Karst aquifers strongly differ from aquifers developed in porous or fractured media (White, 1988; Bakalowicz, 1995, 2005; Ford and Williams, 2007), and the inherent heterogeneity and anisotropy often found in karst aquifers makes it necessary to undertake studies using a wide range of approaches (Doctor et al., 2000; Goldscheider and Drew 2007). These methods may include hydrograph analysis, geochemical methods, dye trace testing, aquifer testing, geologic reconnaissance, and geophysical methods to characterize karst aquifers.

Estimating an aquifer's anisotropic characteristics through use of azimuthal earth resistivity surveys offer the advantages of being relatively simple, non-invasive, rapid, and cost-effective (Habberjam, 1979, Taylor and Fleming, 1988). The square array resistivity method is especially adept at characterizing geo-electrical anisotropy due to a higher electrode spacing ratio (i.e., 1:1) as compared to other electrical resistivity survey methods. In addition, the square array has been shown to be useful for estimating fracture (secondary) porosity in crystalline bedrock (Lane et al., 1995) as well as solutionally-derived porosity in carbonate bedrock (Yeboah-Forson and Whitman, 2014; Whitman and Yeboah-Forson, 2015). However, the square array's utility has not been fully evaluated in complexly folded, faulted, and fractured karst settings, much less where a variable epikarst system exists above the carbonate bedrock. The Paleozoic carbonate

rocks of eastern United States have very low matrix permeability so that regional groundwater flow is often controlled by fractures or conduits, in contrast to Tertiary limestones of the Floridian aquifer where higher matrix permeabilities comprise a significant component of the groundwater flow system (Jones and White, 2012).

This study investigates application of the square array to characterize the anisotropy and fracture-derived secondary porosity of the complexly folded, faulted and karstified Cambrian-Ordovician carbonate aquifers of the Spring Creek watershed located within the Appalachian Valley and Ridge Province of Central Pennsylvania. This carbonate aquifer supplies greater than 95% percent of the drinking water to the approximately 100,000 people who live in the watershed. Consequently, understanding the role that anisotropy plays in groundwater is crucial to its long-term management and protection. Figure 2-1 is a map showing the study area location and Figure 2-2 is a geologic map showing the location of each site where square array measurements were collected within this carbonate bedrock setting. The following sections provide a summary of the use of electrical resistivity surveying, including the square array in karst settings, the study area's geologic setting, surveying methodology, results, and discussion of the square array's utility in characterizing this carbonate bedrock aquifer.

Background

The purpose of conducting earth resistivity surveys is to determine the subsurface resistivity distribution by making resistance measurements on the ground surface in order to gain geological insights. Near surface resistivity is related to various geological parameters including soil type, lithology, geologic structure, fracture density, fracture orientation, porosity, pore fluid content, degree of pore saturation, and pore fluid conductivity (Keller and Frischknecht, 1966). Geologic structure of a bedrock aquifer, including strike, dip, and the presence of one or multiple

sets of subsurface joints or fractures, collectively forms the geologic "fabric" of a hydrostratigraphic unit. Together these geologic features can create an aquifer's anisotropy, resulting in preferred groundwater and contaminant flow paths. In much the same way the geologic structure and fracture sets can influence groundwater flow under a hydraulic head gradient (potential), these features can also control the transmission of an electrical current through the subsurface given an electrical potential, especially where relatively conductive clays or formation waters occur in bedrock fractures.

Azimuthal direct-current electrical resistivity methods for detection of bedrock fractures using collinear arrays have been successfully conducted by many researchers in a variety of geologic settings (Mallik et al., 1983; Taylor, 1984; Leonard-Mayer, 1984; Taylor and Fleming, 1988; Lieblich et al., 1991; Ritzi and Andolsek, 1992; Watson and Barker, 1999; and Busby, 2000). Furthermore, electrical resistivity methods have been utilized to estimate aquifer hydraulic properties such as hydraulic conductivity and transmissivity (Kelly, 1977; Hiegold et al., 1980; Kosinski and Kelly, 1981; Sri Niwas and Singhal, 1981 and 1985; and de Lima and Sri Niwas, 2000) based on the corollary mathematical relationships between Ohm's Law and Darcy's Law that describe electrical current and groundwater flow, respectively (Ahmed et al. 1988). The correlation between subsurface electrical current flow and groundwater flow is founded on the principal that each follows the path of least resistance from high to low potential. Groundwater and electrical current flow are similar as both are transported through the interconnected pore volumes (Revil and Cathles 1999).

The utility of standard collinear electrical resistivity surveying methods has been demonstrated by multiple researchers for hydrogeologic characterization in carbonate bedrock settings, including detecting the presence of voids, caves, and other karst features, as well as fracture

orientation. Roth et al., (2002) correlated collinear resistivity arrays and geotechnical borings to detect fractures and voids in the karst of Northampton County, Pennsylvania. McGrath et al., (2002) used a combination of earth resistivity and microgravity measurements in England and Wales to assist with groundwater vulnerability mapping in regional karst formations. Gibson et al., (2004) combined the use of resistivity with magnetometry for void detection in Ireland in a karst area with glacial overburden. El-Qady et al., 2005 used resistivity in combination with ground penetrating radar for void detection in a karst region of Egypt. Szalai et al., (2002 and 2018) identified fractures and fracture zones using earth resistivity null arrays in combination with "pricking probe" surveys in the karst region of Hungary. Moreira et al., (2018) used square, equatorial dipole–dipole, Wenner and Schlumberger to characterize vertical fractures in a karst region of Brazil. Several researchers (Taylor and Fleming, 1988; Ritzi and Andolsek, 1992; Steinich and Marin, 1996) have conducted azimuthal resistivity surveying in carbonate bedrock to characterize karst aquifer anisotropy.

The square array technique was originally developed by Habberjam and Watkins (1967) as an alternative to conventional Wenner or Schlumberger arrays when dipping subsurface bedding or foliation are present. In this particular case the different array types were conducted over a vertical fault (at an un-specified location in Great Britain) demonstrating the square array's greater sensitivity to fault related anisotropy. Habberjam (1972) showed that a square array is more sensitive to anisotropy in the subsurface and requires less surface area than collinear arrays. In that study, 74 square array soundings were made in the Yorkshire coal measures, including interbedded shale, which was noted as having a shallow dip with some foliation and bedding planes, and thus they obtained relatively low anisotropy coefficients, with a mean of 1.13 and a maximum of 1.26. A second set of measurements were collected in the Northwest Anglesey area

of Great Britain, which consists of highly folded and faulted metamorphic rocks with Ordovician shales and vertical igneous dykes, thus expected to have greater anisotropy and heterogeneity. The anisotropy coefficients that they obtained in this area had a mean of 1.42 and a maximum of 2.55. The Habberjam (1972) study does not provide site locations nor specific field geology measurements on outcrops, thus the results from square array data were not correlated to or validated against site-specific geologic estimates of anisotropy. However, the study compared the overall results from two geologically distinct regions, illustrating the method's sensitivity to anisotropy in geologic settings that are relatively simple with little structure versus a setting with folded and faulted structure.

Additional studies have used the square array technique successfully for identifying crystalline bedrock fracture orientation. Matias and Habberjam (1984) used the square array along two traverses, one 250 meters long with 13 stations and one 500 meters long with 32 stations near Inglesby, Great Britain. These traverses measured the resistivity and anisotropic conditions of the Ingletonian and Ashgillian formations, which represent exposed steeply dipping basement bedrock (70° or more) with general strike directions northwest-southeast. The geologic structure also includes two major strike parallel faults that separate the Great Scar limestone in the west from the Ashgillian, and also separate the Ashgillian from the Ingletonian formation in the east. The square array was useful in this setting by correlating anisotropy with bedrock strike as well as with resistivity contrasts across fault lines between each of the formations.

The square array has been used to detect productive fracture zones in crystalline bedrock for groundwater supply (Darboux-Afouda and Louis, 1989; Sehli, 1990), and Lane et al. (1995) used azimuthal square-array resistivity soundings to detect fractures in bedrock in the Mirror Lake watershed in Grafton County, New Hampshire. Soundings were conducted at a site where

crystalline bedrock underlies approximately 7 meters of glacial drift. Measured apparent resistivity values changed with the orientation of the array, indicating that a dominant fracture set or foliation in the bedrock is oriented at 030°. This results was verified by inspection of a bedrock outcrop with fractures nearly 250 meters away. Assuming that measured anisotropy was due to fractures, the secondary porosity was estimated to range from 0.01 to 0.10, however this result was not field verified. In addition, the fracture orientation interpretations were compared to azimuthal seismic refraction surveys and azimuthal Schlumberger resistivity soundings with resulting strike estimates of 022° and 037°, respectively.

Matias (2002) used the square array to carry out several resistivity soundings in Chapel-le-Dale located in the Three Peaks Region of the West Yorkshire Moors in Great Britain. The soundings were conducted in an area where schists and greywackes are concealed by drift at different depths and have been previously mapped with an approximate NW–SE strike. Coefficient of anisotropy values of 1.04 and 1.81 were estimated for the drift overburden and for the anisotropic basement, respectively, with geo-electrical strike coincident with previously mapped bedrock strike.

Boadu et al., (2005) conducted azimuthal square array surveys at ten sites to characterize bedrock fracture orientation, fracture porosity, and coefficients of anisotropy on farms in Ghana (Nsawam District) where groundwater is suspected to be impacted from over-application of pesticides and fertilizers. The geologic setting consists of metamorphic phyllites, schists, and quartzite with intense folding, fracturing, and faulting. Results from this integrated geological and geophysical study indicate two dominant fracture directions in the study area (NW-SE and NE-SW) that correlated with orientations of minimum resistivity from square array data sets.

Analyses of the resistivity data indicate that the fracture porosity within the study area ranges from 0.001 to 0.015 which agreed reasonably well with field mapping of fracture geometry.

Yeboah-Forson and Whitman (2014) used the square array to investigate electrical anisotropy at 13 sites in the Biscayne Aquifer of southeastern Florida. The measured coefficient of electrical anisotropy generally ranged from 1.01 to 1.12 with a maximum value of 1.36 measured at one site. The observed electrical anisotropy from these studies was used to estimate hydraulic anisotropy (ratio of maximum to minimum hydraulic conductivity) which ranged from 1.18 to 2.83. The greater anisotropy occurred on the Atlantic Coastal Ridge and were interpreted to result from increased dissolution rates of the oolitic facies of the Miami formation limestone while the least anisotropy occurred in low elevation areas on the margin of the Everglades to the west in the bryozoan-dominated facies. The predominate trend of minimum resistivity and maximum hydraulic conductivity was E-W/SE-NW beneath the ridge and E-W/SW-NE farther west. Square array minimum resistivity values were correlated to cross-bedded strike orientation at one available nearby outcrop. The anisotropy directions are similar to the predevelopment groundwater flow direction from previous studies thus suggesting that the observed anisotropy is related to the paleo-groundwater flow in the Biscayne Aquifer. Using the same dataset, Whitman and Yeboah-Forson (2015) investigated how resistivity varies spatially and with depth in the upper 15 m of the carbonate aquifer. Porosity was estimated from the modeled formation resistivity and observed pore fluid resistivity with Archie's Law. Resistivity in the saturated zone ranged from 30 to 320 ohm-m, with resistivity being constant or increasing with depth at many sites in the western portions of the study area while the center of the Atlantic Coastal Ridge exhibited a distinct low resistivity zone (less than 45 ohm-m) at elevations ranging between -5 and -10 meters. The estimated porosity ranged between 14% and 71% with modal

values near 25%, where porosity structure varies with depth and spatially. Western sites exhibited a high porosity zone at shallow depths best expressed in a NE–SW trending zone of 40–50% porosity situated near the western margin of the Atlantic Coastal Ridge. The highest porosity (>50%) is seen at elevations below -5 meters at sites in the center of the Atlantic Coastal Ridge and likely corresponds to solution features. The general NE–SW trend of the resistivity and porosity structure suggests a causal connection with the Pleistocene paleogeography and sedimentary environments.

In this chapter the square array is applied to demonstrate its utility for characterizing the geo-electrical anisotropy and secondary porosity in a complexly folded, faulted, fractured, karstified carbonate bedrock aquifer, with a well-developed epikarst mantle. The square array's use in a carbonate bedrock setting is further validated through field mapping including independent estimates of secondary porosity via rock outcrop fracture measurements and regional groundwater level recession. This research advances the hydrogeophyscial sciences through a unique application of the square array in this type of karst geologic setting.

Spring Creek Watershed Hydrogeologic Setting

The study area is contained in the Spring Creek watershed in Centre County, Pennsylvania, which is underlain by approximately 2,000 to 2,500 meters of interbedded limestone, dolomite, and minor sandstone of Cambrian and Ordovician age (Parizek et al., 1971). The strata were folded into a series of anticlines and synclines of the Nittany Anticlinorium during the late Paleozoic Alleghenian Orogeny, providing a regional northeast/southwest bedrock strike orientation, ranging from approximately 030-060° with dips ranging from horizontal to slightly overturned (Parizek et al., 1971). Silurian-age sandstones cap the ridges with side slopes consisting of Ordovician-age shales that transition to Cambrian- and Ordovician-age carbonates

that form the valley floor. Erosion has exposed the core of the ancient mountains, resulting in a reverse topography where sandstones once deeply buried in synclines now serve as cap rocks for the regional ridges. In contrast, anticlinal structures lie beneath the carbonate bedrock valleys. Soils in the valley portion of the watershed consist primarily of residual silty clays and silt loams that have been formed from the carbonate bedrock with soil thicknesses varying from no soil mantle to upwards of 30 meters or more of soil.

The existence of carbonate bedrock in the Spring Creek watershed is conducive to the formation of karst features, including caves, sinkholes, sinking streams, and solutionally-enlarged bedding planes, joints, and fractures. Mountain runoff provides a significant portion of the karst aquifer's recharge as it enters the valley's carbonate floor, estimated to be 50% or more of the karst aquifer's total recharge (Konikow, 1969). The Cambrio-Ordovician carbonate formations underlying the Spring Creek watershed are known to store and transmit relatively large volumes of groundwater, primarily through the secondary porosity created by dissolution of carbonate bedrock near bedding planes and fractures (USGS, 2005). Epikarst, as defined herein, is the interface zone between soil and bedrock in karst landscapes, and is characterized by small fractures, conduits and solution pockets that may or may not be saturated with water. Water movement and storage in the epikarst zone appears to play an important role in the hydrologic regime of the karst aquifer within the Spring Creek Watershed, as evidenced by sinking streams that are hydraulically connected to nearby springs.

Groundwater flow in the study area's carbonate bedrock aquifer is anisotropic based on groundwater flow mapping and aquifer testing results, and appears to be primarily controlled by solution features, especially along bedding planes, thrust faults, and formation contacts that influence groundwater movement (Parizek, 1984; USGS, 2005). Groundwater flow can also

occur across bedrock strike along joints, faults and fracture traces (Parizek et al., 1971). Fracture traces are natural linear fracture zones that are expressed as aligned topographic and geologic features less than one mile in length. These features are readily visible on aerial photographs and can include any of the following features: straight stream segments; valley alignment changes; gaps in ridges; gulley development; aligned sinkholes and swallets; localized springs and seepage areas; areas of increased soil moisture as evidenced by enhanced vegetation growth; and soil-tonal alignments (Parizek et al., 1971). Fracture traces mapped by Parizek and Drew (1966) within the study area show a distinct pattern with N/NW and E/NE orientations (see map in Appendix A).

Figure 2-3 is a regional groundwater elevation contour and flow map of the Spring Creek basin, which has a total drainage basin of approximately 453 square kilometer (km), including a 378 square km surface drainage area with a groundwater basin extending approximately 75 additional square km toward the southwest, as mapped in previous investigations by Giddings (1974), Wood (1986), Hunter (1994), and SRBC (1997). The groundwater basin extends beyond the surface drainage basin due to the regional southwest/northeast-trending Birmingham thrust fault, a transmissive feature which spans from the Spring Creek Basin into the adjacent Spruce Creek Basin (Giddings, 1974). In addition, northeast-plunging bedrock may be capturing groundwater from beneath the adjacent Spruce Creek surface basin and causing underdrainage toward Spring Creek. Collectively, the average daily flow at the mouth of Spring Creek is 6.57 cubic meters per second (CMS) based on USGS Milesburg gage data, with groundwater baseflow providing an annual average of approximately 86% of total stream flow (Giddings, 1974). The region relies heavily on groundwater from the carbonate aquifer as the primary drinking water source, providing approximately 0.657 CMS of potable water for the region on a daily basis.

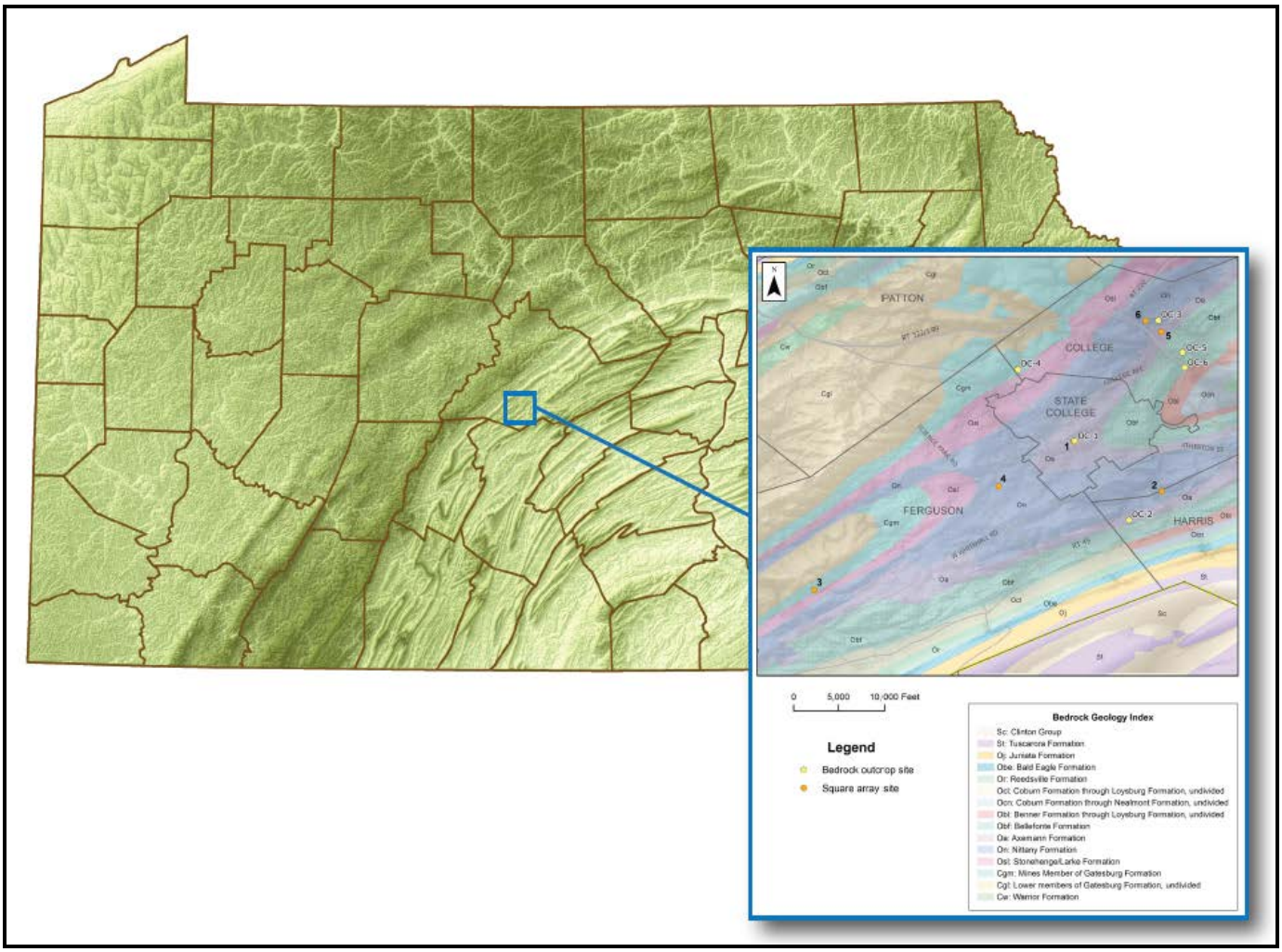

Figure 2-1. Map of the study area location.

Understanding the role of aquifer anisotropy on groundwater flow from bedding planes, fractures, and faults is important for delineating wellfield recharge areas and associated source water protection efforts.

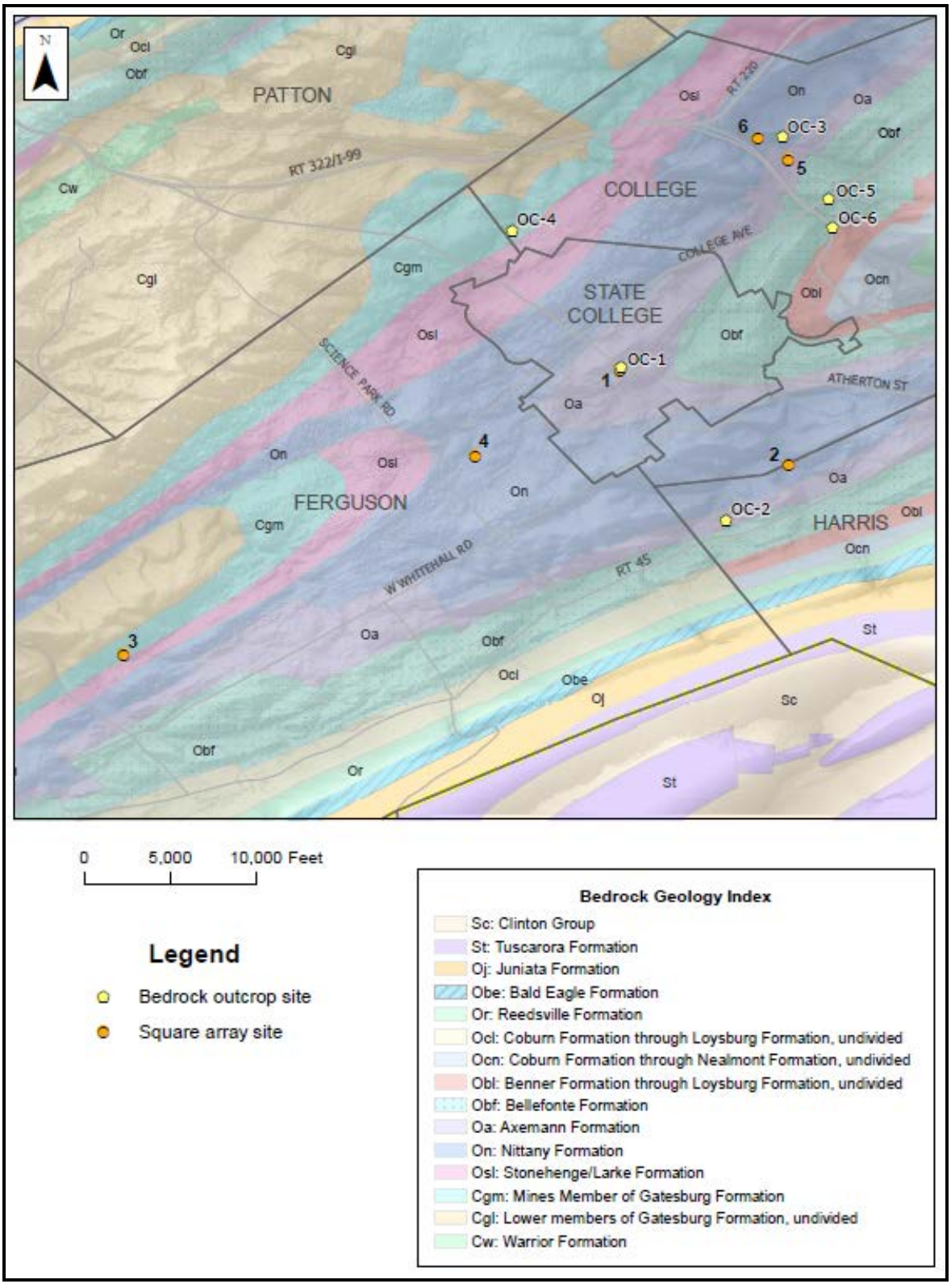

Figure 2-2. Map showing the location of each of the six square array and bedrock outcrop sites located in the Spring Creek Watershed/State College area on a geologic base map.

Methodology

Square array measurements

The square array method consists of using a pair of current electrodes and a pair of potential electrodes positioned at the four corners of a square, with the center point of the square considered as the measuring point, as shown in Figure 2-3. The length of a side of a square is considered as the "a-spacing" for the array size. An electric current is sent between the current electrodes and the resulting voltage drop is measured at the potential electrodes. For each square array a-spacing at a given orientation there are three measurements made, including two perpendicular (alpha and beta) measurements, and one diagonal (gamma) measurement (Figure 2-4).

The azimuthal orientation of a resistivity measurement using the square array is that of the line connecting the current electrodes. Therefore, alpha and beta measurements provide information on the change in the subsurface's apparent resistivity with respect to a 90° change in orientation. The gamma measurement checks the accuracy of the alpha and beta measurements, where, in an isotropic aquifer $\rho_\alpha=\rho_\beta$, and in a heterogeneous, anisotropic aquifer $\rho_\gamma= \rho_\alpha-\rho_\beta$. The array is expanded symmetrically around the center point so the sounding can be interpreted with depth, typically in increments of $A*2^{0.5}$ with a-spacing varying from 5 meters to greater than 50 meters (Habberjam and Watkins, 1967). The array is rotated by a small increment, typically 15°, so that data with sufficient resolution can be collected for interpretation and graphical display.

Apparent resistivity for a square array is determined using the following equation (Habberjam and Watkins, 1967):

$\rho_a=K*V/I$ (Equation 1)

where

$K=3.42*\pi*A$ is the square array geometric factor, and (Equation 2)

A= square-array side length (i.e. a-spacing) in meters.

According to Habberjam (1972), the advantages of the square array include requiring about 65% less area than conventional collinear arrays, providing greater sensitivity to anisotropy than collinear arrays, giving a better point measurement of resistivity, and being less dependent on orientation. In addition, a single full survey can be conducted in a matter of hours and provides a direct earth resistivity measurement without requiring inversion. A potential disadvantage to using the square array is that the layout may be cumbersome, especially in forested areas or severely uneven terrain.

A representative sampling of the Spring Creek watershed was provided by selecting a total of six study areas for square array surveying, as shown in Figure 2-2. Each site is underlain by Cambrian- and Ordovician-age carbonate formations of the Valley and Ridge physiographic province. The sites were selected based on access, surface conditions, and availability of site-specific geologic and hydrogeologic information.

An ABEM 1000 Terrameter electrical resistivity meter was used for collecting field measurements, which consists of a built-in constant current transmitter powered by a clip-on battery pack that is combined with a high resolution receiver. The current and potential connectors on the face of the unit were connected to separate sections of 14-gauge coated wiring that could be extended out to lengths accommodating a- spacings of up to 50 meters. The wiring was then connected to the corresponding current and potential electrodes that were placed in the ground at the four corners of the square to form the array.

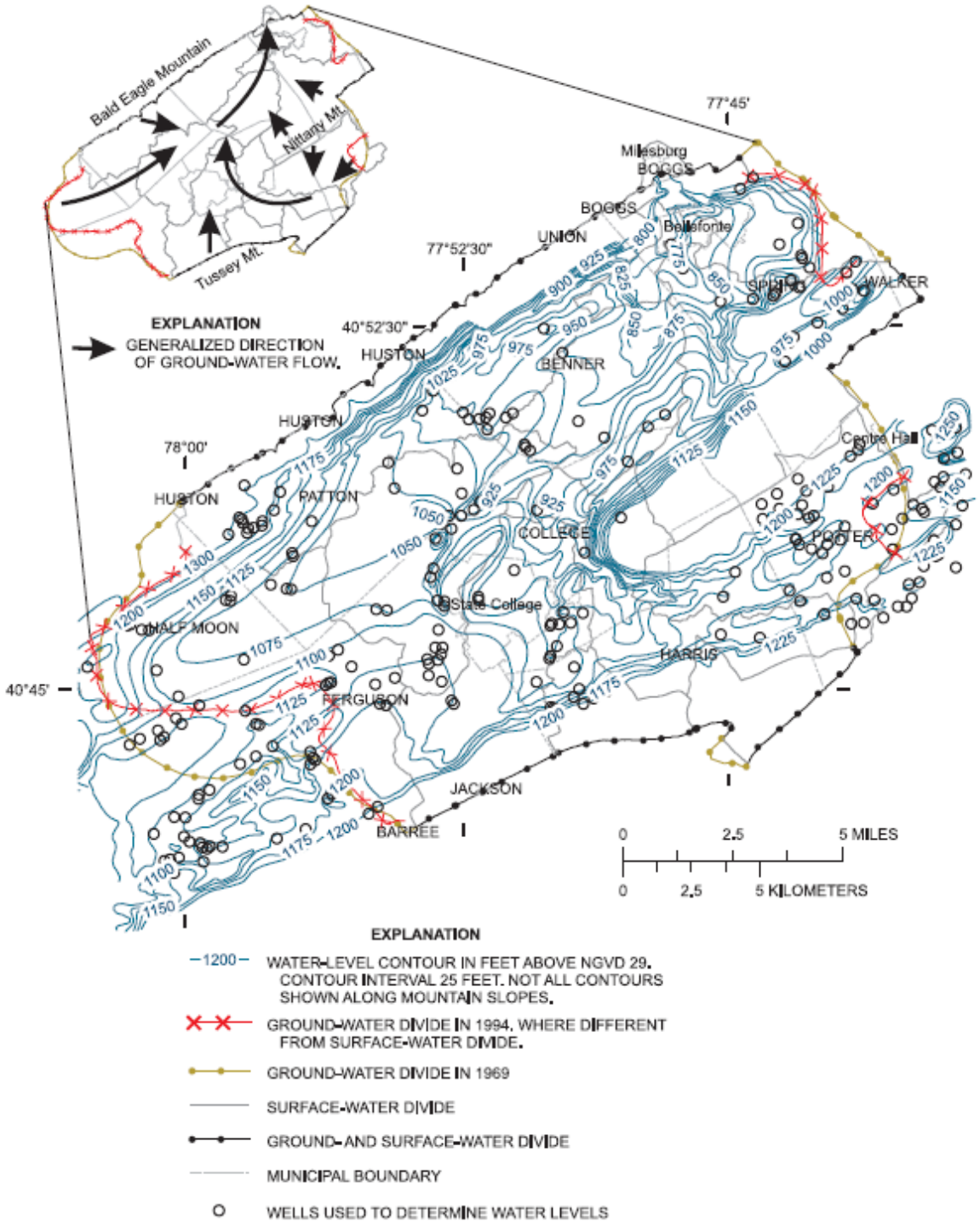

Figure 2-3. Regional groundwater elevation contour map of the Spring Creek basin (USGS, 2005 as modified from SRBC, 1997)

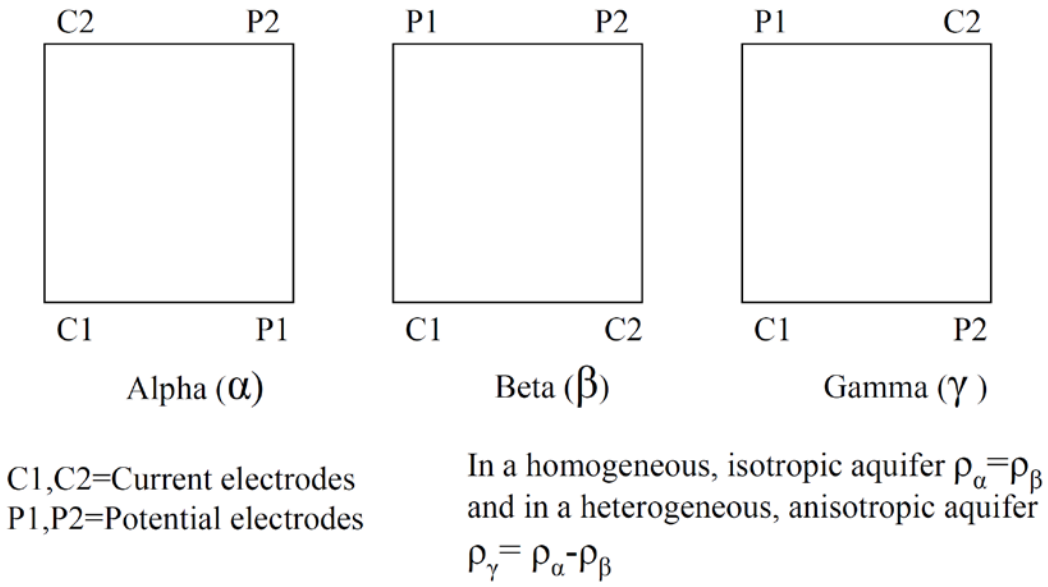

Figure 2-4. **Square array configurations showing the current and potential electrodes locations.**

The current electrodes were initially placed in a north-south orientation using the alpha array. The typical progression of resistance measurements involved starting with an a-spacing of 5 meters and increasing the array size outwardly in a sequential manner to 7.1, 10, 14.2, 20, 28.2, 40, and 50 meters or some combination of these dimensions. Once the alpha measurement was collected for each a-spacing, the wire connections were changed at the meter and measurements were made in the beta array configuration (west-east orientation), which is measured perpendicular to the alpha array's orientation. The perpendicular alpha and beta measurements provide information on the azimuthal variation in the subsurface apparent resistivity, with the measurement orientation parallel to the current electrodes' orientation. Finally the wires were switched to collect gamma resistance measurements (diagonal), which acts as a check on the accuracy of the alpha and beta measurements. If the difference of the alpha and beta field measurements were within 5% of the gamma measurement then then the data were considered valid for that given a-spacing and orientation. Once the series of measurements were made for each a-spacing at a particular orientation, the electrodes were then rotated clockwise by 15°

degrees and the full complement of resistance measurements were collected at each a-spacing. Each measurement was repeated until readings were consistent and recorded on field sheets. The estimated apparent resistivity for a square array measurement was then calculated by using Equation 1. The estimated apparent resistivity values at a given a-spacing were calculated and plotted against azimuth to create a radar plot for interpretation.

The maximum apparent resistivity is considered to be transverse apparent resistivity (ρ_{at}) while the minimum apparent resistivity is considered to be longitudinal apparent resistivity (ρ_{al}), per Habberjam (1972). The coefficient of anisotropy (λ) for each a-spacing of the square array was calculated as using the following equation (Habberjam, 1972):

$$\lambda = (\rho_{at} / \rho_{al})^{1/2} \quad \text{(Equation 3).}$$

The coefficient of anisotropy provides a measure of the anisotropy for a given site. Typical coefficients are between 1 and 2, however they can be greater than 7 in certain settings (Frischknecht and Keller, 1966).

Measuring Secondary Porosity

Square array data can be used to estimate secondary porosity in fractured bedrock aquifers by modifying Taylor's (1984) method developed for collinear arrays in saturated, clay-free, non-shale rocks. To calculate secondary porosity, it is first necessary to calculate the anisotropy (N) from the square array field data, using Habberjam's method (1975) where:

$$N = [(T + S)/(T - S)]^{1/2} \quad \text{(Equation 4)}$$

$$T = A\text{-}2 + B\text{-}2 + C\text{-}2 + D\text{-}2; \quad \text{(Equation 5)}$$

$$S = 2[(A\text{-}2 - B\text{-}2)^2 + (D\text{-}2 - C\text{-}2)2]^{½}; \quad \text{(Equation 6)}$$

and A, B, C, and D are defined as

$$A = [(\rho_{a3} + 3\rho_{a1})/2 + (\rho_{a4} + r_{a2})/(2)^{½}][(2 + (2)^{½}]; \quad \text{(Equation 7)}$$

$$B = [(\rho_{a1} + 3\rho_{a3})/2 + (\rho_{a2} + \rho_{a4})/(2)^{½}][(2 + (2)^{½}]; \quad \text{(Equation 8)}$$

$$C = [(\rho_{a4} + 3\rho_{a2})/2 + (\rho_{a1} + \rho_{a3})/(2)^{½}][(2 + (2)^{½}]; \quad \text{(Equation 9)}$$

$$D = [(\rho_{a2} + 3\rho_{a4})/2 + (\rho_{a3} + \rho_{a1})/(2)^{½}][(2 + (2)^{½}]. \quad \text{(Equation 10)}$$

The secondary porosity (Φ) is then estimated by:

$$\Phi=[3.41*10^{4}*(N-1)*(N^{2}-1)]/[N^{2}*C*(\rho_{max}- \rho_{min})] \quad \text{(Equation 11)}$$

where:

ρ_{max} = maximum square-array apparent resistivity for given a-spacing;

ρ_{min} = minimum square array apparent resistivity for a given a-spacing; and

C = specific conductance of groundwater in microsiemens per centimeter (used 250 µs/cm).

An independent estimate of secondary porosity was estimated from fractures in intact bedrock outcrops at sites shown in Figure 2-2, by measuring fracture frequency, spacing, dimensions (length and depth), and associated aperture within each unit volume. Using these measurements, a fracture-based "void" space estimate for a given volume of rock was used to calculate secondary porosity. Because bedrock outcrop estimates of secondary porosity can be variable based on the local conditions, outcrop measurements were averaged to obtain a representative regional average.

A second independent estimate of secondary porosity was made using groundwater level and stream baseflow data obtained from available county-based US Geological Survey monitoring

wells and stream gauges during recessional periods for groundwater levels and stream flow during dry or drought conditions. During a significant period with little or no precipitation, groundwater levels and stream flow will be in recession, and groundwater baseflow becomes the primary source of the stream's flow. A significant drought condition allows correlation of the measured decrease in the aquifer's level to estimate the volume of bedrock drained to support the known volume of stream flow over the recession period, which equates to the effective porosity. In a karst aquifer, the primary porosity is typically quite low (White, 1988), therefore the effective porosity is the secondary porosity, which is equivalent to the aquifer's specific yield.

Results

The results of square array measurements for each of the test sites, named as Sites 1 through 6, are shown in Figures 2-5 through 2-10 as radar plots, with the associated data summarized in Table 2-1. The square array a-spacings varied at different sites from 5 to 50 meters at Site 1, 10 to 50 meters at Sites 2 and 4, and 40 to 50 meters at Sites 3, 5, and 6. In general, smaller a-spacings (5 to 10 meters) provide resistivity measurements most sensitive to the site soils, the intermediate a-spacings (14.1 to 28.3 meters) give measurements sensitive to the epikarst/weathered bedrock, while the larger a-spacings (40 and 50 meters) provide measurements sensitive to deeper saturated bedrock and associated anisotropy. Collectively, these apparent resistivity measurements allow the effectiveness of the square array to be evaluated for characterizing both epikarst and deeper bedrock geo-electrical properties. Of particular interest is the ability of the electrical current to effectively penetrate through the relatively conductive epikarst into deeper bedrock with the larger a-spacings to characterize aquifer anisotropy. Tables 2-1, and 2-3 through 2-7 summarize calculated apparent resistivity values, including the minimum, maximum and mean values for each site, and the coefficient of

anisotropy, as presented below. Table 2-2 contains the estimated secondary porosity values from the square array and bedrock outcrop measurements.

Site 1

Site 1 is located on the Axemann Formation (fine to coarse-grained limestone). The Site 1 square array data are summarized in Table 2-1 and are shown as a radar plot in Figure 2-5 for each a-spacing and orientation. As can be seen in Figure 2-5, the resistivity data for a-spacings of 5 to 20 m plot similarly in a semi-circular manner with decreasing apparent resistivity values as the a-spacing increases, which would be indicative of soils and epikarst overlying the bedrock. The data for the 28.3 to 50 m a-spacings each plot in a more distinct elliptical pattern, which is indicative of more competent bedrock with discrete bedding planes or fracture orientation, indicating the bedrock is exhibiting stronger geo-electrical anisotropy. The maximum resistivity (232 and 226 ohm-m at 40 and 50 m, respectively) is oriented at 150° while the minimum resistivity (67 and 55 ohm-m at 40 and 50 m, respectively) is at 060°. These resistivity values are within the typical range of 50-500 ohm-m for limestone bedrock (Reynolds, 1997). In addition, the 060° orientation of minimum resistivity values for the 28.3- to 50-m a-spacings correlate well with the nearby field-mapped bedrock strike of 054° from nearby outcrop OC-1 (see Figure 2-2 for location and Appendix A for outcrop photos). Figure 2-6 illustrates increasing coefficients of anisotropy with increased a-spacings, which is expected as electrical current penetrates deeper into more competent bedrock with more discrete bedding planes and fractures. The mean apparent resistivity decreases with greater a-spacings, which is likely a result of encountering saturated bedrock. As summarized in Table 2-2, the secondary porosity

Table 2-1. Site 1 square array apparent resistivity values and statistics.

A-spacing	Azimuth (degrees)/Apparent resistivity (ohm-m)												Statistics			
(meters)	0	15	30	45	60	75	90	105	120	135	150	165	Min	Max	Mean	Anisotropy
5	237	179	184	222	246	259	213	267	266	260	195	201	179	267	228	1.22
7.1	253	162	162	218	232	251	197	262	288	246	204	205	162	288	226	1.33
10	276	141	121	163	214	208	160	280	330	282	186	223	121	330	220	1.65
14.1	217	107	98	130	179	162	124	211	240	201	158	187	98	240	172	1.56
20	176	81	77	92	128	116	87	161	168	166	146	156	77	176	133	1.52
28.3	197	84	75	75	89	75	74	153	184	184	146	192	74	197	133	1.63
40	232	93	81	74	67	68	72	121	194	214	168	209	67	232	133	1.86
50	226	100	84	73	55	71	72	102	178	210	161	186	55	226	127	2.03

for the 40- and 50-meter a-spacing is estimated to be 26.7% and 25%, respectively, however a measurement from the nearby rock outcrop, OC-1, indicates a 3.6% fracture-based porosity (see Appendix A for field measurements of fracture dimensions).

Site 2

Site 2 is located on the Nittany Formation (fine to coarse-grained dolomite). The Site 2 square array data are summarized in Table 2-3 and are shown as a radar plot in Figure 2-7 for each a-spacing and orientation. As can be seen in Figure 2-7, the resistivity data for the 10-m a-spacing plot in a semi-circular manner, which would be indicative of soils and epikarst overlying the bedrock. The resistivity data for the 20-50 m a-spacings each plot in a more distinct elliptical pattern, which is indicative of more competent bedrock with discrete bedding planes or fracture orientation, indicating the bedrock is exhibiting stronger geo-electrical anisotropy. Site 2's preferred subsurface electrical current flow direction and is coincident with the nearby field-mapped bedrock strike of 055° at OC-2 (see Figure 2 for location and Appendix A for photos). Figure 2-8 illustrates increasing mean apparent resistivity and coefficients of anisotropy with increased a-spacings, indicating the rock is more competent with depth. As summarized in Table 2-2, the secondary porosity is estimated to be 4.2% and 3.3% for the 40- and 50-m a-spacing

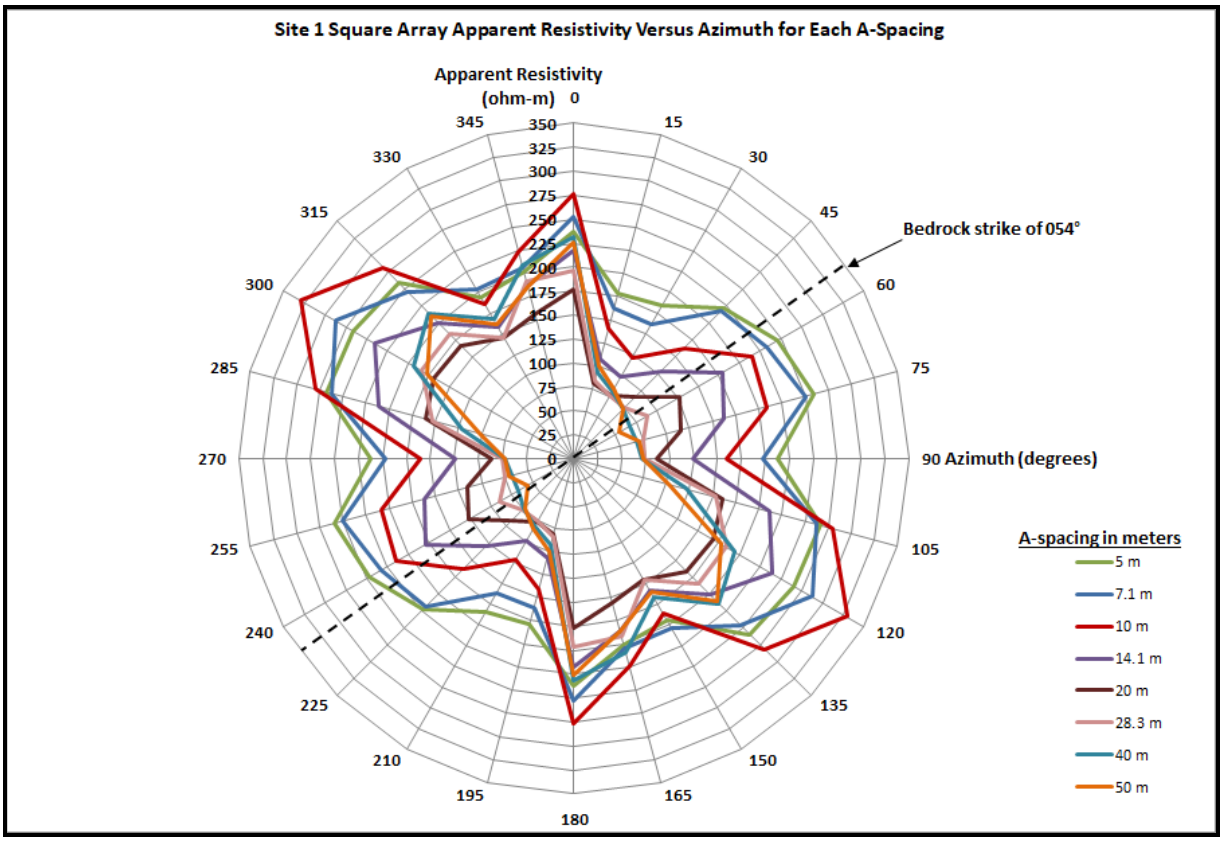

Figure 2-5. Square array Site 1 radar plot of apparent resistivity versus azimuth.

square array measurements, respectively, while the nearby OC-2 outcrop-based secondary porosity is 1.5%.

Site 3

Site 3 is located on the Mines Member of the Gatesburg Formation (fine to coarse-grained dolomite). The site's resistivity data plot as an ellipse, as shown in Figure 2-9, with the major axis formed by the data at the 40-m (495 ohm-m) and 50-m (504 ohm-m) a-spacings, with an orientation of 120°. The minor axis of the ellipse is oriented at 030°, with resistivity values at the 40 and 50 meter a-spacing of 287 and 328 ohm-m respectively, with the preferred current flow in this direction. The range of resistivity values for Site 3's 40 and 50-m a-spacings are within the typical range of 50-500 ohm-m for limestone (Reynolds, 1997). Mapped bedding in

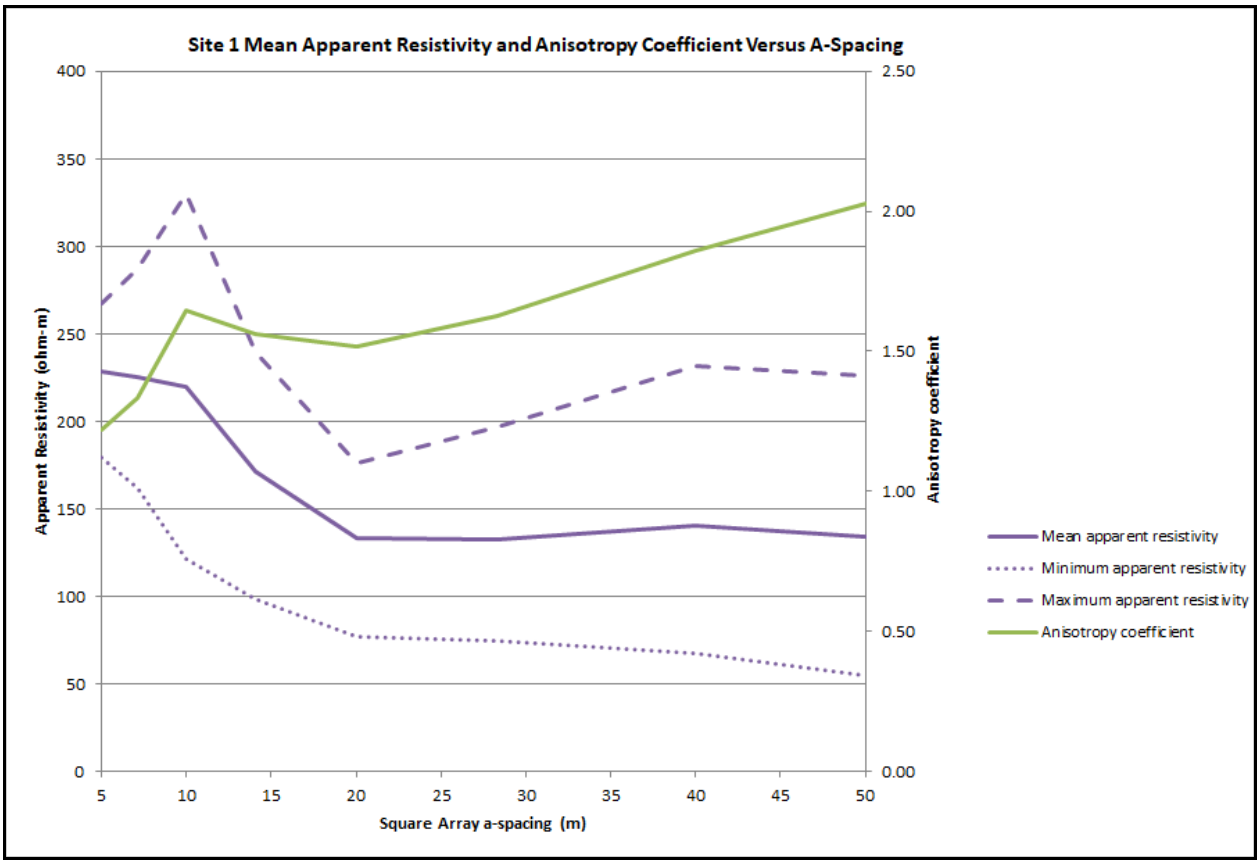

Figure 2-6. Site 1 apparent resistivity and coefficient of anisotropy vs square array a-spacing.

Table 2-2. Summary of Secondary Porosity Estimates from Square Array and Field Measurements

Location	Square Array Secondary Porosity (%)	Location	Square Array Secondary Porosity (%)	Location	Bedrock Secondary Porosity (%)
Site 1-40 m	26.7%	Site 1-50 m	25.0%	Outcrop 1	3.6%
Site 2-40 m	4.2%	Site 2-50 m	3.3%	Outcrop 2	1.5%
Site 3-40 m	1.9%	Site 3-50 m	4.2%	Outcrop 3	3.6%
Site 4-40 m	1.8%	Site 4-50 m	0.7%	Outcrop 4	1.0%
Site 5-40 m	3.6%	Site 5-50 m	4.4%	Outcrop 5	3.0%
Site 6-40 m	4.2%	Site 6-50 m	2.7%	Outcrop 6	0.3%
				Outcrop 7	4.8%
Average*	3.1%	Average*	3.1%	Average	2.6%

*The Site 1 porosity data was not included for average purposes due to possible influence by conduit porosity

Table 2-3. Site 2 square array apparent resistivity values and statistics.

A-spacing	Azimuth (degrees)/Apparent resistivity (ohm-m)												Statistics			
(meters)	0	15	30	45	60	75	90	105	120	135	150	165	Min	Max	Mean	Anisotropy
10	266	319	321	325	334	318	364	313	361	337	322	318	266	364	325	1.17
20	271	280	276	271	249	232	250	244	265	266	332	295	232	332	269	1.20
40	375	357	321	290	285	284	224	334	383	420	419	419	224	420	343	1.37
50	431	386	349	306	307	312	326	365	405	453	458	458	306	458	380	1.22

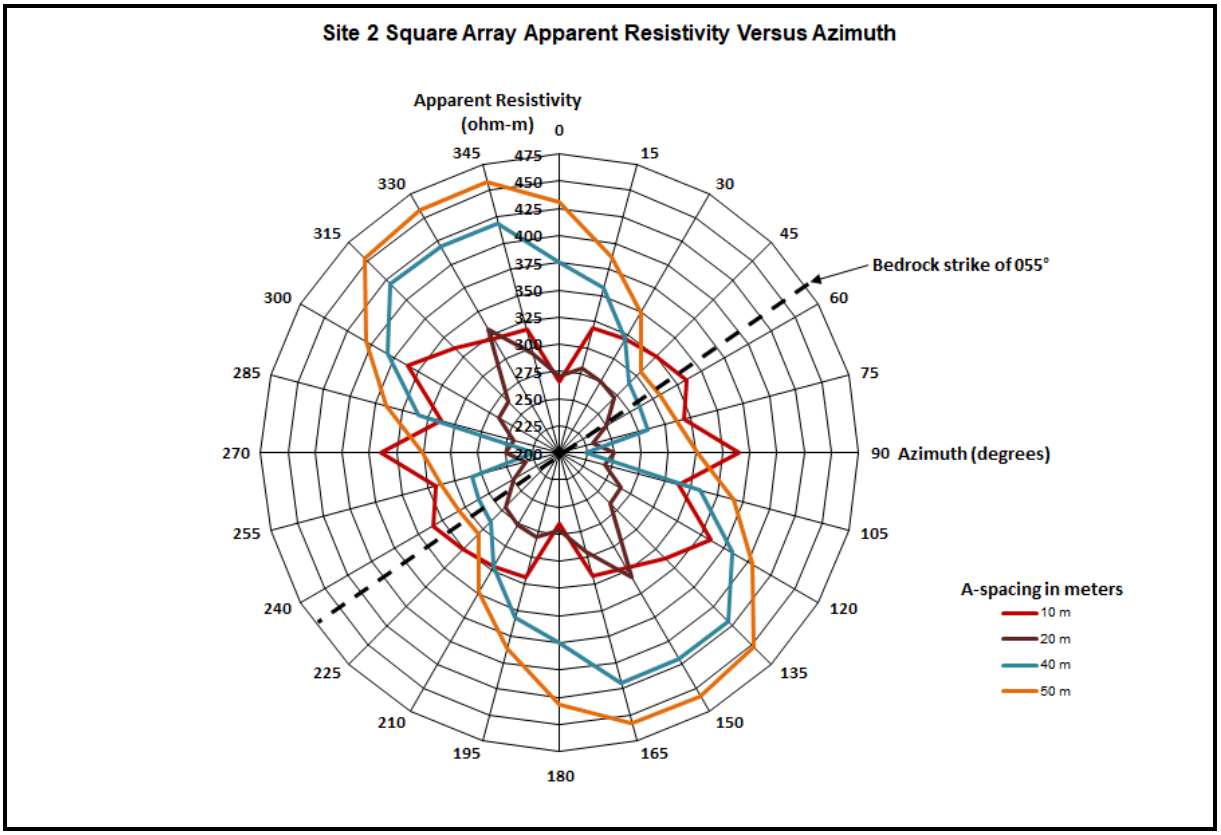

Figure 2-6. Square array Site 2 radar plot of apparent resistivity versus azimuth.

the vicinity of Site 3 has a strike of approximately 035°, which is nearly parallel to the resistivity minima. The mean resistivity values contained in Table 2-3 increase for the 40-m to 50-m a spacing from 386 to 419 ohm-m, respectively, as do the corresponding coefficients of anisotropy from 1.33 to 1.48, likely due to more competent yet increasingly anisotropic bedrock with depth.

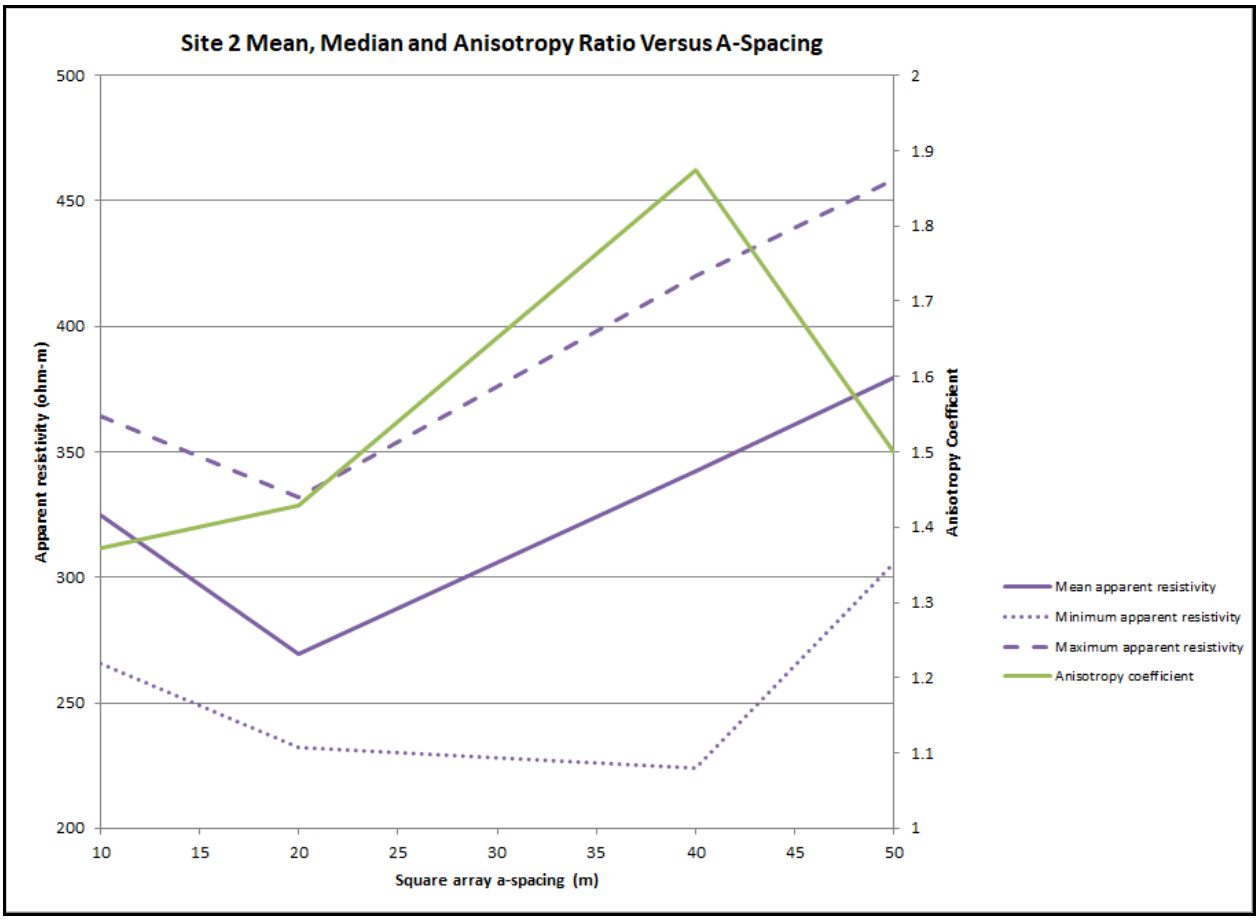

Figure 2-7. Site 2 apparent resistivity and coefficient of anisotropy vs square array a-spacing.

Table 2-4. Site 3 square array apparent resistivity values and statistics.

A-spacing	Azimuth (degrees)/Apparent resistivity (ohm-m)												Statistics			
(meters)	0	15	30	45	60	75	90	105	120	135	150	165	Min	Max	Mean	Anisotropy
40	321	278	287	331	349	366	426	464	495	461	451	399	278	495	386	1.33
50	233	290	328	401	444	437	502	512	504	495	460	427	233	512	419	1.48

Based on the 40- and 50-meter a-spacing square array measurements the secondary porosity is estimated to be 1.9% and 4.1%, respectively, as contained in Table 2-2.

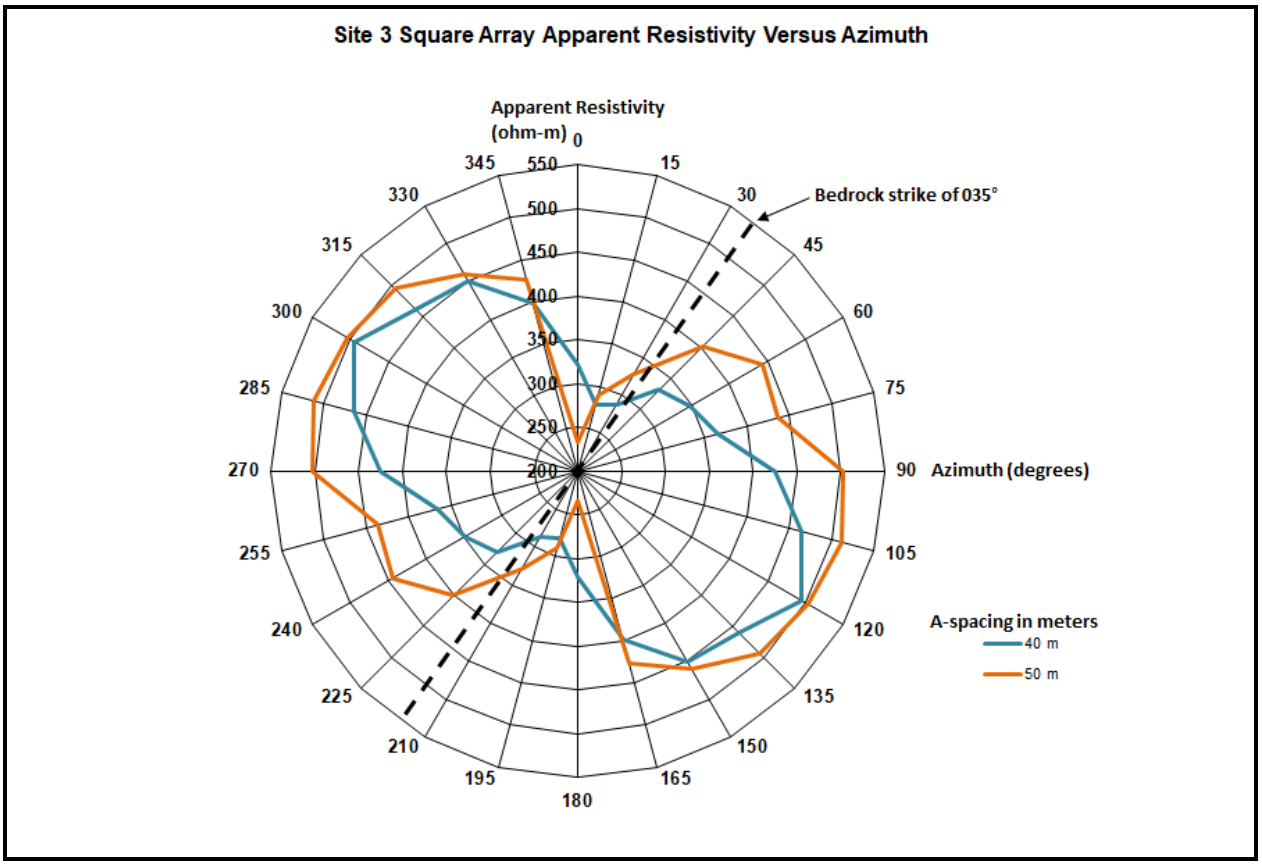

Figure 2-8. **Square array Site 3 radar plot of apparent resistivity versus azimuth.**

Site 4

Site 4 is also located on the Nittany Formation (fine to coarse-grained dolomite). The Site 4 square array data are summarized in Table 2-5 and are shown as a radar plot in Figure 2-10 for each a-spacing and orientation. As can be seen in Figure 2-10, the resistivity data for a-spacing 10-m plot in a semi-elliptical manner with the major axis oriented north/south, though the anisotropy coefficient of 1.14 is fairly low, with mean apparent resistivity of 195 ohm-m, which may be indicative of thin soils underlain by epikarst. The 20 m a-spacing data takes on an a more defined elliptical shape with the major axis running approximately east/west, though the anisotropy coefficient of 1.16 remains fairly low with mean apparent resistivity of 247 ohm-m. Therefore, the bedrock is interpreted to be weathered. Site 4's resistivity data plot as an ellipse

with the highest apparent resistivity values at the 40 and 50 meter a-spacings corresponding to orientations of approximately 105° with resistivity values of 342 and 319 ohm-m, respectively, as shown in Figure 2-10. The minor axis of these ellipses occur perpendicular at an orientation of approximately 015° with a corresponding resistivity value of 237 and 256 ohm-m for the 40 and 50 meter a-spacings, respectively, indicating a preferred electrical flow in this direction. The range of resistivity values for Site 4's 40- and 50-m a-spacings are within the typical range of 50-500 ohm-m for limestone (Reynolds, 1997). The resistivity minima orientation of 015° is essentially parallel to the nearby measured bedrock strike of 019°. The mean resistivity decreases slightly from the 40- to 50-m a-spacings with values of 342 to 319 ohm-m, respectively, with corresponding decreases in the coefficient of anisotropy of 1.20 and 1.15. Based on the 40- and 50-meter a-spacing square array measurements the secondary porosity is estimated to be 1.8% and 0.7%, respectively (Table 2-2).

Site 5

Site 5 is also located on the Axemann Formation (fine to coarse-grained limestone). The site's resistivity data has major elliptical axes at an orientation of 000° for the 40-m and 50-m a-spacings with corresponding resistivity values of 177 and 191 ohm-m, respectively, as shown in

Table 2-5. Site 4 square array apparent resistivity values and statistics.

A-spacing	Azimuth (degrees)/Apparent resistivity (ohm-m)												Statistics			
(meters)	0	15	30	45	60	75	90	105	120	135	150	165	Min	Max	Mean	Anisotropy
10	210	224	172	190	198	185	183	178	216	191	187	208	172	224	195	1.14
20	215	225	232	241	252	279	287	290	264	241	226	218	215	290	247	1.16
40	254	237	251	280	301	311	331	342	333	250	311	316	237	342	293	1.20
50	281	256	259	277	284	303	304	319	315	318	239	307	239	319	289	1.15

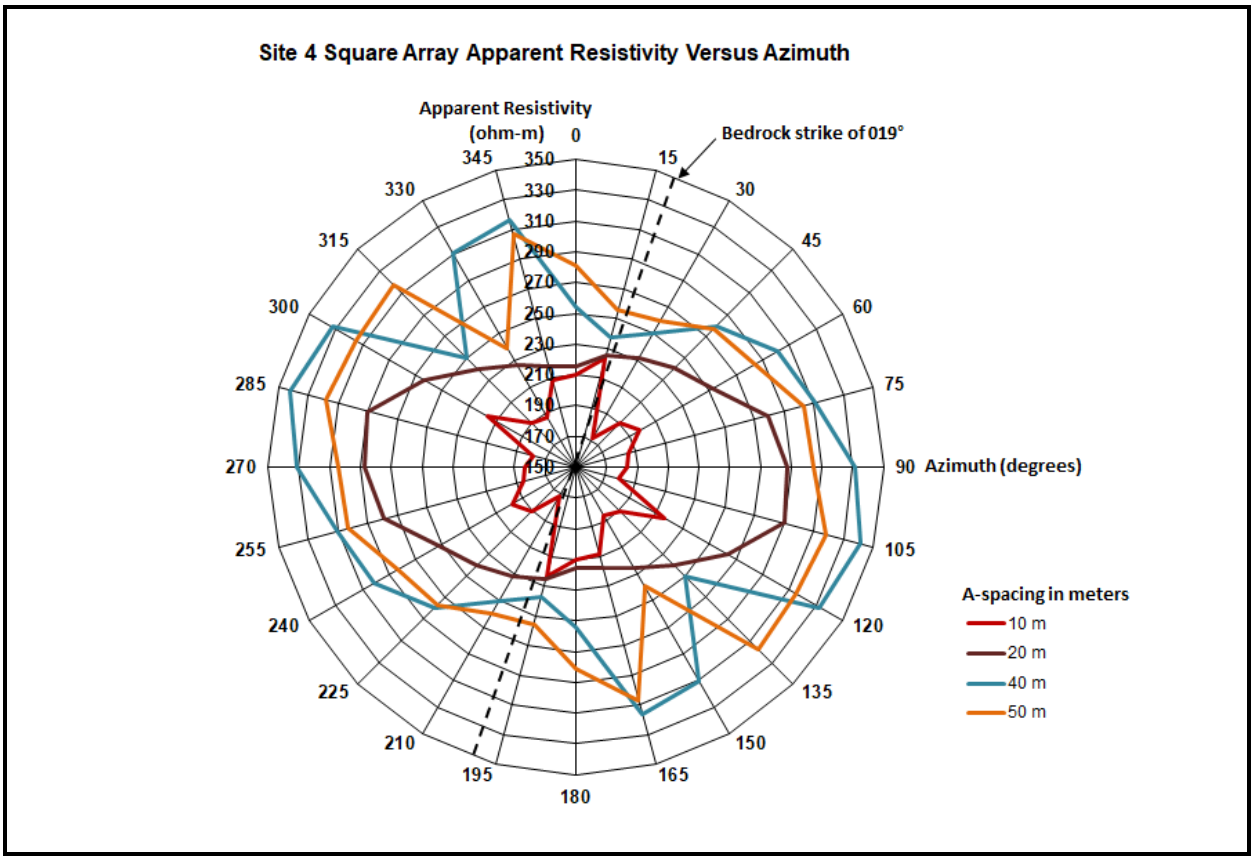

Figure 2-9. **Square array Site 4 radar plot of apparent resistivity versus azimuth.**

Figure 2-12. The minor axes of these ellipses have an orientation of 090° with corresponding resistivity values of 142 and 139 ohm-m for the 40 and 50 meter a-spacings, respectively. The range of resistivity values for Site 5's 40- and 50-m a-spacings are within the typical range of 50-500 ohm-m for limestone (Reynolds, 1997). The preferred electrical current flow at Site 5 is along the resistivity minima 090°, which may be related to a fracture trace, that typically run east-west on a regional basis. It is worth noting the presence of a secondary resistivity minima that occurs at 030° for both a-spacings, which is parallel to bedrock strike of 030°. As summarized in Table 2-6, the mean resistivity values increase slightly from the 40- to 50-m a-spacing from 157 to 161 ohm-m, respectively, which correspond to the coefficients of anisotropy with values of 1.12 to 1.17, again indicating more competent rock with increasing depth. Based

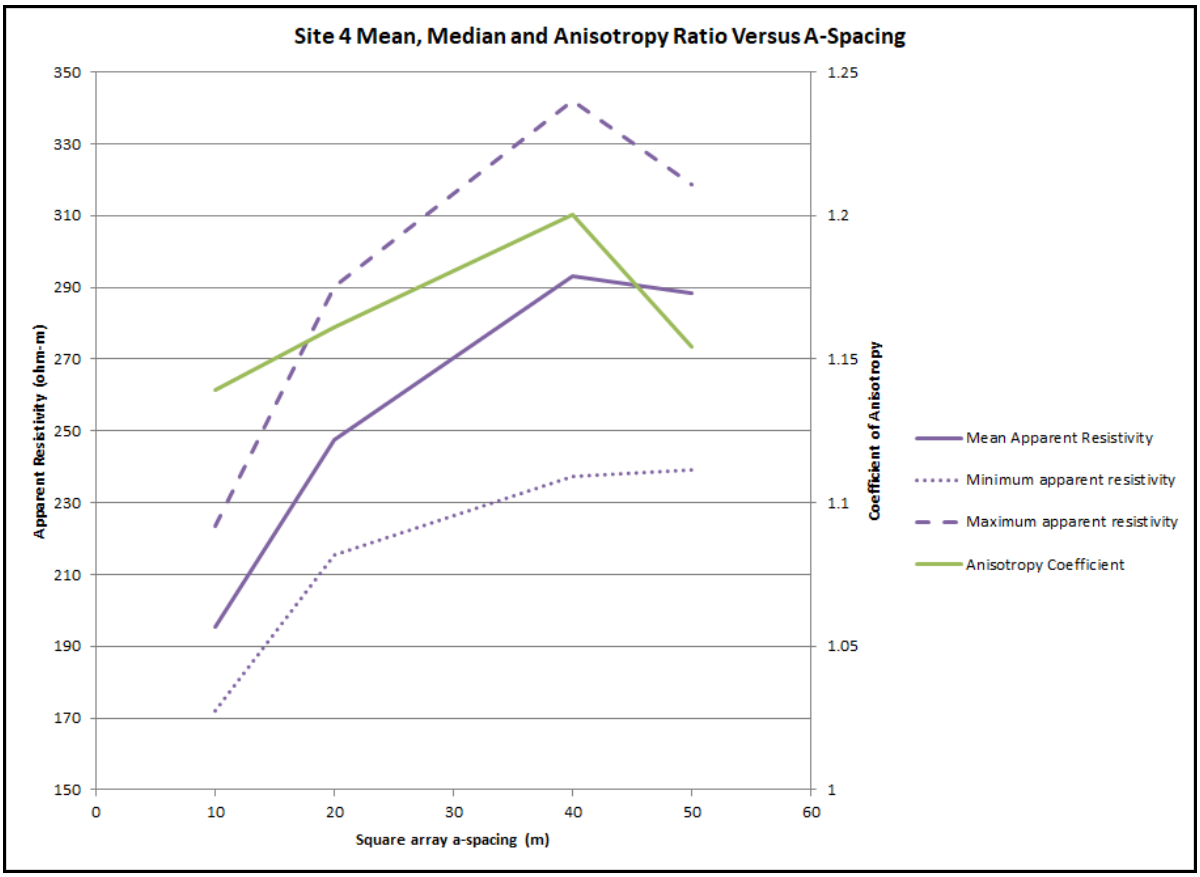

Figure 2-10. Site 4 apparent resistivity and coefficient of anisotropy vs square array a-spacing.

on the 40- and 50-meter a-spacing square array measurements, the secondary porosity is estimated to be 3.6% and 4.4% (Table 2-2).

Site 6

Site 6 is also located on the Nittany Formation (fine to coarse-grained dolomite). The Site 6 resistivity data reveal major axes of the ellipses for the 40 and 50 meter a-spacings corresponding to orientations of approximately 090° and 105° with resistivity values of 641 and 573 ohm-m, respectively. The minor axes of the ellipses correspond to orientations of 000° and 015°, with accompanying resistivity values of 260 and 258 ohm-m for the 40 and 50-m a-spacings, respectively. The minimum and mean resistivity values measured at Site 6 are within

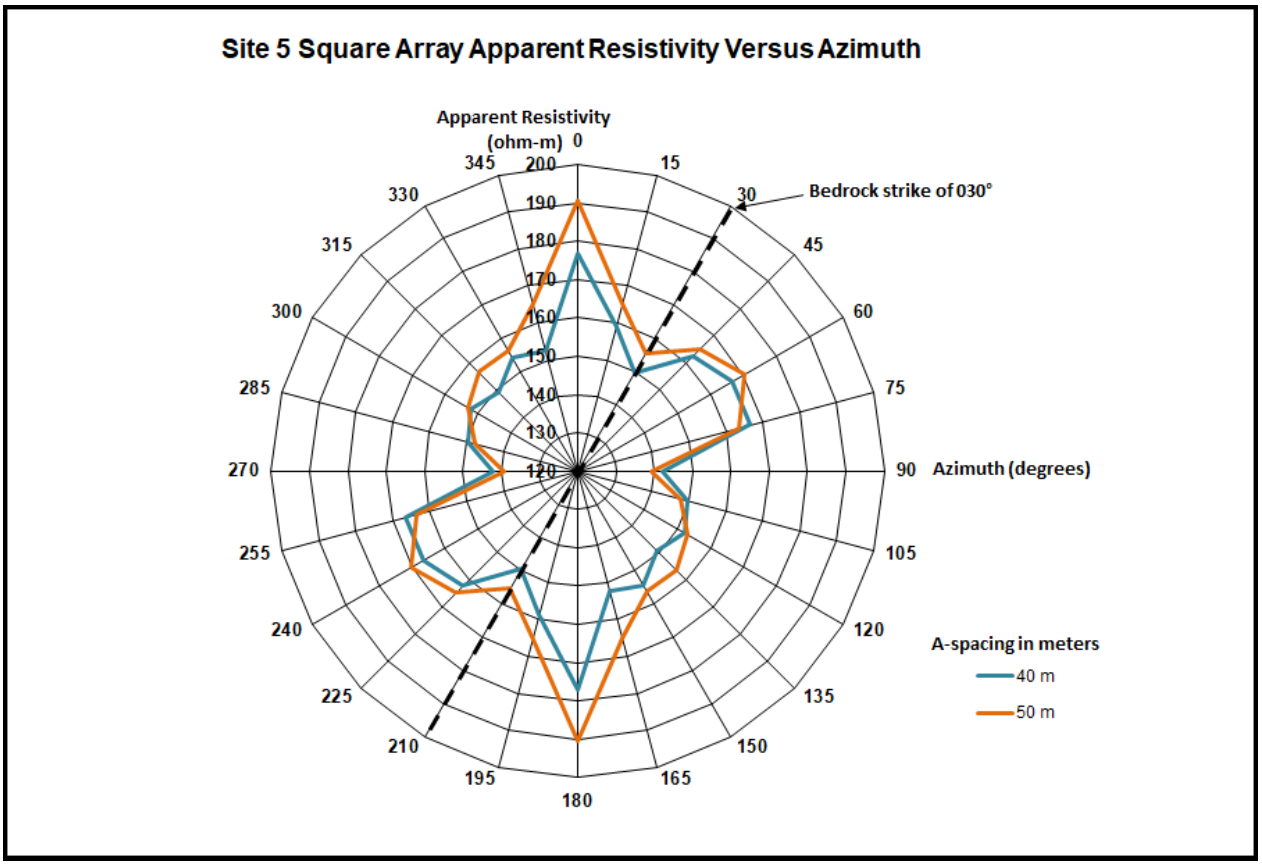

Figure 2-11. Square array Site 5 radar plot of apparent resistivity versus azimuth.

Table 2-6. Site 5 square array apparent resistivity values and statistics.

A-spacing	Azimuth (degrees)/Apparent resistivity (ohm-m)												Statistics			
(meters)	0	15	30	45	60	75	90	105	120	135	150	165	Min	Max	Mean	Anisotropy
40	177	159	150	162	167	167	142	150	152	149	154	152	142	177	157	1.12
50	191	165	155	165	170	163	139	148	153	157	156	165	139	191	161	1.17

the typical range of 50-500 ohm-m for limestone (Reynolds, 1997), however the maximum resistivity values are out of this typical range, which may be attributed to minimal fracturing in the rock. Mapped bedding in the vicinity of the site has a strike of 030°, which is subparallel to

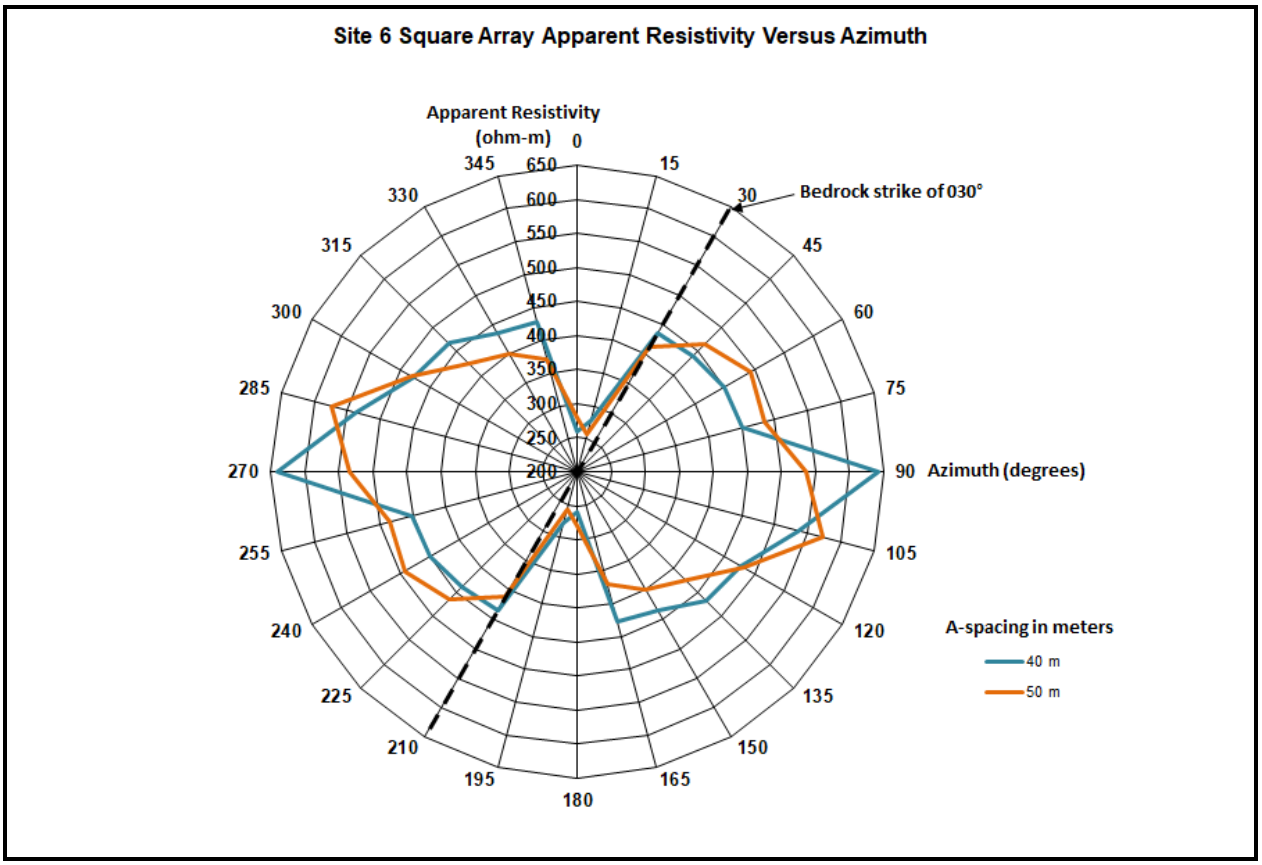

Figure 2-12. Square array Site 6 radar plot of apparent resistivity versus azimuth.

Table 2-7. Site 6 square array apparent resistivity values and statistics.

A-spacing	Azimuth (degrees)/Apparent resistivity (ohm-m)												Statistics			
(meters)	0	15	30	45	60	75	90	105	120	135	150	165	Min	Max	Mean	Anisotropy
40	260	278	434	440	449	451	641	536	477	467	434	428	260	641	441	1.57
50	279	258	413	465	493	484	535	573	481	426	400	372	258	573	432	1.49

the resistivity minima for the 50 m a-spacing. As shown in Figure 2-13, the mean resistivity values decrease slightly from the 40-m (441 ohm-m) to 50-m (432 ohm-m) a-spacings. The coefficients of anisotropy decrease from a value of 1.57 to 1.49 for the 40-meter to 50-meter a-spacings, respectively. Based on the 40- and 50-meter a-spacing square array, measurements of secondary porosity are estimated to be 4.2% and 2.7% (Table 2-2).

Discussion

In this section, a discussion of the square array method's ability to effectively characterize the resistivity, anisotropy and secondary porosity in a fractured, carbonate bedrock setting overlain by an epikarst mantle of variable thickness is presented. The square array resistivity data from each of the six square array sites indicate several consistencies that can be useful for geologic characterization. Thus, as initially postulated by Habberjam (1967), the square array is a useful technique for measuring earth resistivity in that it provides both directionally variable and independent (i.e., mean) values of earth resistivity, and determines geo-electrical anisotropy using Taylor's (1984) method (equation 11) to estimate secondary porosity. The determination of resistivity, anisotropy, and secondary porosity values from the square array are validated through comparisons to published values and independent field measurements, as discussed below.

The fundamental purpose of using the square array in this study is to estimate realistic earth resistivity values in carbonate bedrock at varying orientations, which then allows determination of other useful parameters (i.e., coefficients of anisotropy and secondary porosity). The six sites within the study area consist of residual soils (typically silt loam to clay loam) near the surface that are underlain by weathered bedrock (epikarst) with variable thickness (0 m to greater than 10 m) that gradually becomes more competent with depth. The ability of electrical current to penetrate through the relatively conductive mantle of soils and epikarst of varying thickness to provide reliable carbonate bedrock resistivity value using the square arrays was achieved. This is demonstrated by comparing the square array apparent resistivity values for each a-spacing and orientation (overall resistivity minimum and maximum of 55 and 641 ohm-m, with mean values ranging from 127 to 441 ohm-m) with the typical range of published resistivity values for clay to

silt loams (50-150 ohm-m) and carbonate bedrock and (50-5,000 ohm-m) per Reynolds (1997). Once a realistic range of carbonate bedrock resistivity values have been acquired at a site using a sufficient range of a-spacings (40 and 50 m) and orientation intervals (015°) using the square array, then further geophysical characterization can occur.

The second focus of this study is to characterize the geo-electrical anisotropy of this folded, faulted, fractured, carbonate aquifer using the square array data. As reviewed previously, we are aware of no studies that have documented the square array method's effectiveness in geologically-complex fractured carbonate overlain by an epikarst mantle of variable thickness. Based on the square array resistivity values collected at each site, the regional carbonate aquifer is shown to be geo-electrically anisotropic, with resistivity minima that are parallel or at least sub-parallel to bedrock strike or fractures at each site, where present. Coefficients of anisotropy for the 40- and 50-m a-spacings at the six study areas range from 1.12 to 2.03, which is within the typical range of 1 to 2 that is observed in many bedrock settings (Frischknecht and Keller, 1966). Regional groundwater flow has been mapped to be strike parallel (from southwest to northeast) in much of the Spring Creek watershed's carbonate aquifer, especially in the center of Nittany Valley where most square array surveys were conducted. The orientation of the square array resistivity minima for the 40- and 50-m a-spacings at each of the six sites correlate well with regional bedrock strike (ranging from 030° to 060°), which also is typically coincident with regional groundwater flow direction based on previous mapping (Giddings, 1974; SRBC, 1997). When comparing these square array results to the work in carbonate terrain of the Floridian aquifer by Whiman and Yeboah-Forson (2015), the fractured carbonate anisotropy coefficients are generally higher, as would be expected when compared to a carbonate setting with dissolution-derived matrix porosity. Overall, the anisotropy orientation agrees with known

geologic structure, where resistivity minima for the 40- and 50-m a-spacings are coincident with bedding plane or fracture orientation. In addition, the magnitude of the coefficients of anisotropy measured for each site are within the typical range of 1 to 2, and generally increase with increasing a-spacings. Therefore, based on both known geologic structure and published coefficient of anisotropy values (Frischknecht and Keller, 1966), the square array's ability to effectively characterize bedding plane or fracture orientation and the associated anisotropy has been established in this complex fractured carbonate bedrock setting.

Finally, the secondary porosity measurements associated with fractures and bedding planes estimated from the square array measurements range from 0.7% to 4.4% across the 40-m and 50-m a-spacing for Sites 2-6 with overall mean porosity of 3.1%. The Site 1 porosities of 25-26.7% may be conduit related and therefore were not included in the average values. The range of bedrock secondary porosity estimated from fracture dimensions in outcrops at locations OC-1 to OC-7 range from 0.3% to 4.8%, with an average of 3.2%. These two independent sets of secondary porosity data agree well. The average regional secondary (effective) porosity as measured from watershed-scale groundwater/streamflow recession range from 1.5% (Giddings, 1974) and 1.3% from this study using USGS monitoring well groundwater and stream gage data (see Appendix A). These regional estimates of secondary porosity from groundwater and streamflow recession data are somewhat lower than the average values from both the square array and outcrop measurements. However, the secondary porosity estimates fall well within the range of estimated values by Parizek et al., (1971), with an effective porosity range of 0.3-5% for the Nittany Formation (dolomite), which underlies a significant portion of the watershed study area and agrees well with the range presented in this study. A potential cause of the lower regional estimates is that non-carbonate bedrock (sandstone ridges and shale mountain slopes)

comprise approximately 20% of the Spring Creek watershed, which typically have lower secondary porosities. Additionally, some of the carbonate bedrock is relatively shaley, especially the Coburn and Salona Formations which occur along the base of the ridges near the valley edges and would have lower secondary porosity.

Summary and Conclusions

In summary, application of the square array method to six sites within the fractured carbonate bedrock valley of the Spring Creek basin in central Pennsylvania demonstrates that the square array apparent resistivity data correlate well with known bedrock structure. In particular, the resistivity minima for larger a-spacings of 40 meters and 50 meters at each site paralleled bedrock strike or mapped fractures, where present. In addition, estimates of secondary porosity from the 40- and 50-meter a-spacings of the square array generally compared favorably to independent estimates of bedrock structure and secondary porosity from previously published studies, outcrop measurements, and groundwater level/streamflow recession data. The results of this study validate that the square array method can be used effectively in complex karst settings to characterize bedrock anisotropy and secondary porosity when compared to field measurements of bedrock outcrops and groundwater data.

In this setting, the square array can provide a robust method for estimating realistic earth resistivity values; correlating geo-electrical anisotropy with orientations of bedding plane strike, fracture strike, and mapped groundwater flow; and estimating secondary porosity values that correlate with outcrop-based, fracture porosity measurements, and effective porosity based on streamflow/aquifer level recession estimates. One of the advantages of using the square array over collinear arrays is that it requires a smaller footprint. The results of this study show that this advantage holds even in karst areas with an epikarst mantle, where a-spacings of only 40 meters

to 50 meters are needed to effectively characterize the resistivity and anisotropy of the carbonate bedrock.

Collectively, the results of this study provide valuable information for investigations of water supply, source water protection, and groundwater remediation. In study areas where geologic data are limited due to lack of carbonate bedrock exposure from thick soil and epikarst cover, or where well control is sparse or non-existent, the square array may be especially useful for obtaining estimates of key bedrock aquifer properties.

References

Ahmed, S., G. Marsily, and A. Talbot. 1988. Combined use of hydraulic and electrical properties of an aquifer in a geostatistical estimation of transmissivity. Ground Water 26, no. 1: 78–86.

Bakalowicz, M., 2005. Karst groundwater: a challenge for new resources. Hydrogeology Journal, 13, 148–160.

Boadu, F., Gyamfi, J., and Owusu, E., 2005. Determining subsurface fracture characteristics from azimuthal resistivity surveys: A case study at Nsawam, Ghana, Geophysics, Vol. 70, No. 5 (September-October 2005); P. B35–B42, 10.1190/1.2073888

Busby, J.P., 2000. The effectiveness of azimuthal apparent-resistivity measurements as a method for determining fracture strike orientations, *Geophysical Prospecting*, vol. 48, pp. 677-695.

Chen, Z., Auler, A.S., et al, 2017. The World Karst Aquifer Mapping project: concept, mapping procedure and map of Europe. Hydrogeology Journal, 25, 771–785.

Darboux-Afouda, R., and Louis, P. 1989. Contribution of electrical anisotropic measurements in the search for crystal fracture aquifers in Benin. Geophysical Prospecting. v. 37, pp. 91-105.

de Lima, O and Niwas, S, 2000. Estimation of hydraulic parameters of shaly sandstone aquifers from geoelectrical measurements, Journal of Hydrology 235(1):12-26, August 2000.

El-Qady, G.,Hafez, M., Abdalla, M.A., and Ushijima, K., 2005. Imaging subsurface cavities using geoelectric tomography and ground-penetrating radar. Journal of Cave and Karst Studies, v. 67, no. 3, p. 174–181.

Ford, D.C. and Williams, P., 2007. Karst Hydrogeology and Geomorphology. Wiley, Chichester.

Gibson, P.J., Lyle, P., and George, D.M., 2004. Application of resistivity and magnetometry geophysical techniques for near-surface investigations in karstic terranes in Ireland. Journal of Cave and Karst Studies, v. 66, no. 2, p. 35-38.

Giddings, M.T., 1974. Hydrologic budget of Spring Creek drainage basin, Pennsylvania. Ph.D. Dissertation, The Pennsylvania State University.

Habberjam, G.M., 1975. Apparent resistivity, anisotropy, and strike measurements, *Geophysical Prospecting*, vol. 23, pp. 211-247.

Habberjam, G.M., and Watkins, G.E., 1967. The use of a square configuration in resistivity prospecting, *Geophysical Prospecting*, vol. 15, pp. 221-235.

Habberjam, G.M., 1979. Apparent resistivity observations and theuse of square array techniques. Geoexploration Monographs No. 9. Geopublication Associate, Berlin.

Hiegold, P., Cartwright, G., Reed, P., 1979. Aquifer Transmissivity from Surficial Electrical Methods, Groundwater. v. 17, no. 4, pp. 338-345.

Jones, W.K. & White, W.B., 2012. Karst. In: White, W.B. & Culver, D.C. (Eds) Encyclopedia of Caves. Academic Press, Waltham, Ma, 430–438.

Keller G.V. and Frischknecht F.C. 1966. Electrical Methods in Geophysical Prospecting. Pergamon Press, Inc., Pergamon Press, New York, 523 pp.

Kelly, W. E., 1977. Geoelectric Sounding for Estimating Aquifer Hydraulic Conductivity, Groundwater, Volume 15, Issue 6, p. 420-425.

Konikow, L.F., 1969. Mountain runoff and its relation to precipitation, groundwater and recharge to the carbonate aquifers of Nittany Valley, Pennsylvania: University Park, Pa., The Pennsylvania State University, M.S. thesis, 128 p.

Kosinski, W.K. and Kelly, W.E., 1981. Geoelectric Soundings for Predicting Aquifer Properties. Groundwater, 19, 163-171. https://doi.org/10.1111/j.1745-6584.1981.tb03455.x

Lane 1995, J.W., Haeni, F.P., and Watson, W.M., 1995. Use of a square-array direct current resistivity method to detect fractures in crystalline bedrock in New Hampshire, *Ground Water*, vol. 33, no. 3, 476-485.

Lattman, L.H., and Parizek, R.R., 1964. Relationship between fracture traces and the occurrence of ground water in carbonate rocks, *Journal of Hydrology*, vol. 2, pp. 73-91.

Leonard-Mayer P.J., 1984. A Surface Resistivity Method for Measuring Hydrologic Characteristics of Jointed Formations. Report of Investigations 8901, Bureau of Mines, United States Department of the Interior.

Lieblich, D.A., Lane, J.W., Jr., and Haeni, F.P. 1991. Results of integrated surface-geophysical studies for shallow subsurface fracture detection at three New Hampshire sites, in Expanded Abstracts with Biographies. SEG 61st Annual International Meeting. Houston, Texas. November 10-14, 1991. Houston, Texas. Society of Exploration Geophysicists. pp. 553-556.

Parise, M., Gabrovsek, F., Kaufmann, G., and Ravbar, N., 2018. Recent advances in karst research: from theory to fieldwork and applications, General Assembly of the European Geosciences Union.

Mallik, S.B., Bhattacharya, D.C., and Nag, S.K. 1983. Behaviour of fractures in hard rocks--A study by surface geology and radial VES method. Geoexploration. v. 21, pp. 181-189.

Matias, M.J.S., and Habberjam, G.M., 1984. A field example of the use of anisostropy parameters derived from resistivity soundings, *Geophysical Prospecting*, vol. 32, 725-739, pp. 725-739.

Matias, M.J.S., 2002. Square array anisotropy measurements and resistivity sounding interpretation, *Journal of Applied Geophysics*, vol. 49, pp. 185-194.

McGrath, R., Styles, P., Thomas, E., 2002. Integrated high-resolution geophysical investigations as potential tools for water resource investigations in karst terrain, Env. Geol. 42:552. https://doi.org/10.1007/s00254-001-0519-2.

Moreira, S.S., Bacellar, L.A.P., Aranha, P.R.A, 2019. A comparative evaluation of vertical fractures using different azimuthal electrical resistivity survey arrays, *Near Surface Geophysics*, Volume 17, Issue 4.

Niwas, S., Singhal, D.C., 1981. Estimation of aquifer transmissivity from Dar-Zarrouk parameters in porous media, Journal of Hydrology, Elsevier.

Parizek, R.R., White, W.B., and Langmuir, D., 1971. Hydrogeology and Geochemistry of Folded and faulted carbonate rocks of the central Appalachian type and related land use problems: Pennsylvania State University Circular 82.

Revil, A., and L.M.I. Cathles. 1999. Permeability of shaly sands, Water Resources Research 35, no. 3: 651–662.

Reynolds, J.M., 1997. An Introduction to Applied and Environmental Geophysics, 2nd Edition, Wiley Publishing.

Ritzi R.W. Jr and Andolsek R.H. 1992. Relation between anisotropic transmissivity and azimuthal resistivity surveys in shallow, fractured, carbonate flow systems. Ground Water 30, 774-780.

Roth, M.J.S., Mackey J.R., Mackey, C., and Nyquist, J.E., 2002. A case study of the reliability of multi-electrode earth resistivity testing for geotechnical investigations in karst terrains Engineering Geology, Volume 65, Issues 2–3, Pages 225-232.

Sehli, A. S., 1990. Contribution of electrical prospecting to the geophysical study of discontinuous media: International Symposium on Applications of Geophysics to Water Prospecting in Arid and Semi-Arid Areas, UNESCO, Proceedings.

Siddiqui, S.H., and Parizek, R.R., 1971. Hydrogeologic factors influencing well yields in folded and faulted carbonate rocks in central Pennsylvania, Water Resources Research, Vol. 7, No. 5.

Steinich, B., and Marin, L., (1996). Hydrogeological Investigations in Northwestern Yucatan, Mexico, Using Resistivity Surveys, Groundwater, Vol. 34, Issue 4.

Szalai, S., Szarka. L., Prácser, E., Bosch, F., Müller, I., Turberg, P., 2002 Geoelectric mapping of near-surface karstic fractures by using null arrays, Geophysics (2002) 67 (6): 1769-1778.

Szalai, S., Kovács,A., Kuslits, L., Facskó, G., Gribovszki, K.,Kalmár, J. and Szarka, L., 2018. Characterisation of Fractures and Fracture Zones in a Carbonate Aquifer Using Electrical Resistivity Tomography and Pricking Probe Methods. Journal of Geoscience and Environment Protection, 6, 1-21.https://doi.org/10.4236/gep.2018.64001.

Taylor, R.W., and Fleming, A.H., 1988. Characterizing jointed systems by azimuthal resistivity surveys, *Ground Water*, vol. 26, no. 4, pp. 464-474.

Watson K.A. and Barker R.D. 1999. Differentiating anisotropy and lateral effects using azimuthal resistivity offset Wenner soundings. Geophysics 64, 739-745.

White, W.B. 1988. Geomorphology and Hydrology of Karst Terrains. Oxford University Press, New York.

White, W.B. 2002. Karst hydrology: recent developments and open questions. Engineering Geology, 65, 85–105.

Whitman, D., and Yeboah-Forson, A. D., 2015. Electrical resistivity and porosity structure of the upper Biscayne Aquifer in Miami-Dade County, Florida, Journal of Hydrology 531 (2015) 781–791.

Yeboah-Forson, A., D. Whitman, D., 2014. Electrical Resistivity Characterization of Anisotropy in the Biscayne Aquifer, Groundwater 52, no. 5: 728–736.

Chapter 3

Evaluating Shale Bedrock Geo-Electrical Anisotropy at the Susquehanna Shale Hills Critical Zone Observatory Using Square and Wenner Arrays to Optimize Data Inversion and Model Results

Abstract

Geo-electrical anisotropy associated with inclined bedding planes and fractures in bedrock is often not factored into apparent resistivity results, much less data inversion, which can lead to misleading model results. In particular, the "paradox of anisotropy" occurs where resistivity data are collected in areas of inclined bedding planes or fractures where longitudinal apparent resistivity is greater than transverse apparent resistivity, which is opposite of when true resistivity values are considered. This paper evaluates the effects of anisotropy on earth resistivity measurements in a fractured shale bedrock setting at the Susquehanna Shale Hills Critical Zone Observatory (SSHCZO) in central Pennsylvania using square and Wenner arrays. The square array can be used to determine the magnitude and orientation of anisotropy, as it is not subject to the paradox of anisotropy, whereas collinear arrays are, including the Wenner array. This study shows that in fractured shale bedrock, the anisotropy effects can be significant, as is the paradox of anisotropy, which can lead to significant inaccuracies in resistivity models if not factored into the input data. In this study, the square array is used to evaluate site anisotropy at variable depths through the soils and bedrock profile, including fractured, weathered and un-weathered bedrock intervals. The square array's anisotropy coefficient was then factored into apparent resistivity data from strike parallel and perpendicular 2-D Wenner arrays to correct for the paradox of anisotropy. The corrected 2-D resistivity data were then inverted to provide model results, to establish longitudinal resistivity values that are lower than transverse resistivity

values, as would be expected. In addition, a series of ten parallel 2-D Wenner arrays were run and used to create 3-D models of the site's resistivity distribution using anisotropy corrections from the square array data for comparison against 3-D models without this correction. Ultimately, using the square array's coefficients of anisotropy to adjust the input model data resulted in a 3-D resistivity model that provided useful hydrogeologic insights into shallow groundwater interflow at the SSHCZO site that can applied toward future modelling and research efforts. This study demonstrates a useful methodology for correcting collinear resistivity data from the paradox of anisotropy to develop realistic 2-D and 3-D resistivity models that provide hydrogeologic insights in the critical zone.

Introduction

Electrical resistivity surveying methods are commonly utilized to characterize subsurface conditions in fractured bedrock settings to identify depth to bedrock, the presence of voids or fracture zones, or for hydrogeologic investigations including water supply well siting or groundwater remediation projects. These resistivity surveys often use collinear arrays, such as the Wenner, Schlumberger, or dipole-dipole methods to collect apparent resistivity data for inversion into a two-dimensional (2-D) model of the subsurface resistivity distribution within the area of interest.

Bedrock is considered to be isotropic if the value of a physical parameter, such as resistivity or permeability, is the same in all directions and is anisotropic if these parameter values vary with orientation (Anderson, 1999). Characterizing whether bedrock behaves isotropically or anisotropically with respect to electrical resistivity is important for both geophysical and hydrogeological studies. Forms of anisotropy (including resistivity) that can occur in consolidated bedrock materials may develop during sedimentary deposition due to layering of

the bedrock sediments in a preferred direction, especially with platy minerals (Watson and Barker, 1999). Post-depositional anisotropy can occur due to bedrock fracturing, that may be further enhanced by dissolution or weathering. Conducting azimuthal electrical resistivity surveys where inclined bedding planes or fractures occur will likely cause variations in apparent resistivity values with respect to changes in orientation, therefore providing useful insights into the direction of bedrock geo-electrical anisotropy.

The use of azimuthal collinear arrays for comparing differences in resistivity with respect to orientation should be considered in terms of the “paradox of anisotropy”, as originally described by Maillet and Doll (1932) and later named by Keller and Frischknecht (1966). As summarized by Luling (2013), the paradox of anisotropy associated with geo-electrical surveying was first noted after Schlumberger introduced wireline electric logging in 1927 for vertical oil and gas wells, which primarily intercepted horizontal sedimentary formations. The electrical borehole log measurements of this era consisted of injecting a vertically flowing current that was expected to provide a value representative of the vertical conductivity. Conversely, the logs consistently provided readings that approximated the horizontal conductivity, apparently not sensitive to the vertical conductivity, which ultimately became known as the paradox of anisotropy. Maillet and Doll (1932) proved that any vertically-aligned electric measurement where horizontal laminations occur would only be sensitive to the horizontal conductivity, which has been since independently derived by several researchers (van der Pauw, 1961; Wasscher, 1961; Bhattacharya and Patra, 1968; Hagiwara, 1994; Al-Garni and Everett, 2003). This same phenomena occurs when conducting surface electrical resistivity surveys using collinear arrays.

Normally when conducting collinear electrical resistivity surveys, the electrical current will preferentially flow along inclined bedding planes or fractures, especially where these features contain relatively conductive clays and/or fluids, such as groundwater. As a result, the orientation of the minimum true resistivity value is parallel to the bedding planes or fractures and the maximum true resistivity orientation is perpendicular to the bedding planes and fractures. However, when conducting collinear earth resistivity arrays in bedrock with dipping bedding planes or fractures, the orientation of maximum measured apparent resistivity is parallel to the strike of bedrock or the primary fracture sets, while the strike-parallel apparent resistivity is measured by the minor axis of the resistivity ellipse, which is normal to the fracture strike on the ellipse (Keller and Frischknecht, 1966; Bhattacharya and Patra, 1968). This occurrence of the paradox of anisotropy is realized when plotting an azimuthal resistivity ellipse using apparent resistivity data from collinear arrays in bedrock with inclined bedding planes or fractures as shown in Figure 3-1 and explained in more detail in later sections. This study explores the potential for using earth resistivity surveying to quantify anisotropy in shale bedrock at the SSHCZO (Figure 3-2) using the square and Wenner arrays (Figure 3-3). The US National Research Council (2001) defines a critical zone (CZ) from the upper vegetative canopy through groundwater. Critical zone observatories (CZOs) have been created to facilitate multi-disciplinary teams of collaborative researchers (including fields of geology, hydrology, climate science, ecology, soil science, geochemistry, geomorphology, and social science) to quantify current fluxes of solutes, water, energy, gases, and sediments to provide insights into historic and future fluxes (Brantley et al., 2017). The current focus of the SSHCZO is to upscale the current understanding the 0.08 km^2 Shale Hill's catchment basin to a regional scale in the 120 km^2 Shaver's Creek watershed, which includes a wider array of lithologies and landscapes,

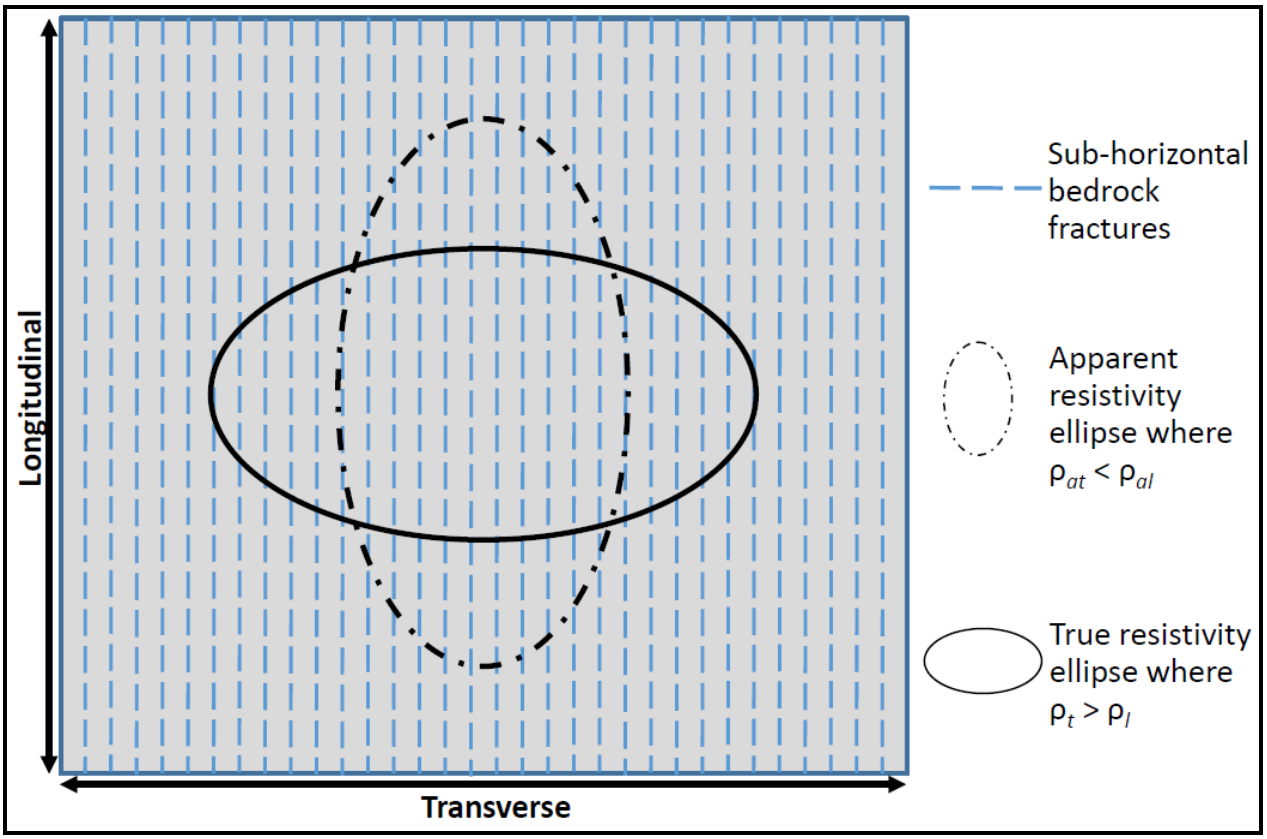

Figure 3-1. **True and apparent resistivity ellipses for collinear arrays in homogeneous, anisotropic fractured bedrock showing the paradox of anisotropy, adapted from Watson and Barker (1999).**

including agriculture, managed forests, and minor development (Brantley et al., 2018). At the SSHCZO, the majority of subsurface water flows laterally to the catchment outlet as interflow through the upper 5 to 8 meters of highly fractured bedrock occurring beneath the hillslope with the remaining water recharging the regional groundwater system (Sullivan et al., 2016). Given the key role that interflow plays in catchment flow and groundwater recharge at the SSHCZO, the square and Wenner resistivity arrays have been applied to characterize the shallow subsurface conditions. The resistivity data was collected to characterize site-specific anisotropy and identify zones of enhanced permeability to provide insights on the subsurface water flow regime, particularly within the interflow zone. Figure 3-4a shows the locations of SSHCZO

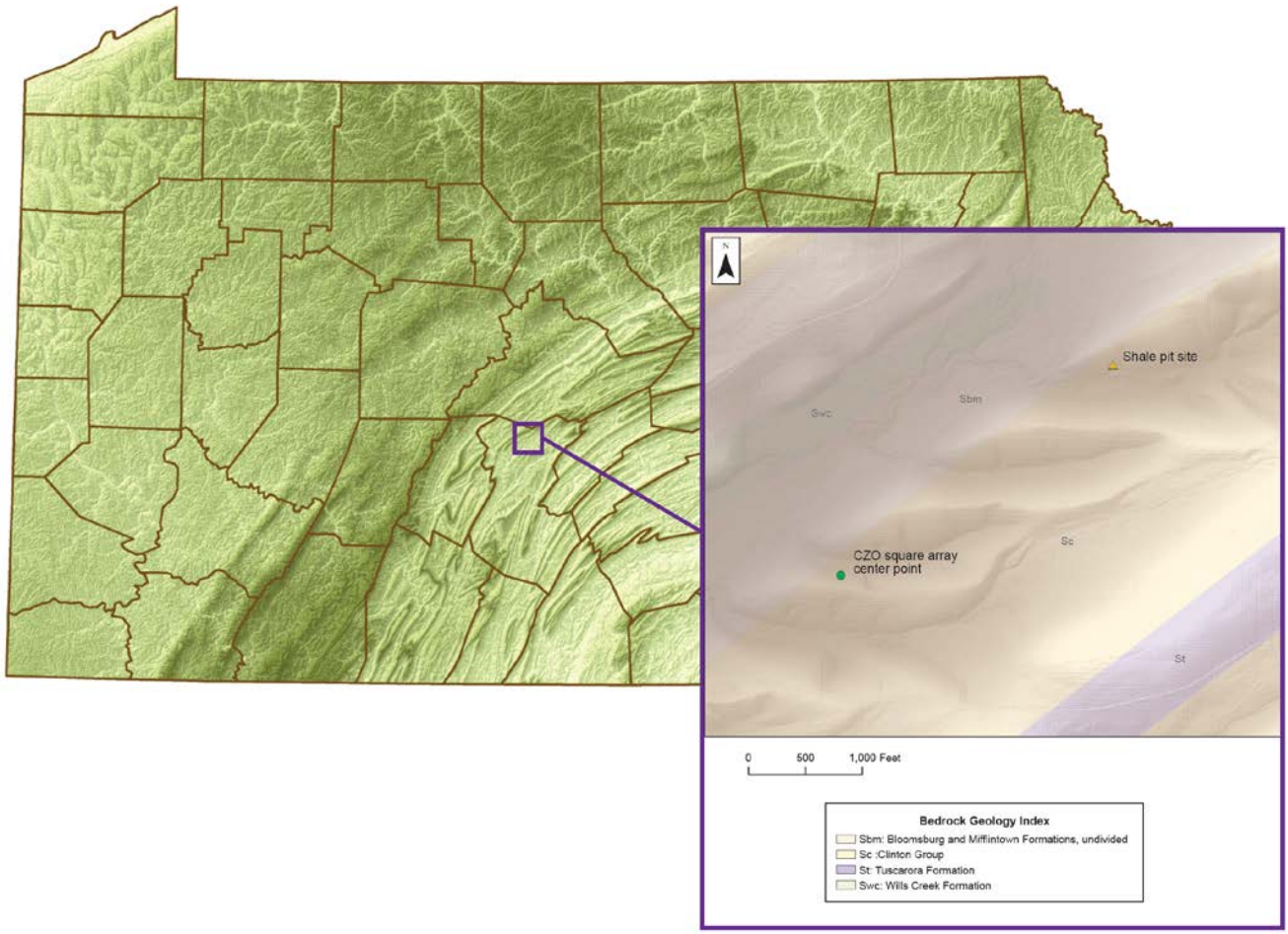

Figure 3-2. Map showing the study area, resistivity data collection area and nearby shale pit outcrop.

groundwater monitoring points and lithologic information while Figure 3-4b shows the catchment's potentiometric surface (upper map), and the lower maps show estimated groundwater ages and seasonal depth of the interflow zone (Sullivan et al., 2016).

The Wenner array at the SSHCZO site was collected at several orientations, including normal and parallel to both bedrock strike and the site's slope, and used to generate 2-D models of the subsurface conditions, including interflow zone geometry. Square array data were also collected

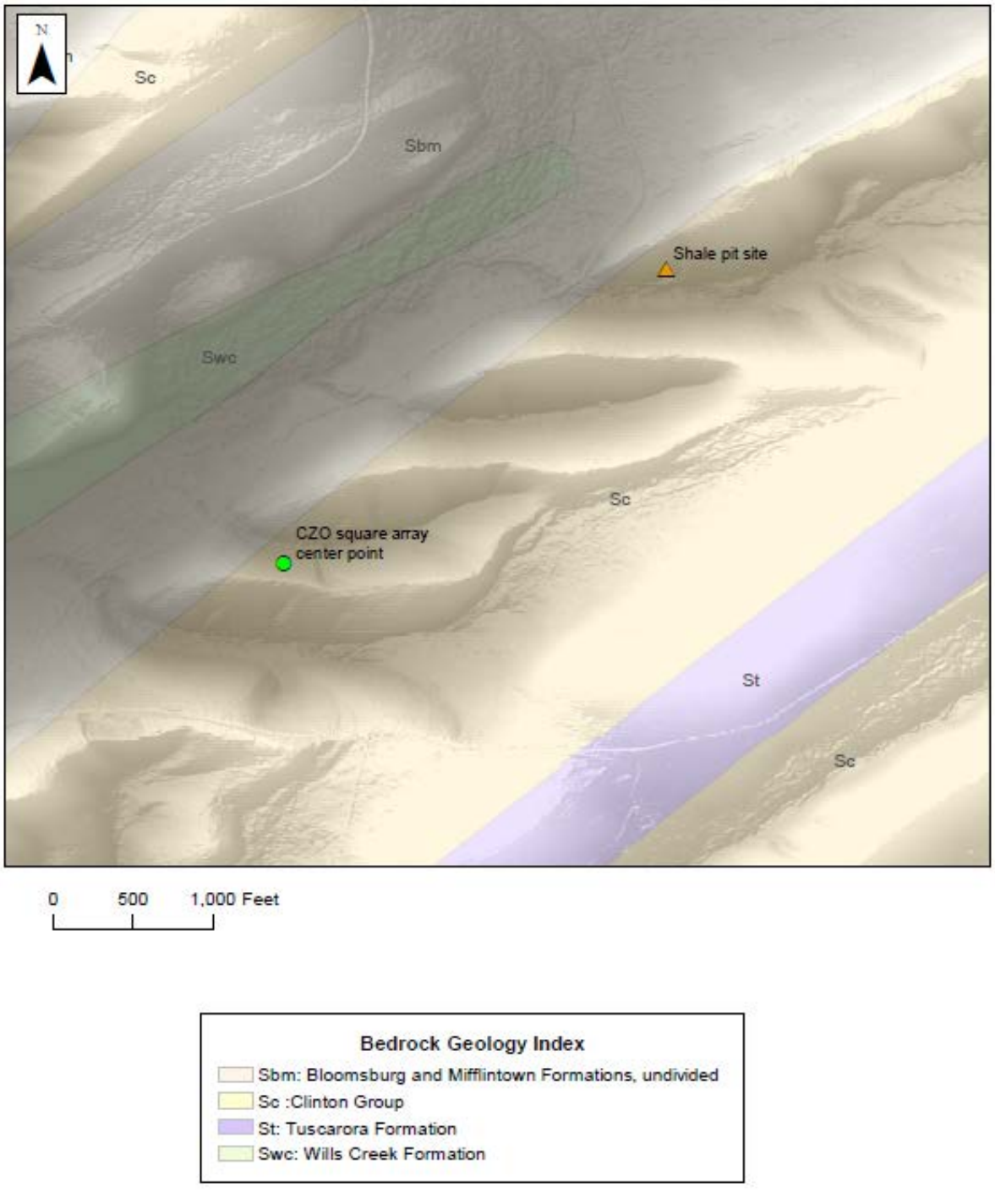

Figure 3-3. Geologic map of the SSHCZO square array site.

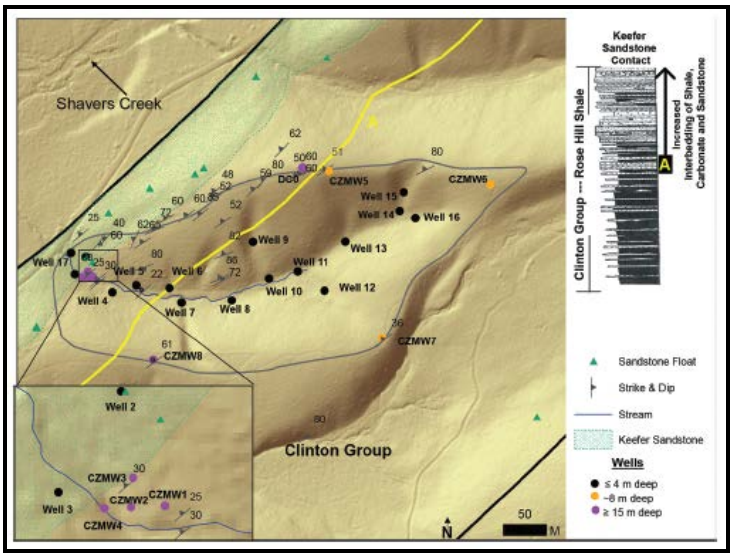

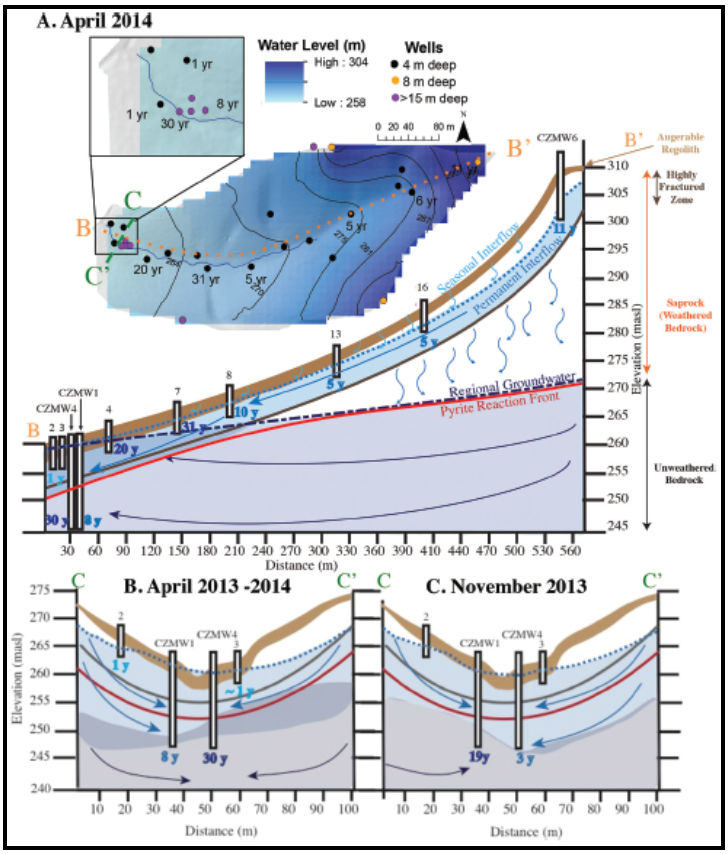

Figure 3-4. Figure 3-4a (upper) shows the locations of SSHCZO groundwater monitoring points and lithologic information while Figure 3-4b (lower) shows the catchment's potentiometric surface, while the lower maps show estimated groundwater ages and seasonal depth of the interflow zone (Sullivan et al., 2016).

in the same area to evaluate the shale bedrock's anisotropy for comparison to the Wenner array data. As already mentioned, the square array is more sensitive to bedrock anisotropy and is not subject to the paradox of anisotropy where inclined bedding planes or fractures exist (Habberjam, 1967). This study shows that the combination of Wenner and square array resistivity data can provide information on the presence and severity of anisotropy, and whether the paradox of anisotropy is significant when estimating apparent resistivity and developing 2-D resistivity models. A final aspect to this work is compilation of a "pseudo" 3-D resistivity model using a series of parallel 2-D arrays to further evaluate the potential for geo-electrical anisotropy and develop more accurate resistivity models.

This study establishes a series of steps to ensure that representative apparent resistivity values are estimated and to correct for the paradox of anisotropy prior to data inversion to develop more realistic 2-D and 3-D models resistivity models. The overall significance of this study is to demonstrate how square array data, which provides estimates of the shale bedrock anisotropy, can be used to resolve the paradox of anisotropy inherent to collinear arrays, and thus provide the foundation for developing realistic 2-D and 3-D resistivity models. These 2-D and 3-D models can then be used by researchers to gain insights into the geometry of interflow and groundwater flow systems in the CZ for further evaluation, including the location of saturated interflow and vertical groundwater recharge zones. Once these features are identified, additional data collections efforts can then be applied to further characterize key aspects of the SSHCZO interflow zone geology, such as the potentiometric surface, hydraulic gradient, flow rates, saturated interval thickness, and horizontal/vertical flow components. The following sections of this study provide a summary of the study area's geologic setting, resistivity survey methodologies, model results, a preliminary interpretation of interflow zone based on the model

results, and finally a discussion about using a variety of resistivity methods for characterizing the geo-electrical properties in a shale bedrock setting.

Background

As described in the previous chapter, earth resistivity surveys are conducted by collecting an array of surface resistance measurements, which are inverted into subsurface apparent resistivity values to aid in characterizing the study area's subsurface geology. Near surface resistivity is related to various geological parameters including soil type, depth to bedrock, lithology, geologic structure, fracture density, fracture orientation, porosity, pore fluid content, degree of pore saturation, and pore fluid conductivity (Keller and Frischknecht, 1966). Bedrock geologic structure including strike, dip, subsurface joints, and fractures collectively influence an aquifer's anisotropy resulting in preferred groundwater and contaminant flow paths. Similar to the influence geologic structure and fracture orientation has on groundwater flow under a hydraulic gradient, these structural features can also control the transmission of an electrical current with an electrical potential, especially where groundwater or clays occur in bedrock fractures.

The use of electrical resistivity methods for estimating aquifer hydraulic properties and using azimuthal collinear arrays for detecting anisotropy related to bedrock fracture orientations in a variety of geologic settings has been summarized in Chapter 2. These relationships are founded on the corollary relationships between Ohm's Law and Darcy's Law that describe electrical current and groundwater flow, respectively, where each follows the path of least resistance from high to low potential (Taylor and Fleming, 1988).

The square array technique was originally developed by as an alternative to conventional Wenner or Schlumberger arrays when dipping subsurface bedding or foliation was present

(Habberjam and Watkins, 1967). The square array has been used in aforementioned studies to characterize metamorphic and sedimentary geologic settings, including carbonate, coal, and shale bedrock. In this study the Wenner and square arrays are applied to characterize the geo-electrical anisotropy in the Rose Hill shale at the SSHCZO to provide hydrogeologic insights of the shallow groundwater flow system, as described in greater detail below.

Apparent resistivity measured parallel to inclined bedding or fractures is termed apparent longitudinal resistivity (ρ_{al}) while earth resistivity data from measurements perpendicular to inclined bedding or fractures is called apparent transverse resistivity (ρa_t) with mean apparent resistivity (ρ_{am}) equaling (Bhattacharya and Patra, 1968):

$$\rho_{am}=(\rho_{al} * \rho_{at})^{1/2} \quad \text{(Equation 1).}$$

This previously described paradox of anisotropy is caused by using the current magnitude to estimate apparent resistivity, while the actual electro-potential differences are measured using the current density (Taylor, et al., 1988). Another way to explain the paradox is that longitudinal true resistivity (ρ_l) is less than transverse true resistivity (ρ_t) and the current density will be greatest along the relatively conductive bedding or fracture planes as compared to across the plane (Bhattacharya and Patra, 1968). As a result, when measuring transverse true resistivity (ρ_t) spanning two potential electrodes across a low resistivity fracture, the current will preferentially flow along the fracture plane due to the relatively conductive clays or groundwater in the fracture, thus the current density will be greatest within the fracture and as a result the potential difference between the electrodes will be relatively low.

Mathematically the apparent resistivity ρ_a (in units of ohm-m) for a Wenner array is calculated by (Bhattacharya and Patra, 1968):

$\rho_a = K*V/I$ (Equation 2)

where

K=2*π*a is the Wenner array geometric factor (meters),

a= spacing between potential electrodes (meters),

V=electric potential difference (volts), and

I=current (amps).

The true resistivity, ρ (in units of ohm-m), is determined by:

$\rho = E/J$ (Equation 3)

where

E=electric field intensity (volts/m)

J=current density (amps/m^2).

2-D collinear arrays are commonly run in the field without consideration of the potential for anisotropic conditions to exist. If measured apparent resistivity values are utilized for geologic site characterization or as input for modeling without consideration of anisotropy effects, then misleading results and interpretations may occur. For example, consider a project involving a series of collinear resistivity arrays with varying orientation at a site with multiple survey locations where contaminated groundwater has a distinctly higher resistivity. Those arrays run parallel to bedrock fractures would show higher longitudinal apparent resistivity values compared to transverse apparent resistivity surveys run normal to the fractures based on the paradox of anisotropy. If the anisotropy effect causes a 20% increase in longitudinal apparent

resistivity and the signature of the groundwater being explored for has resistivity that is 20% greater than background conditions, the strike parallel apparent resistivity may indicate the high-resistivity groundwater is present, when in reality it is not. This type of issue can be avoided by factoring the geo-electrical anisotropy effects into the models and interpretations for more realistic site characterization results.

The square array method's relatively limited use has shown it to be a useful technique for characterizing aquifer characteristics such as anisotropy, secondary porosity, and fracture orientation in crystalline bedrock in New Hampshire (Lane et. al, 1995) and more recently in carbonate bedrock of the Biscayne Aquifer in Florida (Yeboah-Forson and Whitman, 2014; Whitman and Yeboah-Forson, 2015). Habberjam (1972) used the square array to characterize the apparent resistivity and coefficient of anisotropy in Ordovician shales in the Northwest Anglesey area of Great Britain. Beyond Habberjam's early work no peer-reviewed studies were found that uniquely addressed the application of the square array in a shale bedrock setting, nor any studies that examined approaches to correcting for the paradox of anisotropy associated with collinear arrays.

The objectives of comparing square array data to collinear array data at the SSHCZO are to: 1) illustrate the square array's advantages for characterizing the direction(s) of geo-electrical anisotropy in shale bedrock, 2) demonstrate that coefficients of anisotropy obtained from the square array can be applied to collinear arrays to adjust for the paradox of anisotropy to obtain more realistic resistivity values, and 3) adjusted 2-D data can be used to develop "pseudo" 3-D models that provide insights into the hydrogeologic geometry of shallow groundwater flow systems, including interflow and vertical groundwater recharge zones at the SSHCZO .

Geologic Setting

The study area is contained within the SSHCZO in Huntingdon County, Pennsylvania, located within the Valley and Ridge Physiographic Province of the Appalachian Mountains (Figure 3-2). The SSHCZO contains a small (0.08 sq. km.), first-order watershed that flows from east-to-west within the Shaver's Creek drainage. The SSHCZO is underlain by the Silurian-age Clinton Group, composed of the Rose Hill Formation, and the overlying Keefer Sandstone, a prominent 1- to 10-meter thick sandstone, which exists in the subsurface at the outlet of the catchment (Sullivan et. al, 2016). Nearby stratigraphic sections of the Rose Hill Formation exposed in the Shavers Creek and Juniata River watersheds reveal that it is comprised primarily of shale with thin interbeds of limestone and sandstone in the upper half (Flueckinger, 1969; Cotter and Inners, 1986). The Keefer Sandstone underlies the outlet of the SSHCZO catchment (Sullivan et. al, 2016), thus the occurrence of the upper section of the Rose Hill with limestone and sandstone interbeds within the SSHCZO and resistivity survey area is likely (Figure 3-4). The catchment is located on the northwest-dipping limb of a third-order, southwest-plunging anticline in the Broadtop Synclinorium, with bedding and dominant fracture strike at approximately 054° with a minor orthogonal fracture set (Brantley et al., 2018). The bedrock dip at the SSHCZO ranges from 40° to 88° to the northwest based on 58 dip measurements from dug pits and well optical televiewer logs (Sullivan et. al, 2016). As part of this study, bedrock structure field measurements were collected at a nearby shale pit as shown in Figure 3-2 with outcrop pictures in Figure 3-4. Field measurements of bedrock strike at the shale pit ranged from 050° to 057°, with a dip of approximately 58° NW, consistent with the SSHCZO site characteristics. The primary joint set was oriented 320°, orthogonal to bedrock strike, with a near vertical dip of 85° SW and spaced approximately 0.2-0.6 m and 0.3-3 m in length. Bedrock exposed at this location

consisted of olive-gray to red-brown shale, weathering to black in some locations with thin bedding (0.05-0.25 cm). Dyson (1967) described the Clinton Group as brownish-gray to olive-gray shaley claystone, and a thinly-bedded, fine-grained sandstone, with dark red, fine-grained "iron" sandstone also present.

The SSHCZO stratigraphy generally consists of up to one meter of silty to silty clay loam underlain by 5-8 meters of "augerable" highly-fractured weathered bedrock, with weathered bedrock occurring at a depth of approximately 10 meters, and un-weathered bedrock 10 meters below grade (Brantley et al. 2018; Sullivan et. al, 2016). A zone of interflow is thought to occur in the highly-fractured weathered bedrock (Appendix B), with regional groundwater mapped to occur near the top of unweathered bedrock and generally flows westward toward the drainage outlet (Sullivan et. al, 2016). It has been estimated that more than 90% of the water that enters the SSHCZO catchment infiltrates the soil and highly-fractured upper bedrock and flows down to the valley along preferential flow lines through the upper soil and upper fractured layers with the remaining water recharging the aquifer (Guo et al., 2014; Zhang et. al, 2014; Sullivan et. al, 2016).

Methodology

A series of both square array and Wenner array resistivity measurements were collected over a common tract within the SSHCZO at the locations shown in Figures 3-2 and 3-3 and described below. The data collection and analysis methods for each type of array are discussed in this section.

Square array measurements

As previously described, the square array method consists of using a pair of current electrodes and a pair of potential electrodes positioned at the four corners of a square, with the center point of the square considered as the measuring point (Figure 2-4). The length of a side of a square is considered as the "a-spacing" for the array size. An electric current is sent between the current electrodes, with the line between them corresponding to the resistivity measurement orientation, and the resulting electro-potential field is measured at the potential electrodes as voltage. For each square array a-spacing at a given orientation there are three measurements made, two perpendicular measurements (alpha and beta), and one diagonal measurement (gamma), (Figure 2-5), thus providing the subsurface's apparent resistivity with respect to a 90° change in orientation. The gamma measurement checks the accuracy of the alpha and beta measurements, where in an isotropic aquifer $\rho_\alpha=\rho_\beta$ and in a heterogeneous, anisotropic aquifer $\rho_\gamma= \rho_\alpha-\rho_\beta$. The array is expanded symmetrically around the center point so the sounding can be interpreted with depth, commonly in increments of $A*2^{1/2}$ with a-spacing typically varying from 5 to 50 or more meters (Habberjam and Watkins, 1967), though any a-spacing within practical reason can be used. The array is rotated by a small increment, typically 15°, so that apparent resistivity with sufficient resolution can be collected for interpretation and graphical display.

The apparent resistivity for a square array is calculated using the following equation (Habberjam and Watkins, 1967):

$\rho_a=K*V/I$ (Equation 4)

where

$K=(2*pi*a)/(2-2^{1/2})$ is the square array geometric factor (Equation 5)

a= square-array side length (i.e. a-spacing) in meters,

V=voltage in volts, and

I=current in amps.

A total of four a-spacings were measured at the SSHCZO site (5 meters, 10 meters, 25 meters, and 50 meters), and for each a-spacing the array was rotated at 15° increments until a full rotation of measurements were collected (from 0° to 165°). The field resistance measurements were used to calculate the apparent resistivity with the above equations. The data were then plotted as apparent resistivity versus azimuth in radar plots, as shown in the results section. The

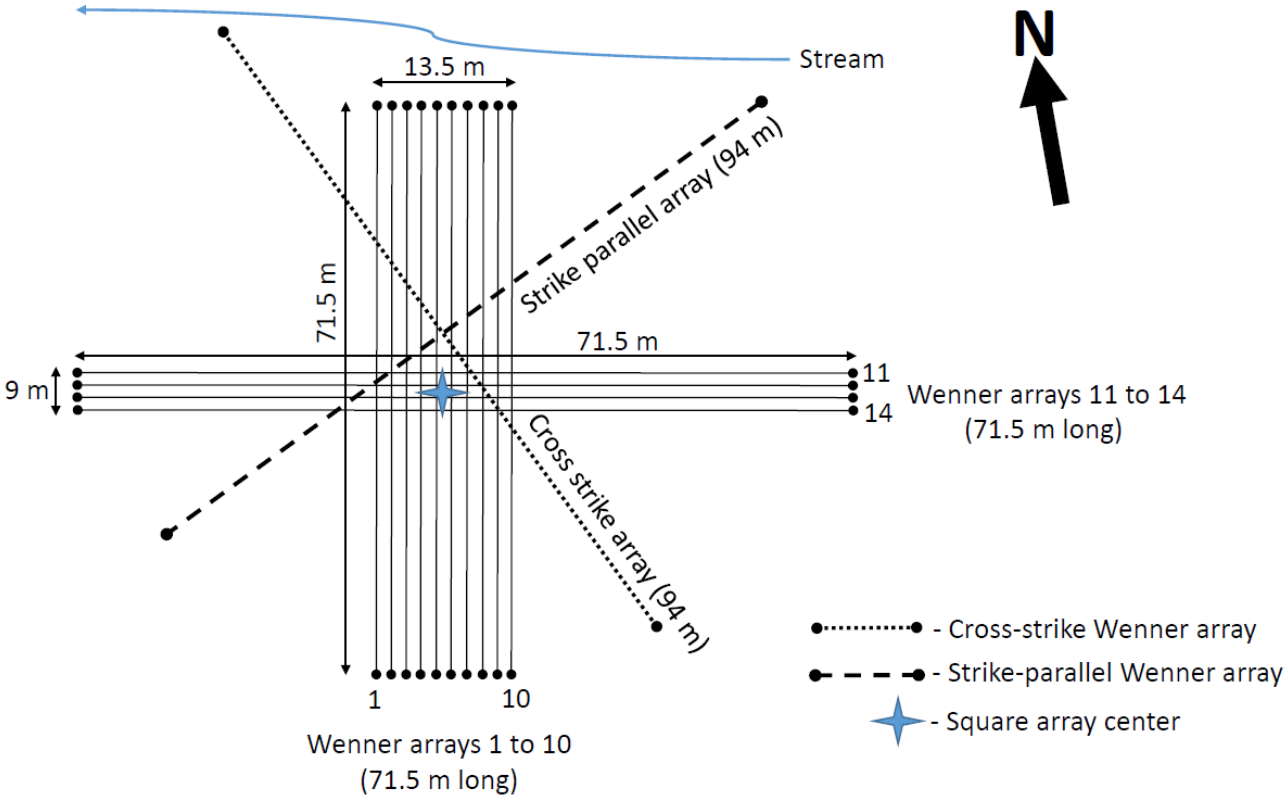

Figure 3-5. Schematic of general layout of square and Wenner arrays at SSHCZO.

Figure 3-6. **Shale outcrop near study area looking north along a joint (upper photo) with close up of shale (bottom photo) with a joint running left to right just above the compass and bedding running top to bottom along photo.**

maximum apparent resistivity is considered to be transverse apparent resistivity (ρ_{at}) while the minimum apparent resistivity is considered to be longitudinal apparent resistivity (ρ_{al}), per Habberjam (1972). The coefficient of anisotropy (λ) for each a-spacing of the square arrays was calculated using the following equation (Habberjam, 1972):

$$\lambda = (\rho_{at} / \rho_{al})^{1/2} \qquad \text{(Equation 6)}$$

Two coefficients of anisotropy (λ) were calculated using Equation 6. The transverse apparent resistivity (ρ_{at}) and longitudinal apparent resistivity (ρ_{al}) were used to estimate λ as shown in Equation 6. A second "averaged" square array coefficient of anisotropy for each a-spacing was estimated for both ρ_{at} and ρ_{al} to somewhat constrain the extremities of the apparent resistivity minimum and maximum values. This averaged value for each ρ_{at} and ρ_{al} was calculated by factoring in the apparent resistivity values spaced 15° on either side of the ρ_{at} and ρ_{al} apparent resistivity values. The two coefficients of anisotropy for each a-spacing were plotted, a curve was fit to the data, and the coefficient was interpolated to then estimate apparent resistivity at

varying electrode spacings. In addition, as discussed in Chapter 2, the square array allows estimates of secondary porosity in fractured bedrock aquifers by modifying Taylor's (1984) method developed for collinear arrays in saturated, clay-free, non-shale rocks. To calculate secondary porosity, it is first necessary to calculate the anisotropy (N) from the square array field data, using Habberjam's method (1975) where:

$$N = [(T + S)/(T - S)]^{1/2} \quad \text{(Equation 7)}$$

where

$$T = A\text{-}2 + B\text{-}2 + C\text{-}2 + D\text{-}2; \quad \text{(Equation 8)}$$

$$S = 2[(A\text{-}2 - B\text{-}2)^2 + (D\text{-}2 - C\text{-}2)2]^{½}; \quad \text{(Equation 9)}$$

and A, B, C, and D are defined as

$$A = [(\rho_{a3} + 3\rho_{a1})/2 + (\rho_{a4} + r_{a2})/(2)^{½}][(2 + (2)^{½}]; \quad \text{(Equation 10)}$$

$$B = [(\rho_{a1} + 3\rho_{a3})/2 + (\rho_{a2} + \rho_{a4})/(2)^{½}][(2 + (2)^{½}]; \quad \text{(Equation 11)}$$

$$C = [(\rho_{a4} + 3\rho_{a2})/2 + (\rho_{a1} + \rho_{a3})/(2)^{½}][(2 + (2)^{½}]; \quad \text{(Equation 12)}$$

$$D = [(\rho_{a2} + 3\rho_{a4})/2 + (\rho_{a3} + \rho_{a1})/(2)^{½}][(2 + (2)^{½}]. \quad \text{(Equation 13)}$$

The secondary porosity (Φ) is then estimated by:

$$\Phi=[3.41*10^4*(N-1)*(N^2-1)]/[N^2*C*(\rho_{max}- \rho_{min})] \quad \text{(Equation 14)}$$

where:

ρ_{max} = maximum square-array apparent resistivity for given a-spacing;

ρ_{max} = minimum square array apparent resistivity for a given a-spacing; and

C = specific conductance of groundwater in microsiemens per centimeter.

Collinear Resistivity Measurements

A total of fourteen Wenner arrays were collected using a Syscal Pro resistivity meter at the SSHCZO site during August 2018. Ten of these arrays were run along the topographic slope (at an orientation of 010°) centered at location shown in Figure 3-5, with an electrode spacing of 1.5 meters, a total of 48 electrode takeouts, and each array spaced 1.5 meters apart in parallel. Four additional collinear arrays were run along grade (at an orientation of 100°), with the same 1.5-meter electrode spacing and each line being 3 meters apart in parallel. The 10 x 4 array grid overlapped from the square array center point outward, thus allowing some crossover of data for comparison of resistivity values from lines run normal to each other and the square array. The parallel 2-D Wenner arrays enabled the creation of a "pseudo" 3-D resistivity model as described below.

In addition, bedrock strike-parallel and cross-strike resistivity surveys using the Wenner array were conducted to determine the subsurface characteristics of the shale at these two orientations. These arrays were run with an electrode spacing of 2 meters and a total of 48 electrode takeouts using a Syscal Pro resistivity meter during June 2019. These arrays were designed to cross over at their center points which then provided an opportunity to estimate geo-electrical anisotropy based on a comparison of resistivity values at orthogonal orientations where the arrays shared this common crossover point. The raw field resistance data were extracted from each array at the center points for each electrode spacing, which provided resistance measurements at varying depths from each array at the center point. The crossover point resistivity data from the two orthogonal arrays allowed a comparison of apparent resistivity values at different electrode spacings, and associated estimations of the coefficient of anisotropy λ for the Wenner arrays using the following equation (Taylor and Fleming, 1988):

$\lambda = (\rho_{at} / \rho_{al})$ (Equation 15).

2-D and 3-D Resistivity Modeling

The collinear resistivity array data were modelled using an inversion algorithm to obtain estimates the subsurface resistivity values. The RES2DINV software program was utilized to invert each of the individual collinear arrays, while RES3DINV was used to collate the 2-D arrays into a "pseudo" 3-D earth resistivity model. For both programs, a finite-difference or finite-element modeling subroutine was used to calculate the apparent resistivity values, and a non-linear smoothness-constrained least-squares optimization technique was used to estimate the resistivity of the model blocks (deGroot-Hedlin and Constable, 1990; Loke et al., 2003). Where sloping topography is present, as it is here, the program used a distorted finite-element grid so that the surface of the grid matched the topography (Loke, 2000).

Results

The results of square array, 2-D collinear arrays, and 3-D modelling efforts are presented below.

Square Array

Figure 3-7 shows the apparent resistivity values versus azimuth as radar plots using the square array data, which plot as ellipses for each a-spacing. Based on the square array results for each a-spacing, there is an apparent resistivity minima for each a-spacing between 045° to 060°, which brackets the site's bedrock strike of 054°, with the maxima oriented normal to strike. Table 3-1 summarizes the apparent resistivity data values for each a-spacing, provides the minimum, maximum and mean values, along with the calculated coefficient of anisotropy and "averaged" coefficient of anisotropy. The range of resistivity values is 72-584 ohm-m and mean resistivity ranges from 236-322 ohm-m, which are consistent with those of consolidated shale,

having a relatively wide range of approximately 20-2,000 ohm-m (Reynolds, 1997). As shown in Figure 3-8, the square array anisotropy coefficients increase with a-spacing length from 1.65 for the 5-meter spacing, to 2.61 for the 50-meter a-spacing, with the averaged square array anisotropy coefficients also increasing from 1.46 to 1.95, respectively. The increasing anisotropy trend indicates that as the current penetrates deeper through the soil to the shale bedrock, the bedding planes and fractures create increased anisotropy. Figure 3-8 also provides a best fit logarithmic curve to the data. The range of anisotropy coefficients is relatively high at the site for the larger a-spacings, where typical coefficients are less than 2, however coefficients can be greater than 7 in certain settings (Frischknecht and Keller, 1966). In this case, the high anisotropy may be related to a combination of saturated shale bedding planes and strike parallel fracture sets significantly decreasing the resistivity along strike thus increasing the overall anisotropy.

The secondary porosity was derived from the 10-, 25- and 50-meter a-spacing resistivity values to obtain estimates representative of the saturated bedrock. These secondary porosity estimates are 10.1%, 14.6% and 10.6% for the 10-, 25- and 50-meter a-spacings respectively, with calculations contained in Appendix B.

Wenner Array

Figure 3-9 shows the inversion results of two Wenner arrays run orthogonally to one another both parallel (oriented at 054°) and normal (oriented at 144°) to strike with crossover in the center point of each array. In general the strike parallel model (Figure 3-9a) shows a layer of relatively high resistivity (ranging from ~500 to 1000 ohm-m) in the upper 1-2 meters, which is likely due to relatively dry sandy soils noted at the site (Appendix B). Resistivity values then decrease fairly uniformly and approach 250 ohm-m near the bottom center of the model. The

decreasing resistivity is likely related to increased bedrock saturation where the interflow zone intercepts the water table, which is illustrated in Figure 3-4b. The zone of low resistivity at the

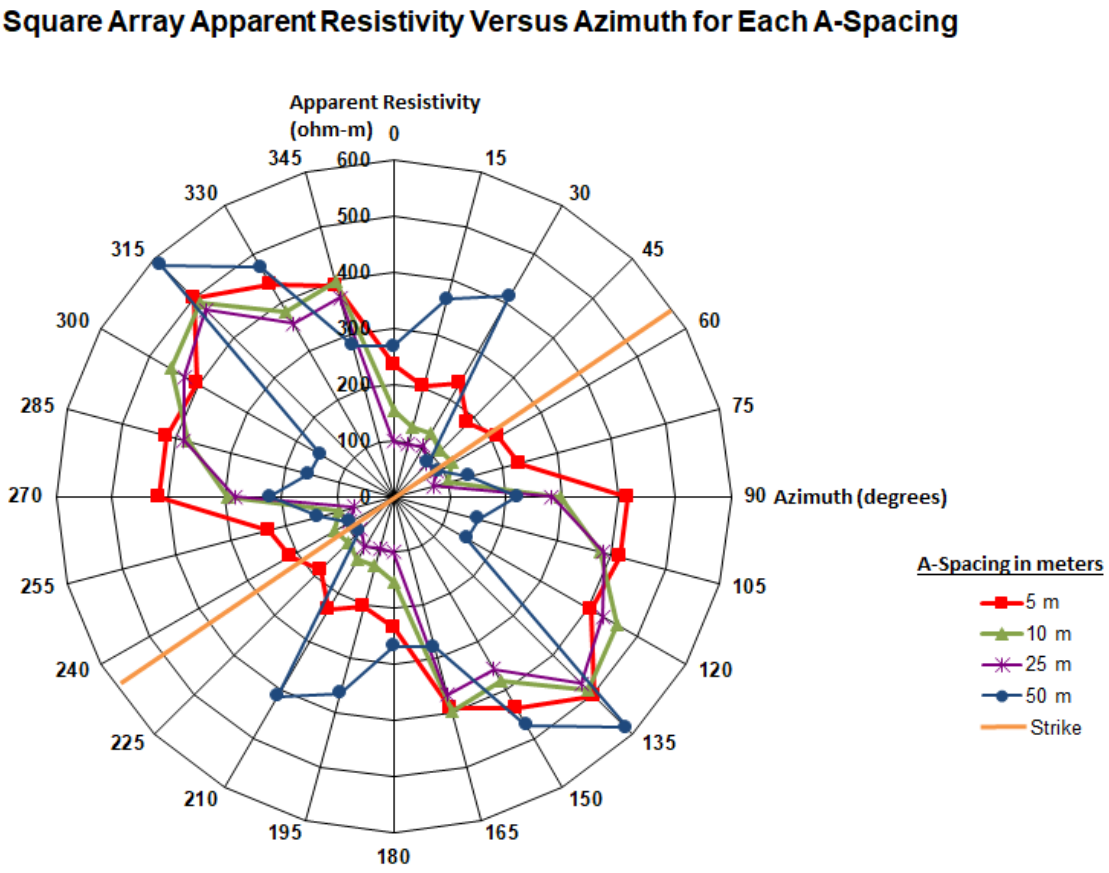

Figure 3-7. SSHCZO site square array resistivity ellipses for each a-spacing.

Table 3-1. Square array apparent resistivity data from the Shale Hills SSHCZO site.

	Azimuth (degrees)/Apparent resistivity (ohm-m)												Statistics			Coefficient of	Avg. Coefficient
(meters)	0	15	30	45	60	75	90	105	120	135	150	165	Min	Max	Mean	Anisotropy	of Anisotropy
5	234	204	232	185	213	230	416	417	404	502	436	390	185	502	322	1.65	1.46
10	154	129	131	116	120	100	296	380	457	488	382	398	100	488	262	2.21	1.90
25	99	96	105	83	88	72	281	386	429	472	356	367	72	472	236	2.55	2.13
50	268	365	413	86	91	139	220	155	150	584	472	279	86	584	268	2.61	1.95

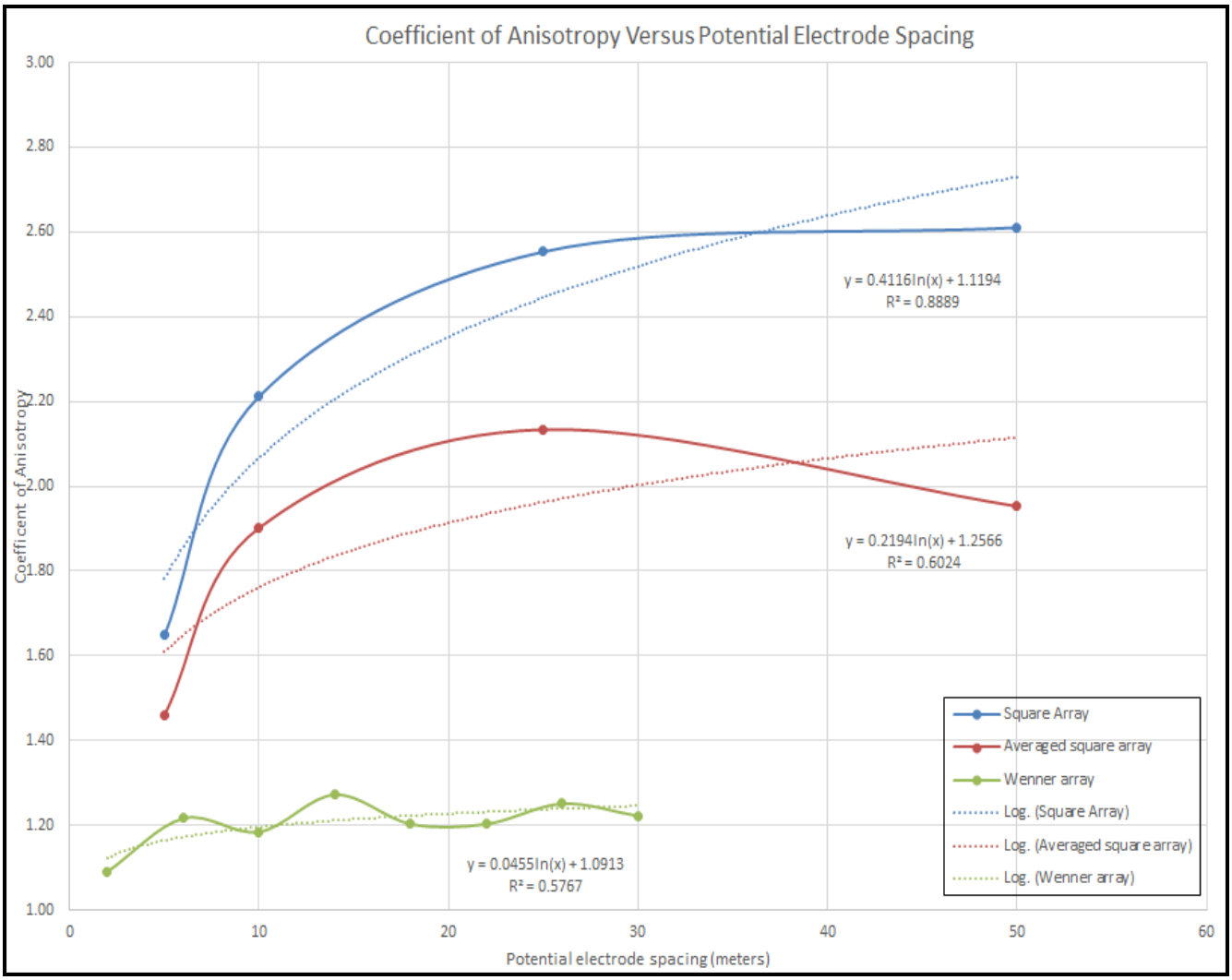

Figure 3-8. Coefficients of anisotropy for square, average square and orthogonal Wenner arrays with logarithmic best fit curves.

NE **SW**

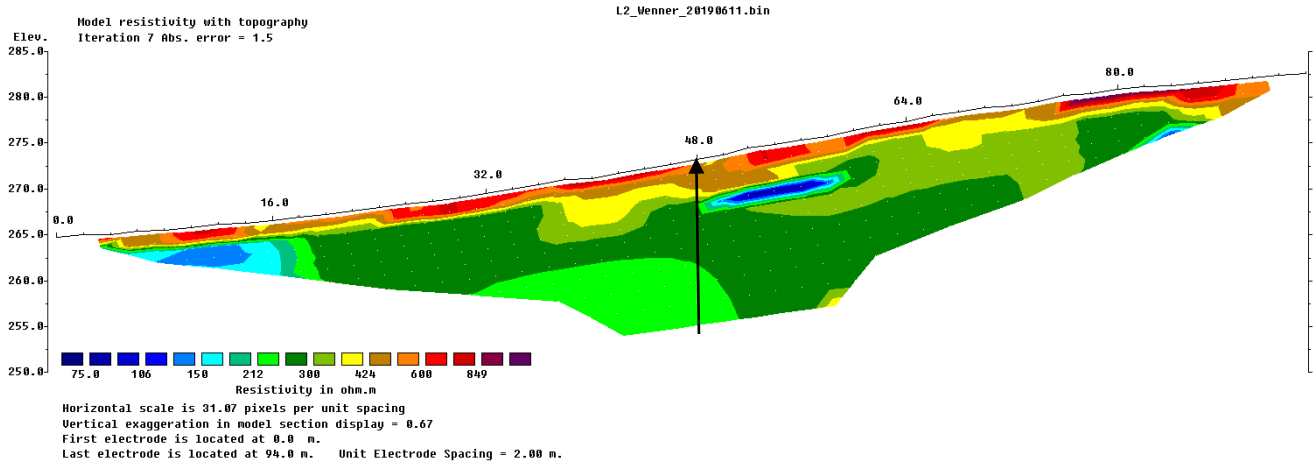

(a) Strike-parallel Wenner array with no anisotropy adjustment (arrow showing array crossover point)

NW **SE**

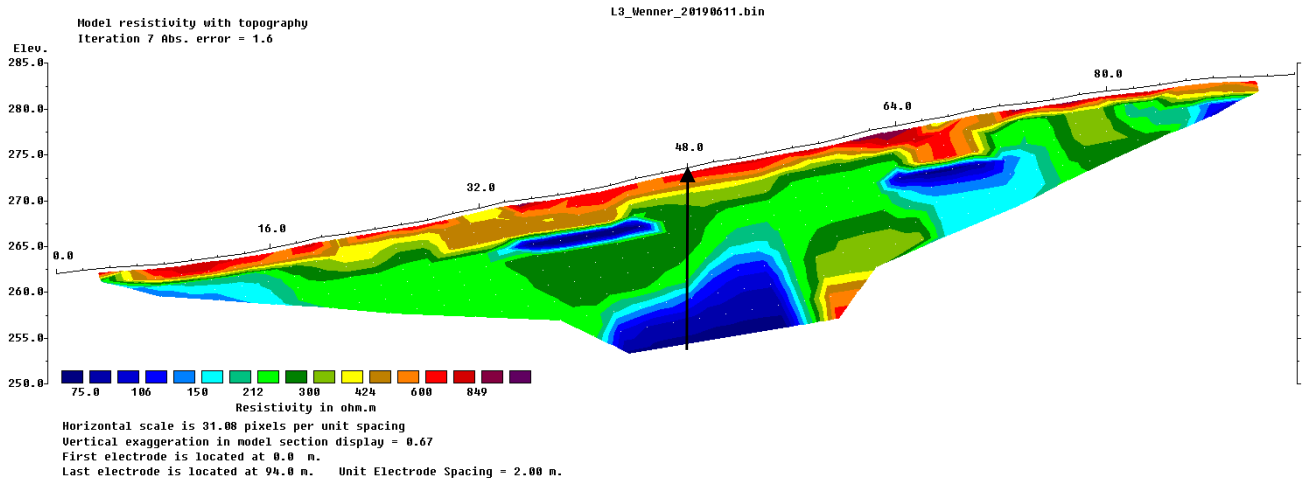

(b) Cross-strike Wenner array with no anisotropy adjustment (arrow showing array crossover point)

Figure 3-9. 2-D Wenner array model results showing resistivity distribution in the subsurface between two orthogonal arrays, with (a) strike parallel and (b) cross-strike orientations.

northeastern edge of the array is due to saturation from the nearby by stream channel. The lens of low resistivity just southwest of the center point at a depth of approximately 5 meters below land surface (mbls) is consistent with perched groundwater within the interflow zone. The cross-strike model (Figure 3-9b) shows a layer of relatively high resistivity (ranging from ~500 to 1000 ohm-m) in the upper several meters, likely due to dry sandier soils. Resistivity values then decrease fairly rapidly with depth in the center of the model, where resistivity values approach 75 ohm-m, particularly toward the northwest, likely due to more saturated conditions where the interflow zone intercepts the water table. Two "lens" of low resistivity occur on either side of the center point in the upper half of the model, which appear to be zones of perched water, consistent with the interflow zone previously discussed. In addition there is a low resistivity zone on the northwestern edge of the model due to the nearby stream. Where these two arrays intersect at their center points, the upper several meters of each model shows relatively high resistivity, from 600 ohm-m near the surface and decreasing to approximately 250 ohm-m near the mid-point of each model. The resistivity values in the lower half of each array begin to diverge significantly, where the cross-strike array has resistivity values decreasing with depth to 75 ohm-m while the strike parallel array maintains a higher resistivity of approximately 225 ohm-meters, a three-fold difference that is consistent with the paradox of anisotropy, but not consistent with expected true resistivity values.

The paradox of anisotropy is also present in the sets of orthogonal collinear arrays used to develop the 3-D model presented later in this paper. The locations of Wenner arrays 5 and 12 are oriented at 010° and 100°, respectively, as shown in Figure 3-5, with a cross-over point coincident with the square array center. The midpoint of the north-south oriented Wenner array has a resistivity value of approximately 250 ohm-m (Figure 3-10a), while the midpoint of the

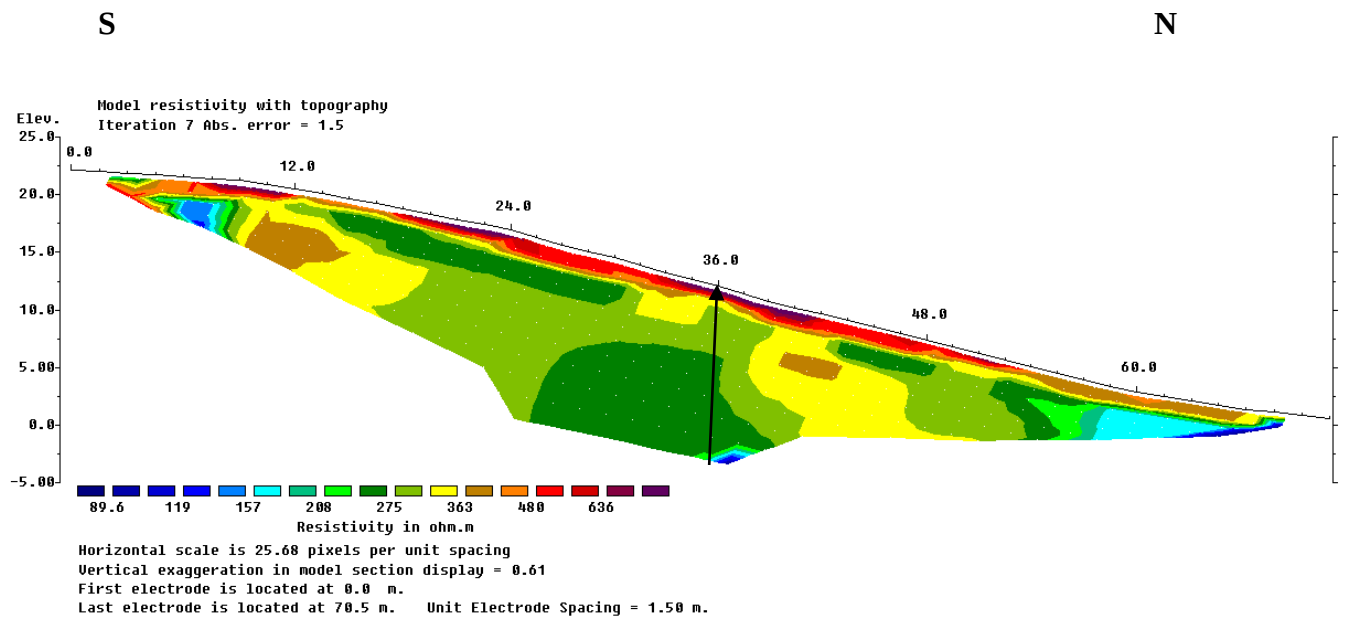

(a) North-south oriented Wenner array with no anisotropy adjustment (arrow showing array crossover point)

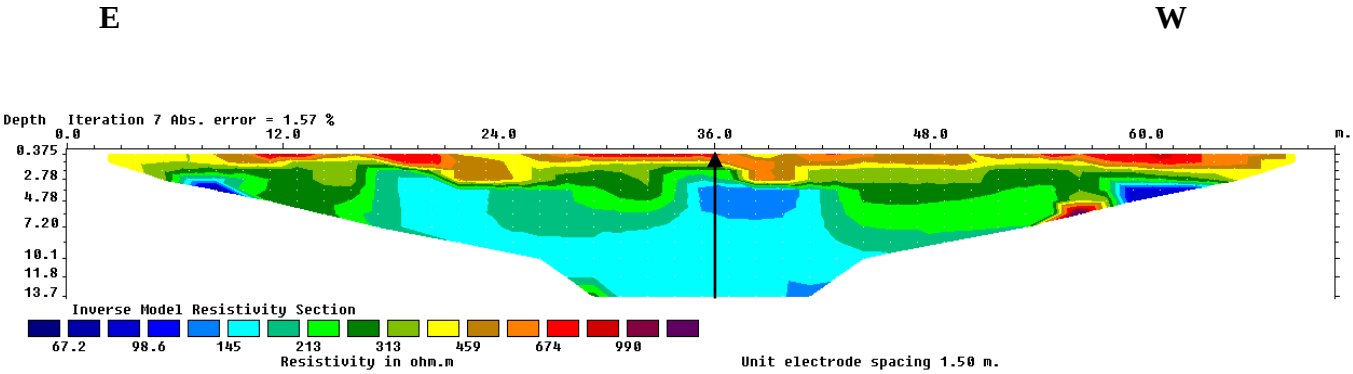

(b) East-west oriented Wenner array with no anisotropy adjustment (arrow showing array crossover point)

Figure 3-10. 2-D Wenner array model results showing resistivity distribution in the subsurface between two orthogonal arrays, with (a) north-south and (b) west-east models with no anisotropy adjustment.

east-west oriented Wenner array has a resistivity value of approximately 150 ohm-m (Figure 3-10b). For comparison, square array's 25-meter a-spacing data in the north-south direction is

lower (99 ohm-m), with higher resistivity (~280 ohm-m) in the east-west direction. Therefore, the paradox of anisotropy is still present where resistivity arrays are oriented orthogonal to one another without regard to bedrock strike, though not as pronounced when compared to arrays run parallel and normal to bedding or fracture strike. In addition, previous resistivity data collected by DeLisser (2016) in the eastern area and current data collection in western area of the SSHCZO indicate the paradox of anisotropy is present in these data sets, and thus appears to be a pervasive phenomena. The results of comparing resistivity values to assess anisotropy between collinear and square arrays at the SSHCZO highlight that the effects are significant and can affect geophysical interpretations unless accounted for in modeling efforts, as presented in the discussion section.

Discussion

The ability to use results from the square array data to correct for the paradox of anisotropy observed in the 2-D Wenner array profiles is addressed here. Following the definition of longitudinal true resistivity (ρ_l) and transverse true resistivity (ρ_t) illustrated in Figure 3-1, the resistivity values at the intersecting (cross-over) point of the strike parallel and perpendicular lines (Figure 3-8) are taken as ρ_t and ρ_l, respectively. That is, in this setting with inclined bedding planes and fractures, the strike parallel array theoretically gives the transverse true resistivity, while the strike perpendicular line gives the longitudinal true resistivity. Therefore, knowing the paradox of anisotropy occurs through the resistivity profile at the cross-over point of these two orthogonal arrays, an effective anisotropy correction applied to the apparent resistivity values from the 2-D Wenner arrays should yield models with ρ_t and ρ_l thus defined.

As discussed above, the square array provides independent values of longitudinal and transverse apparent resistivity that are not subject to the paradox of anisotropy, from which coefficients of

anisotropy can be calculated for each a-spacing. These coefficients have been used to "correct" the original Wenner array resistance measurements, which were used in the RES2DINV code to produce the 2-D Wenner profiles in Figures 3-9 and 3-10. The corrected resistance measurements were then used in the RES2DINV code to generate new "anisotropy corrected" 2D Wenner profiles. Table 3-2 summarizes the results of the corrections to demonstrate the effectiveness of these corrections. Based on the SSHCZO's geologic setting, four intervals have been selected to compare the 2-D model results for assessing the effectiveness of adjusting the original resistance values based on measured anisotropy for data inversion purposes. These four intervals in the models include: 1) soils from 0-1 meters, 2) highly-fractured rock from 1-5 meters, 3) weathered rock from 5-10 meters, and 4) bedrock from 10-15 meters. The approximate range of resistivity values from each of the models along the vertical profile at their cross-over point is summarized in Table 3-2 below.

Table 3-2. Summary of modeled resistivity value ranges with and without anisotropy corrections.

Resistivity model depth interval (m)	No correction resistivity values (1) (ohm-m)		Square array correction resistivity values (ohm-m)		Averaged square array correction resistivity value (ohm-m)	
	Transverse	Longitudinal	Transverse	Longitudinal	Transverse	Longitudinal
0-1 (soils)	600-800	600-800	700-850	300-400	700-850	350-450
1-5 (fractured rock)	250-600	300-600	450-700	150-300	450-700	200-350
5-10 (weathered rock)	150-250	225-300	350-450	100-150	300-450	125-200
10-15 (bedrock)	<150	<225	200-350	<100	175-300	100-125

(1)-Note that the uncorrected transverse and longitudinal values are subject to the paradox of anisotropy, therefore the listed transverse resistivity values are equivalent to longitudinal values and vice versa.

NE **SW**

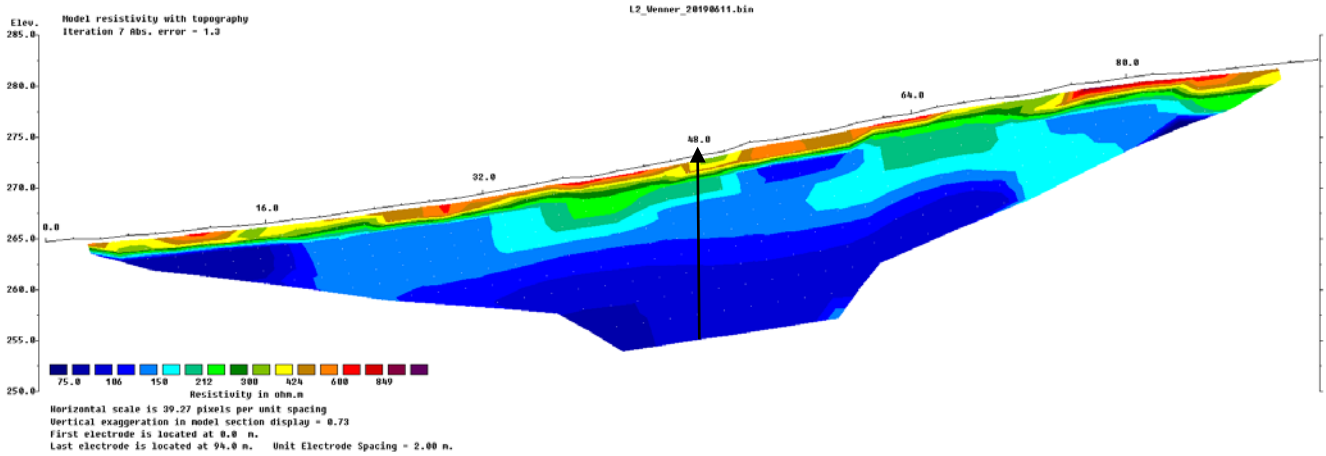

(a) Strike-parallel Wenner array with square array anisotropy adjustment (arrow showing array crossover point)

NW **SE**

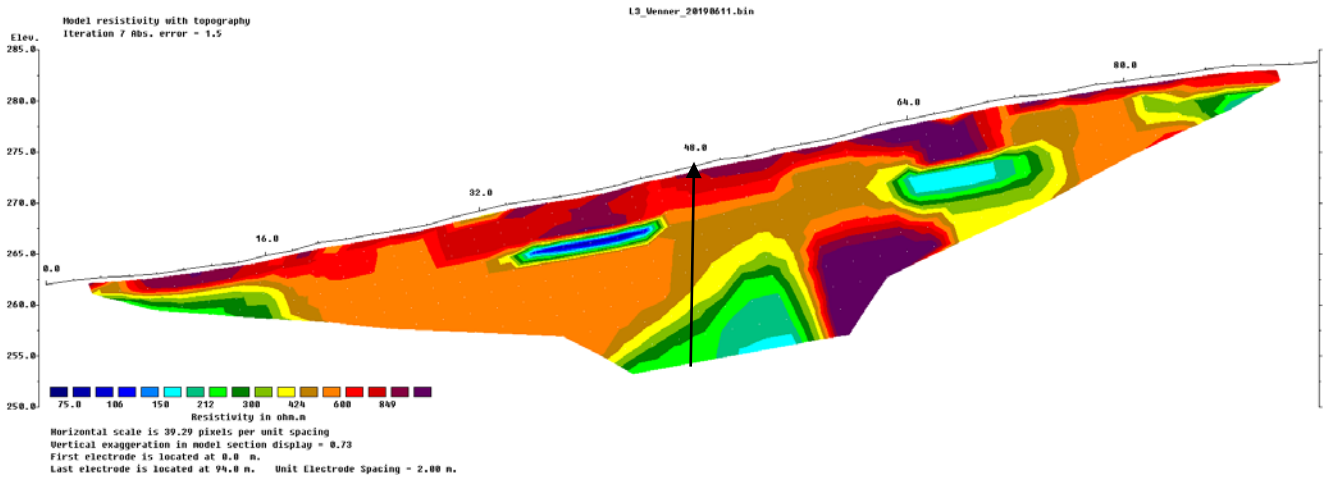

(b) Cross-strike Wenner array with square array anisotropy adjustment (arrow showing array crossover point

Figure 3-11. 2-D Wenner array model results showing resistivity distribution in the subsurface between two orthogonal arrays, with (a) strike-parallel and (b) cross-strike models with square array coefficients of anisotropy adjustment.

NE **SW**

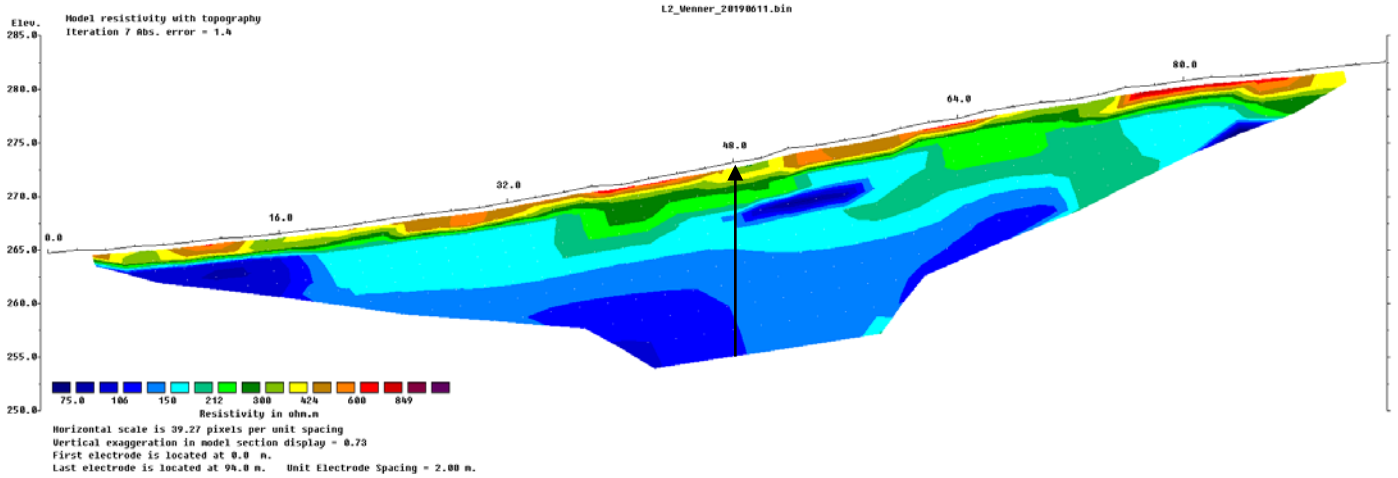

(a) Strike-parallel Wenner array with square array average anisotropy adjustment (arrow showing array crossover point)

NW **SE**

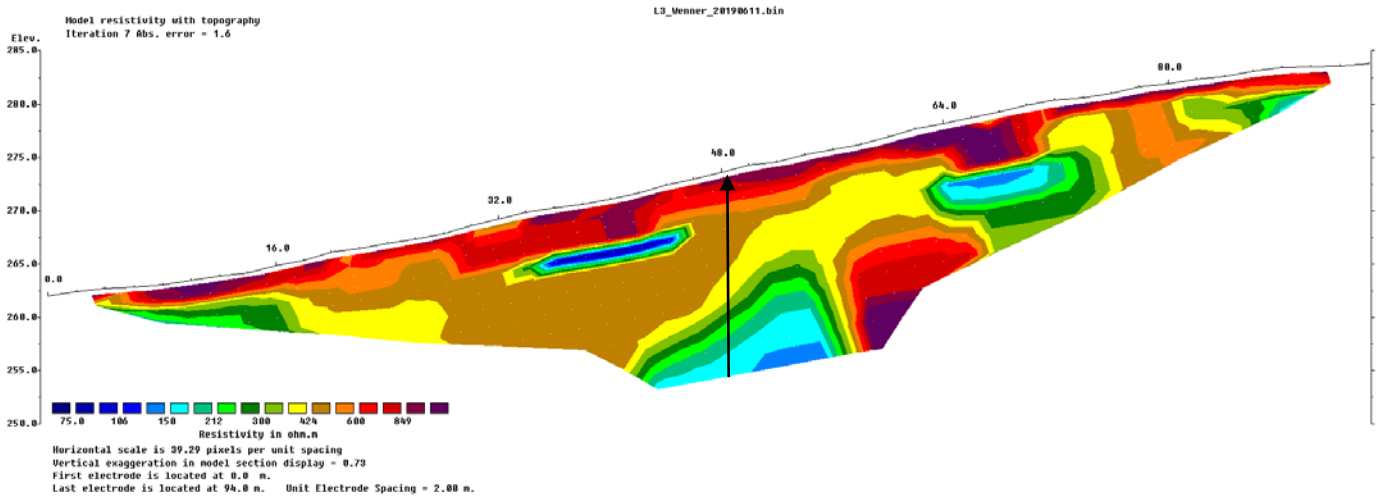

(b) Cross-strike Wenner array with square array average anisotropy adjustment (arrow showing array crossover point)

Figure 3-12. 2-D Wenner array model results showing resistivity distribution in the subsurface between two orthogonal arrays, with (a) strike-parallel and (b) cross-strike models with square array averaged coefficients of anisotropy adjustment.

Figure 3-11 shows the inversion results of the Wenner arrays after using the square array coefficients of anisotropy to correct for anisotropy (see Table 3-1 for data and Figure 3-8 for coefficient of anisotropy versus a-spacing). When comparing resistivity values for each model scenario at their respective cross-over points, the relatively high coefficients appear to cause a large disparity in resistivity values near the soil interval (0-1 m), from approximately 700-850 ohm-m normal to strike (transverse) versus 300-400 ohm-m parallel to strike (longitudinal). This large difference decreases through the highly-fractured rock interval (1-5 m) with resistivity values ranging 450-700 ohm-m (transverse) versus 150-300 ohm-m (longitudinal). The weathered rock interval (5-10 m) shows resistivity values ranging 350-450 ohm-m (transverse) versus 100-150 ohm-m (longitudinal). The bedrock interval (10-15 m) shows resistivity values ranging 200-350 ohm-m (transverse) versus less than 100 ohm-m (longitudinal). These values are representative of the range found in shales (20-2,000 ohm-m per Reynolds, 1997) and provide lower resistivity values parallel to strike in contrast to higher values shown with the uncorrected model.

The averaged square array coefficient of anisotropy values are lower than the coefficient of anisotropy calculated from the square array's longitudinal and transverse apparent resistivity values. Using the averaged square array coefficient of anisotropy values creates "less contrast" in the model resistivity values. When the corrected models are compared to the expected ρ_t and ρ_l values as defined in Figure 3-1 (see last four columns of Table 3-2), both coefficients appear to yield reasonable matches in the resistivity values for the bottom three layers (1-15 m depth), but neither coefficient seems to yield a good match to resistivity values in the soil layer. It should be noted that both corrected cross-strike models in Figures 3-11(b) and 3-12(b), highlight two lenses (near the 32 and 64 meter intervals) of low resistivity that occur within the typical

depth of the interflow zone. Neither model indicates a vertical low-resistivity zone beneath either lens, thus suggesting that water is perched at these locations but is not necessarily recharging groundwater to the deeper aquifer. This may be indicative of insufficient vertical permeability (i.e. fracturing) to allow downward flow.

Figure 3-13 shows the plan view (X-Y) of the 3-D model results compiled from the series of 10 parallel arrays run along slope, at an orientation of 010°. The model reveals decreasing resistivity with depth, with values ranging from 800 to 1,000 ohm-m near the surface (upper 1.6 m), which is fairly consistent with the results from strike parallel and cross-strike models previously discussed, although these resistivity values are the upper end of the near surface resistivity values. The resistivity values generally decrease fairly rapidly below 1.6 meters to between 200-300 ohm-m and stay relatively stable from 2.6 to 8.3 meters, which is within and consistent with the expected resistivity range for the saturated interflow zone. Below 8.3 meters it would appear as though saturated conditions are reached near the center of the model with resistivity values decreasing to approximately 150 ohm-m.

Figure 3-14 shows the plan view (X-Y) of the 3-D model results compiled from the same series of ten parallel arrays that have been corrected for anisotropy. When comparing the apparent resistivity values of cross-grade to grade-parallel Wenner arrays, the paradox of anisotropy still occurs, though as expected it was less severe than with the strike-parallel and cross-strike Wenner arrays. The ten parallel arrays had lower resistivity values that coincided with higher square array resistivity values at a similar orientation and vice versa. Therefore, to correct for the paradox of anisotropy, the resistance values from which the ten parallel arrays were made have been adjusted upward by the “averaged” square array coefficient. This adjustment used the averaged coefficient of anisotropy between the 015° (averaged with apparent resistivity at 000°

S **N**

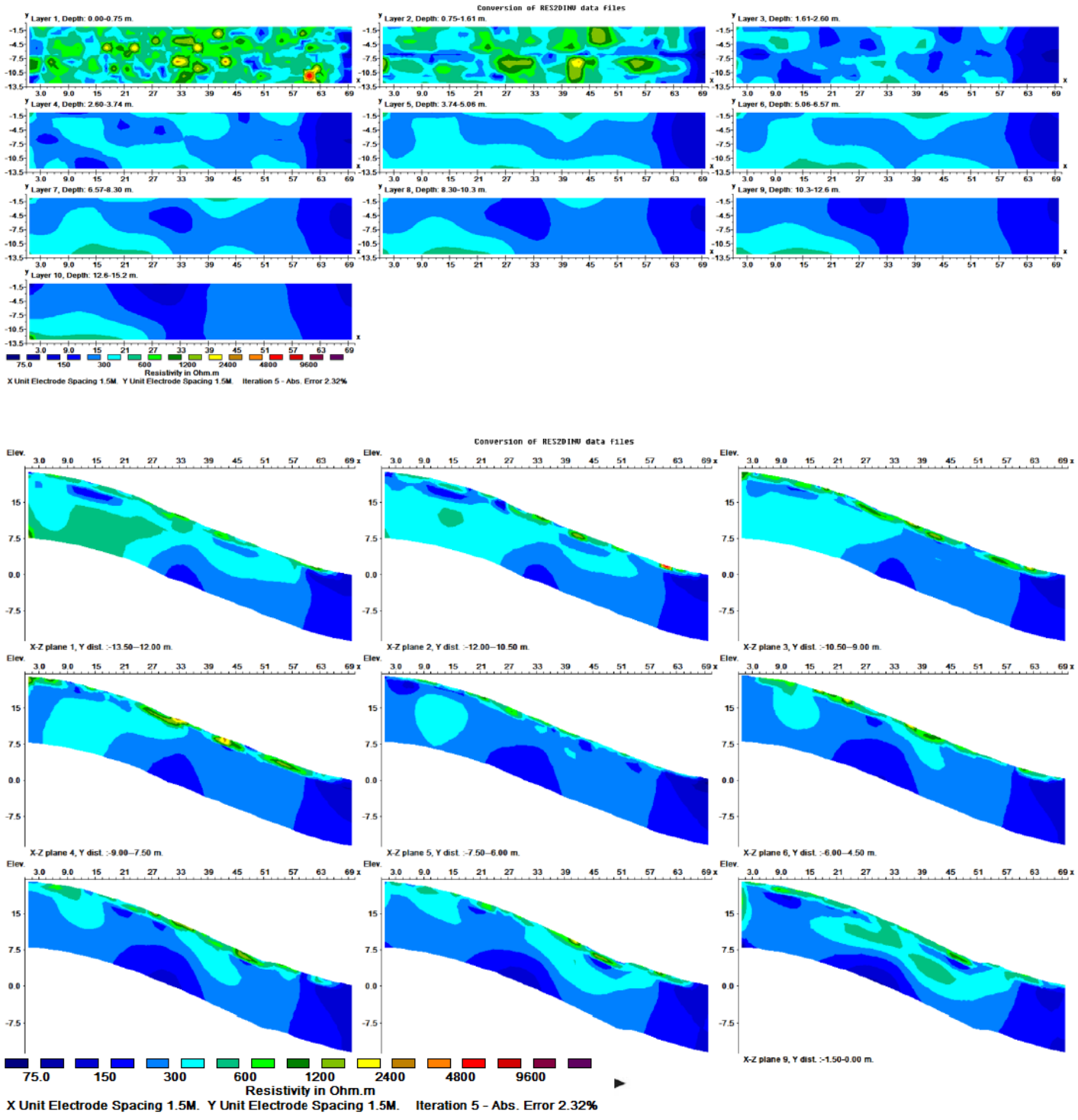

Figure 3-13. Uncorrected 3-D resistivity model showing plan view (upper image) vs cross section view (lower image)

S **N**

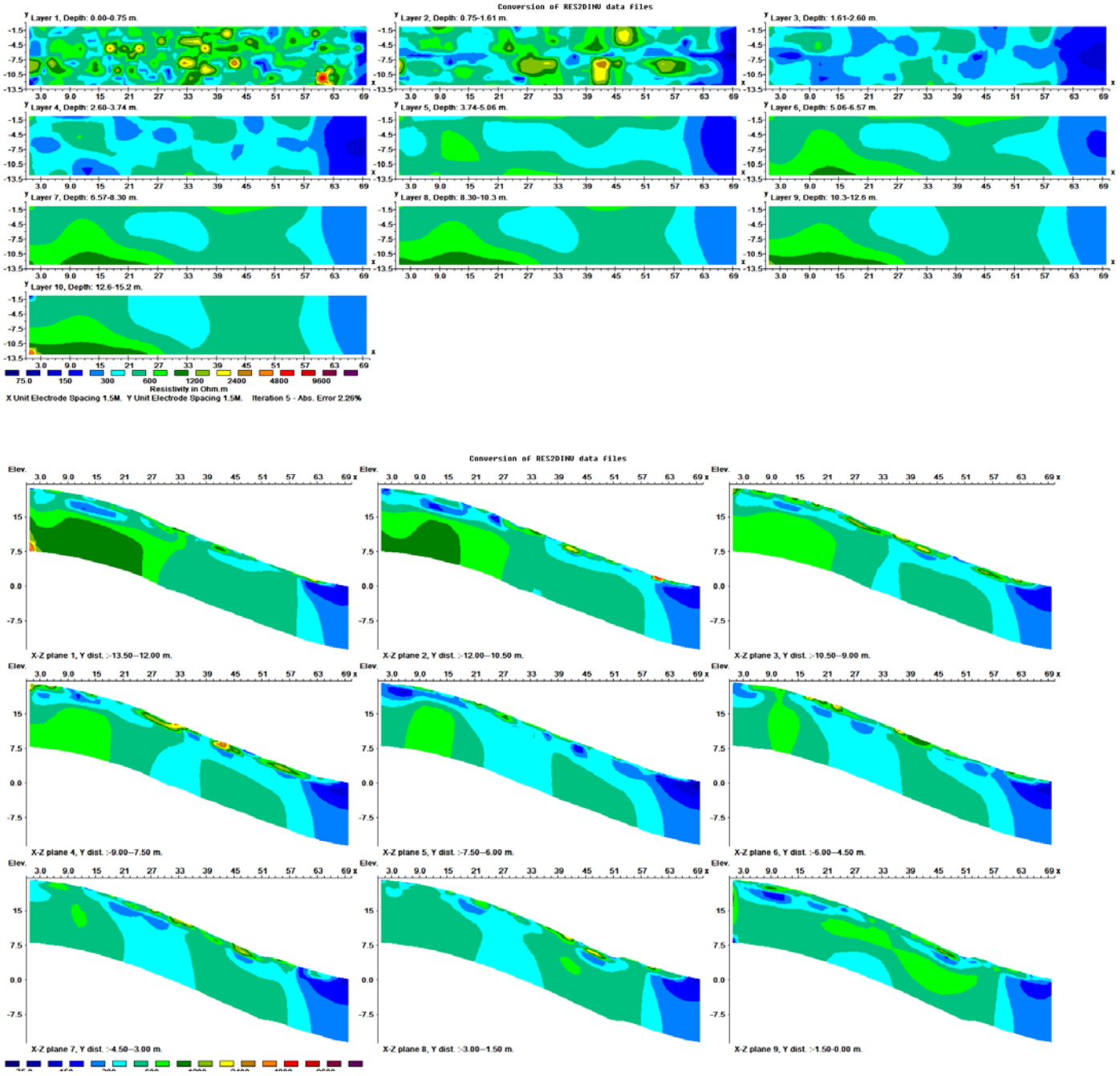

Figure 3-14. Plan view 3-D model corrected for anisotropy showing plan view (upper image) vs cross section (lower image).

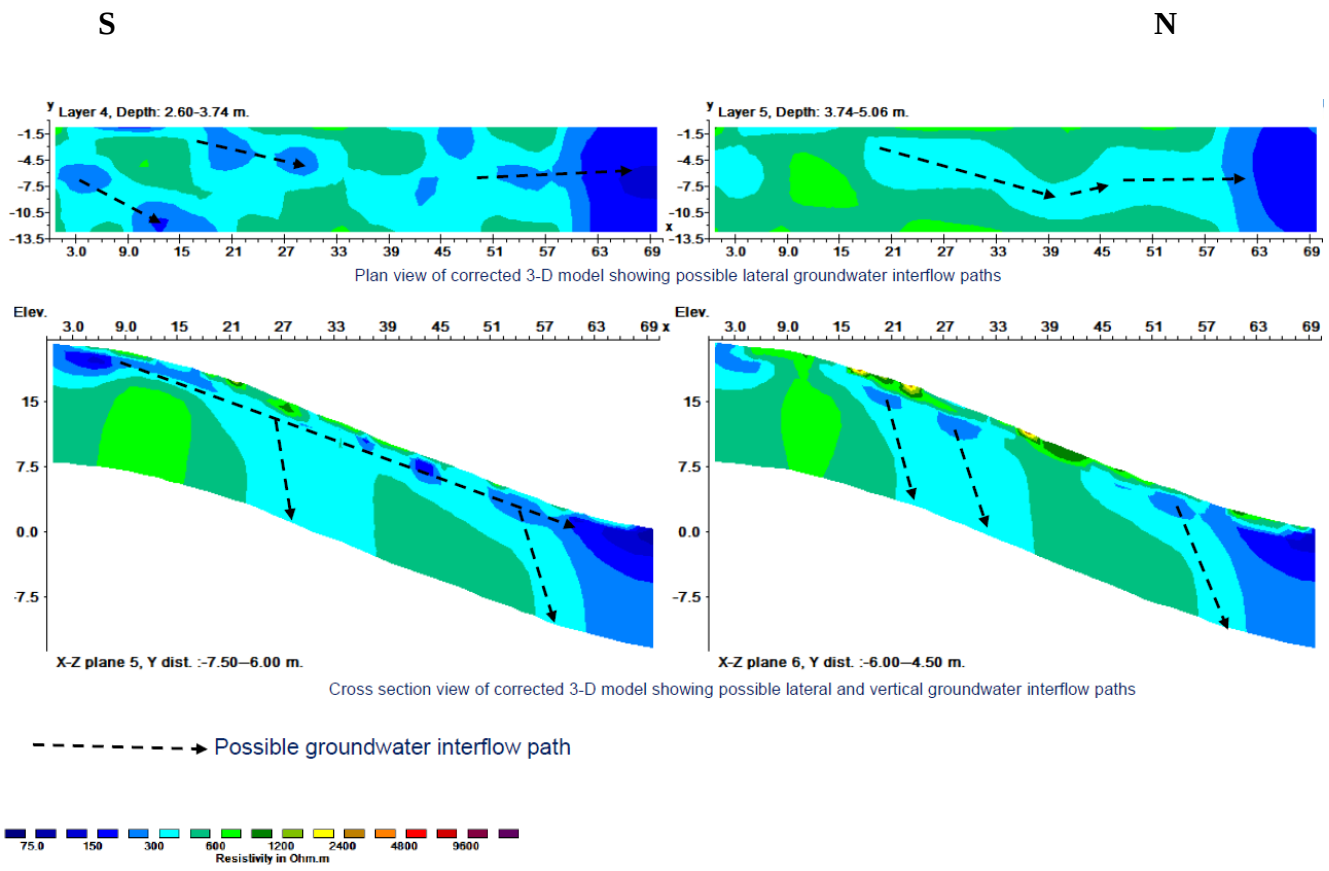

Figure 3-15. Corrected 3-D model slices showing plan view (upper image) and cross-section view (lower image) of potential lateral and vertical groundwater interflow paths with dashed arrows.

and 030°) and 105° (averaged with apparent resistivity at 090° and 120°) square array apparent resistivity values to increase Wenner apparent resistivity values commensurately, which were then collated and inverted using RES3DINV. The revised 3-D model is very similar to the original 3-D model with the pattern of resistivity distribution as shown in Figure 3-13. However, the apparent resistivity values were shifted upward by factors ranging from 1.36 (5-m average coefficient of anisotropy) to 1.91 (25-m averaged coefficient of anisotropy), which is reflected in the data inversion. The adjusted resistivity model values range from 800 to >2,000 ohm-m near the surface (upper 1.6 m) and decrease fairly rapidly below 1.6 meters to between 500-600 ohm-

m to 8.3 meters. Below 8.3 meters, saturated conditions appear to be reached near the center of the model with resistivity values decreasing to approximately 450 ohm-m.

The significance of applying the square-array derived anisotropy correction is illustrated where the corrected 3D resistivity model highlights the preferential flow paths within the interflow zone of the SSHCZO. In the uncorrected model (Figure 3-13), the relatively low resistivity values (300-400 ohm-m) within the interflow zone (~1.5-5 meters), make it challenging to see how the pods of lower resistivity (<200 ohm-m) may connect. However, in the corrected model (Figure 3-14), it is easier to connect the pods of lower resistivity and therefore visualize the flow pathway downslope for water migrating through the interflow layer. Figure 3-14 consists of plan and cross-sectional views from the 3-D model results within the highly-fractured rock interflow zone. Figure 3-15 illustrates how the lower resistivity zones can be connected to define lateral interflow pathways (upper image) potentially draining to vertical flow pathways to the regional groundwater table.

It has been noted that 90% of the water entering the catchment is captured as interflow via the fractured rock zone in the upper 8 meters of the subsurface and that the remaining groundwater is directed toward the regional flow system (Guo et al., 2014; Zhang et al., 2014; Sullivan et al., 2016). No shallow wells exist on the south slope near the resistivity array center to verify the presence, depth or thickness of the interflow zone. However, the resistivity data clearly show a zone of low resistivity that is coincident with the SSHCZO's interpreted depth of the interflow zone between 1.5-5 mbls (Figures 3-14 and 3-15). Within this interval, several localized pods of low resistivity occur (150-250 ohm-m) that coincide with vertical zones of low resistivity, that may feed interflow to the regional groundwater system.

The presence of localized pods of lower resistivity within the interflow zone appear to be a common feature of the SSHCZO based on previous work by Delisser (2018). For example, two Wenner resistivity arrays, Lines 4 and 6, were run approximately northwest/southeast and west/east, respectively, and crossover approximately 150 meters southeast of where the square array was conducted (Appendix B). Based on data inversion results (Appendix B), each model contained multiple low resistivity pods near depths of 1.5 to 5 mbls, similar to Figures 3-11 and 3-12 and were subject to the paradox of anisotropy when comparing square and Wenner array resistivity values. Appendix B contains these original and adjusted Wenner array models using the square array coefficient of anisotropy as a correction factor.

Conceptually, the interflow zone may be partially "under-drained" where strike-parallel vertical fracture zones are encountered, thus providing avenues of vertical groundwater migration from the interflow zone to the regional groundwater table. One possible interpretation is that the vertical fractures form a deeper soil profile locally, which retains some interflow in the clay-rich soil and appear as low resistivity pods. Some of the water retained within the low resistivity pod may flow downward along the vertical fractures. The relative amount of vertical flow compared to interflow may be small given relatively tight fracture aperture and potential for clay sediment to form in and plug the fractures. These fractures would still appear to have relatively low resistivity compared to the surrounding un-fractured, un-saturated rock which is consistent with the resistivity models.

This conceptual model could be verified with properly placed nested piezometers that are monitored to determine the degree of a vertical hydraulic gradient. The piezometers could be installed to monitor three intervals: the interflow zone, the vertical migration zone, and the regional groundwater table to confirm the presence and permanence of enhanced zones of

vertical groundwater recharge from interflow. Monitoring well CZMW8 is located south of the square array center point by a distance of approximately 50 meters (Figure 3-4), with a total depth of 30 mbls, casing to 25.43 mbls, and screened to 30 mbls (Sullivan et al., 2016). Based on available historic depth to water records for monitoring well CZMW8 from 2013-2017 from the SSHCZO website, the depth to water ranged from approximately 17.5-19.5 mbls, indicating the likely depth to the regional water table, which may provide a reasonable location for additional interflow and vertical flow monitoring points.

The secondary porosity values derived from Taylor's (1984) method using the square array data for the 10-, 25- and 50-meter a-spacings were 10.1%, 14.6% and 10.6%, respectively. Bedrock porosity at the SSHCZO has been estimated to be approximately 5-6% based on neutron scanning, however this is primarily due to mineral dissolution (Jin et. al, 2016), and therefore does not represent fracture-related porosity. Based on SSHCZO data from the site's deep well groundwater levels (Well CZMW8) versus stream flow recession, a secondary porosity value of approximately 3% is estimated (see Appendix B) which is significantly less than secondary porosity estimates from the square array data. This may be a realistic figure, however, it does not account for baseflow input via interflow, which is likely significant. Using Taylor's (1984) method to calculate the secondary porosity from the square array data based on Archie's Law (1942) is likely affected by the conductivity of the clays in shale, therefore contributing to the overestimation of the secondary porosity.

Summary and Conclusions

The use of azimuthal resistivity surveys in shale bedrock settings provides useful insights into the degree and orientation of geo-electrical anisotropy, which are often overlooked in 2-D surveys, yet are important factors for ensuring representative resistivity survey and modeling results. In particular the square array, known to be more sensitive to bedrock anisotropy, provides strong correlation between resistivity values and inclined bedding plane and fracture orientation, which are important controls on groundwater flow. Use of the square array to characterize bedrock anisotropy provides key initial insights for investigators to then design 2-D or 3-D resistivity surveys, and ultimately factor anisotropy results into the models. In particular the paradox of anisotropy, which has been demonstrated to occur in the SSHCZO's apparent resistivity results, should be factored into the apparent resistivity values for modeled resistivity results to be realistic.

Square array survey results provide the initial necessary anisotropy orientation based on longitudinal and transverse apparent resistivity that can be used to determine orientations of 2-D or 3-D resistivity surveys. The coefficients of anisotropy from the square array and 2-D arrays can be estimated and then factored into the data inversions to aid in model optimization for interpretation toward further geophysical or hydrogeological investigation. In this case of shale bedrock resistivity surveying it is clear that data inverted without anisotropy corrections leads to models with higher resistivity values parallel to bedrock strike and lower values across strike, which will mislead researchers. Correction of 2-D data using the coefficients of anisotropy estimated from orthogonal collinear arrays (i.e., cross strike and strike parallel) provided reasonable model results which offset the paradox of resistivity, with much of the strike parallel model having lower resistivity values than the cross-strike model. The square array's

coefficients of anisotropy were relatively high, especially at depth where values greater than 2 occurred, however this is not unexpected as the square array is especially sensitive to anisotropy. Using the square array coefficient of anisotropy to correct the 2-D Wenner array data may have somewhat overcompensated for any anisotropy effects, thus both artificially decreasing strike parallel and increasing cross-strike resistivity values. In order to reduce the "overcompensation" of the square array's longitudinal and transverse apparent resistivity values, an averaged square array coefficient of anisotropy was estimated by using resistivity values adjacent to the maximum and minimum values, which appears to provide more realistic model results. The corrected model results using averaged square array coefficients of anisotropy ultimately provide clearer insights into the nature of groundwater flow at the SSHCZO, and thus can aid with future research efforts through optimized monitoring point location selection and construction.

In closing, each site's subsurface conditions will be unique while data inversion results are inherently non-unique. In the case of shale at the SSHCZO it has been demonstrated that anisotropy can be significant and therefore it is prudent to be factored into apparent resistivity values for realistic model output. Though the models provided herein are non-unique, the input data has been optimized to the extent possible to provide better results that are more reflective of true resistivity values in this type of setting. The results of this study demonstrate a useful methodology of establishing geo-electric anisotropy with the square array and orthogonal collinear array results to determine if the paradox of anisotropy exists, and if so, how to adjust the collinear measurements to obtain more accurate models.

The SSHCZO resistivity models provide investigators information on the location and geometry of the pods for further characterization and research on their potential role in the catchment's interflow. The presence of low resistivity pods at depths of approximately 1.5 to 5 mbls at

multiple locations correlates with previous work suggesting a significant volume of interflow in the fractured bedrock interval. The resistivity models provide unique insight on the lenticular geometry of these low resistivity pods, indicating a lateral extent on the order of 10 meters with a thickness of several meters. Given these dimensions, it is feasible the pods are significant components of interflow zones, and as suggested may also correlate with fracture zones allowing some vertical groundwater recharge to the regional system, as shown in the 3-D models. These resistivity models are useful for investigators to further characterize the potential significance these pods have on the SSHCZO's catchment interflow as well as interaction with regional groundwater recharge. This methodology can likely be applied in a variety of geologic settings where anisotropy is expected, and provide useful insights into subsurface conditions for investigators, especially in areas where nearby bedrock outcrops do not exist and/or well control is poor.

References

Al-Garni, M. A., and M. E. Everett, 2003. The paradox of anisotropy in electromagnetic loop-loop responses over a uniaxial half-space: Geophysics, 68, 892–899. doi: 10.1190/1.1581041.

Bhattacharya, P.K., and Patra, H.P., 1968. Direct Current Electric Sounding (Methods in Geochemistry and Geophysics, 9.) 135 p., Elsevier Publishing Co., Amsterdam, London, New York.

Brantley, S.L., W.H. McDowell, W.E. Dietrich, T.S. White, P. Kumar, S.P. Anderson, et al. 2017. Designing a network of critical zone observatories to explore the living skin of the terrestrial Earth. Earth Surf. Dyn. 5:841–860. doi:10.5194/esurf-5-841-2017.

Brantley, S.L., T. White, N. West, J.Z. Williams, B. Forsythe, D. Shapich, J. Kaye, H. Lin,Y. Shi, M. Kaye, E. Herndon, K.J. Davis, Y. He, D. Eissenstat, J. Weitzman, R. DiBiase, L. Li, W. Reed, K. Brubaker, and X. Gu. 2018. Susquehanna Shale Hills Critical Zone Observatory: Shale Hills in the context of Shaver's Creek watershed. Vadose Zone J. 17:180092. doi:10.2136/vzj2018.04.0092

Cotter, E., and J.D. Inners. 1986. Silurian stratigraphy and sedimentology in the Huntingdon County area. In: W. Sevon, editor, 51st Annual Field Conference of Pennsylvania Geologists, Juniata College, PA. Dept. of Environmental Resources, Bureau of Topographic and Geological Surveys, Harrisburg. p. 27–39,154–170.

Delisser, T., 2018. Analysis of the Subsurface Structure of Swales in the Shale Hills Catchment Using Electrical Resistivity Tomography, Senior Thesis in Geosciences, The Pennsylvania State University.

Flueckinger, L. A., 1969, Geology of a portion of the Allensville Quadrangle, Centre and Huntingdon Counties, Pennsylvania: Pennsylvania Geological Survey, 4th Series, Progress

Habberjam, G.M., and Watkins, G.E., 1967, The use of a square configuration in resistivity prospecting, *Geophysical Prospecting*, vol. 15, pp. 221-235.

Habberjam, G.M., 1975, Apparent resistivity, anisotropy, and strike measurements, *Geophysical Prospecting*, vol. 23, pp. 211-247.

Habberjam, G.M., 1979. Apparent resistivity observations and theuse of square array techniques. Geoexploration Monographs No. 9. Geopublication Associate, Berlin.

Hagiwara, T., 1996, Em log response to anisotropic resistivity in thinly laminated formations with emphasis on 2-mhz resistivity devices: SPE Formation Evaluation, 211–217.

Jin, L., G. Rother, D. Cole, D. Mildner, C.J. Duffy, and S.L. Brantley, 2011. Characterization of deep weathering and nanoporosity development in shale: A neutron study. Am. Mineral. 96:498–512.doi:10.2138/am.2011.3598

Keller G.V. and Frischknecht F.C. 1966. Electrical Methods in Geophysical Prospecting. Pergamon Press, Inc., Pergamon Press, New York, 523 pp.

Kosinski, W.K. and Kelly, W.E. (1981) Geoelectric Soundings for Predicting Aquifer Properties. Groundwater, 19, 163-171. https://doi.org/10.1111/j.1745-6584.1981.tb03455.x

Lane 1995, J.W., Haeni, F.P., and Watson, W.M., 1995, Use of a square-array direct current resistivity method to detect fractures in crystalline bedrock in New Hampshire, *Ground Water*, vol. 33, no. 3, 476-485.

Loke, M.H., 2000. Electrical imaging surveys for environmental and engineering studies. Geotomo Software tutorial.

Loke, M.H. (2003) RES2DINV-Rapid 2D Resistivity and IP Inversion Using the Least-Squares Method. Geotomo Software Manual, Malaysia.

Maillet, R., and H. G. Doll, 1932, Sur un Théorème Relatif aux Milieux Électriquement Anisotropes et ses Applications à la Prospection Electrique en Courant Continu: Ergänzungshefte für Angewandte, Geophysik, 109–124.

Maillet, R. 1947. The fundamental equations of electrical prospecting. Geophysics 12, no. 4: 529–556.

Matias, M.J.S., and Habberjam, G.M., 1984, A field example of the use of anisostropy parameters derived from resistivity soundings, *Geophysical Prospecting*, vol. 32, 725-739, pp. 725-739.

Matias, M.J.S., 2002, Square array anisotropy measurements and resistivity sounding interpretation, *Journal of Applied Geophysics*, vol. 49, pp. 185-194.

Reynolds, J.M., 1997, An Introduction to Applied and Environmental Geophysics, 2nd Edition, Wiley Publishing.

Ritzi R.W. Jr and Andolsek R.H. 1992. Relation between anisotropic transmissivity and azimuthal resistivity surveys in shallow, fractured, carbonate flow systems. Ground Water 30, 774-780.

Sehli, A. S., 1990, Contribution of electrical prospecting to the geophysical study of discontinuous media: International Symposium on Applications of Geophysics to Water Prospecting in Arid and Semi-Arid Areas, UNESCO, Proceedings.Sehli, 1990

Sullivan, P.L., S. Hynek, X. Gu, K. Singha, T.S. White, N. West, et al. 2016. Oxidative dissolution under the channel leads geomorphological evolution at the Shale Hills catchment. Am. J. Sci. 316:981–1026.doi:10.2475/10.2016.02

Taylor, R.W., and Fleming, A.H., 1988, Characterizing jointed systems by azimuthal resistivity surveys, *Ground Water*, vol. 26, no. 4, pp. 464-474.

U.S. National Research Council Committee on Basic Research Opportunities in the Earth Sciences: Basic Research Opportunities in Earth Science, National Academy Press, Washington, D.C., 2001.

van der Pauw, L. J., 1961, Determination of resistivity tensor and Hall tensor of anisotropic conductors: Philips Research Reports, 16.

Wasscher, J. D., 1961, Note on four-point resistivity measurements on anisotropic conductors: Philips Research Reports, 16, 301–306.

Watson K.A. and Barker R.D. 1999. Differentiating anisotropy and lateral effects using azimuthal resistivity offset Wenner soundings. Geophysics 64, 739-745.

Whitman, D., and Yeboah-Forson, A. D., 2015, Electrical resistivity and porosity structure of the upper Biscayne Aquifer in Miami-Dade County, Florida, Journal of Hydrology 531 (2015) 781–791.

Yeboah-Forson, A., D. Whitman, D., Electrical Resistivity Characterization of Anisotropy in the Biscayne Aquifer, Groundwater 52, no. 5: 728–736.

Zhang, J., H. Lin, and J. Doolittle. 2014. Soil layering and preferential flow impacts on seasonal changes of GPR signals in two contrasting soils. Geoderma 213:560–569. doi:10.1016/j.geoderma.2013.08.035.

Chapter 4

Conclusions

In summary, application of the square array method to the six sites within the fractured carbonate bedrock valley of the Spring Creek basin show that the square array apparent resistivity data correlates well with known bedrock structure. In particular, the resistivity minima for larger a-spacings of 40 and 50 meters at each site paralleled bedrock strike or mapped fractures, where present. In addition, estimates of secondary porosity from the 40- and 50-meter a-spacings of the square array generally compared favorably to independent estimates of bedrock structure and secondary porosity from previously published studies, outcrop measurements and groundwater level/streamflow recession data. The results of this study demonstrate that the square array method can be used effectively in complex karst settings to characterize bedrock anisotropy and secondary porosity.

By comparing the results from the square array method to mapped geologic structure and groundwater flow this study demonstrates that the square array can be used effectively for characterizing the complex geologic setting of fractured carbonate bedrock with epikarst overburden of varying thickness. In this setting, the square array can provide a robust method for estimating realistic earth resistivity values; correlating geo-electrical anisotropy with orientations of bedding plane strike, fracture strike, and mapped groundwater flow; and estimating secondary porosity values that correlate with outcrop-based, fracture porosity measurements, and effective porosity based on streamflow/aquifer level recession estimates. One of the advantages of using the square array over collinear arrays is that it requires a smaller footprint. The results of this study show that this advantage holds even in karst areas with an

epikarst mantle, where a-spacings of only 40 to 50 meters are needed to effectively characterize the resistivity and anisotropy of the carbonate bedrock.

Collectively, the results of this study provide valuable information for investigations of water supply, source water protection, and groundwater remediation. In study areas where there is little or no available geologic data due to lack of carbonate bedrock exposure from thick soil and epikarst cover, or where well control is sparse or non-existent, the square array may be especially useful for obtaining estimates of key bedrock aquifer properties.

The use of azimuthal resistivity surveys in shale bedrock settings provides useful insights into the degree and orientation of geo-electrical anisotropy, which are often overlooked in 2-D surveys yet are important factors for representative survey and modeling results. In particular the square array, provides strong correlation between resistivity values and inclined bedding plane and fracture orientation, which are important controls on groundwater flow. Use of the square array to characterize bedrock anisotropy provides key initial insights for investigators to then design 2-D or 3-D resistivity surveys, and ultimately factor anisotropy results into the models. In particular the paradox of anisotropy, which has been demonstrated in this paper to be present in the shale apparent resistivity results, needs to be factored into the apparent resistivity values used as input for modeled resistivity results to be realistic.

Square array survey results provide the initial necessary anisotropy orientation based on longitudinal and transverse apparent resistivity that can be used to determine orientations of 2-D or 3-D resistivity surveys. The coefficients of anisotropy from the square array and 2-D arrays can be estimated and then factored into the data inversions to aid in model optimization for interpretation toward further geophysical or hydrogeological investigation. In this case of shale bedrock resistivity surveying it is clear that data inverted without anisotropy corrections leads to

models with higher resistivity values parallel to bedrock strike and lower values across strike, which can mislead investigators. Correction of 2-D data using the coefficients of anisotropy estimated from orthogonal collinear arrays (ie cross strike and strike parallel) provided reasonable model results which offset the paradox of resistivity, with much of the strike parallel model having lower resistivity values than the cross-strike model. The square array's coefficients of anisotropy were relatively high, especially at depth where values greater than 2 occurred, however this is not unexpected as the square array is especially sensitive to anisotropy. In order to reduce the "overcompensation" of the square array's longitudinal and transverse apparent resistivity values, an averaged square array coefficient of anisotropy was estimated by using resistivity values adjacent to the maximum and minimum values, which appears to provide more realistic model results.

In closing, each site's subsurface conditions will be unique while data inversion results are inherently non-unique. In the case of shale bedrock it has been demonstrated here that anisotropy can be significant and therefore it is prudent to be factored into apparent resistivity values for realistic model output. Though the models provided herein are non-unique, the input data has been optimized to the extent possible to provide better results that are more reflective of true resistivity values in this type of setting. The results of this study demonstrate a useful methodology of establishing geo-electric anisotropy with the square array and orthogonal collinear array results to determine if the paradox of anisotropy exists, and if so, how to adjust the collinear measurements to obtain more accurate models. This methodology can likely be applied in a variety of geologic settings where anisotropy is expected, and provide useful insights into subsurface conditions for investigators, especially in areas where nearby bedrock outcrops do not exist and/or well control is poor.

Appendix A

Supplementary Material for Chapter 2

Introduction

Appendix A contains regional geologic information, mapping, photos, and field equipment technical information that supplement Chapter 2- An Assessment of the Square Array Resistivity Method's Ability to Geo-Electrically Characterize the Cambrio-Ordovician Karst Aquifers of the Appalachian Valley and Ridge Physiographic Province.

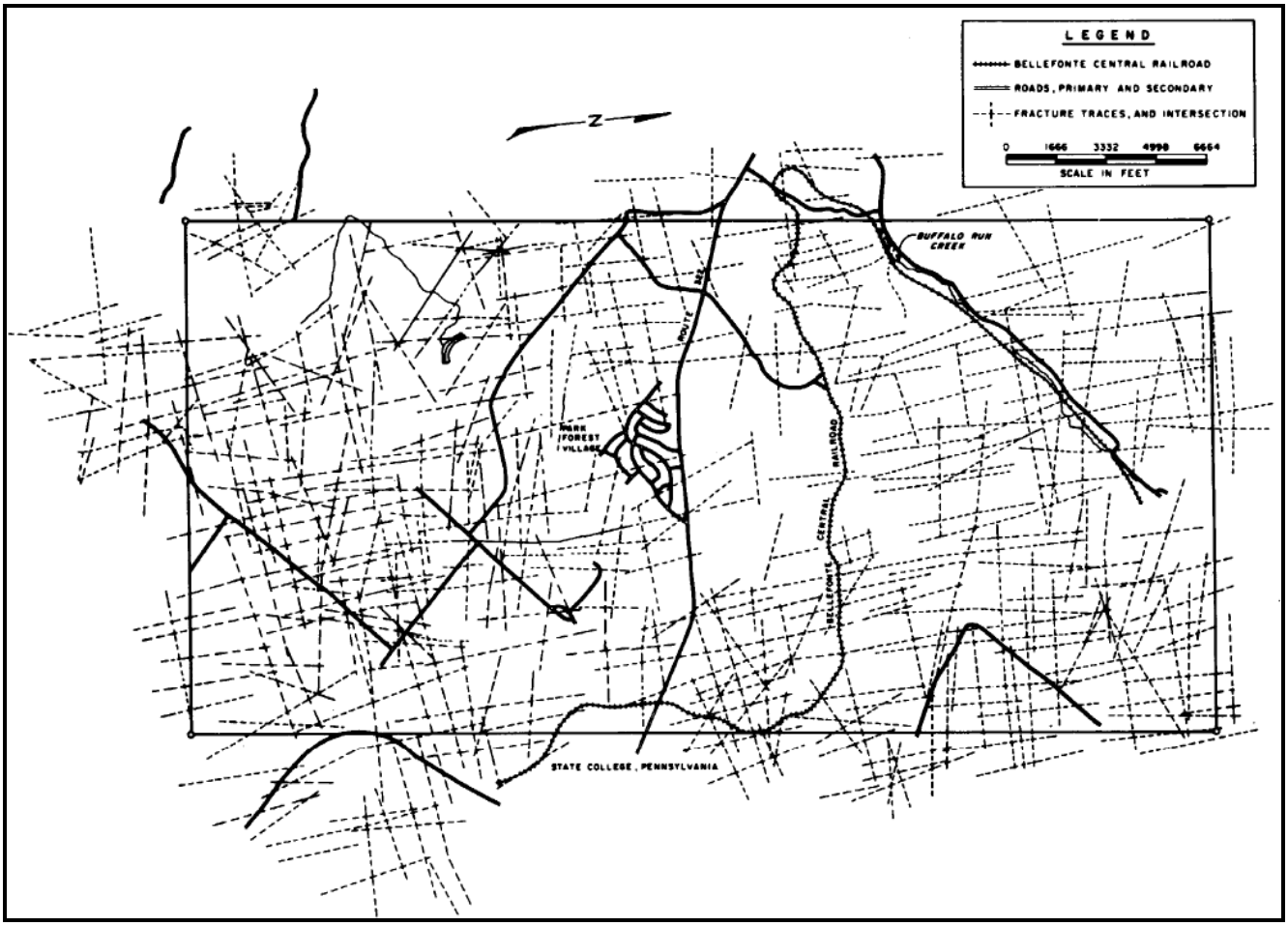

Figure A-1. Regional fracture trace mapping showing preferential N/NW and E/NE orientations of fracture traces within a portion of the study area (Parizek and Drew, 1966).

Equipment Specifications

Earth Resistivity Meter Equipment Specs for the ABEM 100 Terrameter

Terrameter SAS 1000

PRODUCT LEAFLET

Receiver

Isolation	Input channel is galvanically separated
Input Voltage Range	+ / - 400 V
Input Impedance	10 MOhm minimum
Precision	Better than 0.1 % (in the range 4 - 200 ohm at 1 s integration
Accuracy	1 % typical
Resolution	Theoretical 30 nV
Dynamic range	Up to 140 dB plus 64 dB automatic gain (at 1 s integration)
Automatic ranging	+ /- 2.5 V + / - 10 V + / - 400 V

Measuring

Resistivity	YES
SP	YES
IP	YES
Current pulse length	from 0.1 s to 4 s User selectable
IP Windows	Up to ten time windows
IP integration interval	Up to 8 s

Transmitter

Output power	100 W
Current transmission	True Current Transmitter
Output Current Accuracy	Better than 0.5 % at 100 mA
Output Current	1, 2, 5, 10, 20, 50, 100, 200, 500, 1000 mA (operator set or auto ranging)
Maximum Output Voltage	+/- 400 V (800 V peak-to-peak)
Cycle type in resistivity mode	Plus-Minus-Minus-Plus
Cycle type in IP mode	Plus-Zero-Minus-Zero

General

Casing	Rugged Aluminium case meets IEC IP 66
Computer	PC compatible
Display	LCD, 200 x 64 pixels, 8 lines of 40 characters
I / O ports	Multifunction connector with current and potential including RS232 communication for external devices as PC, LOG and Imaging Banana connectors for current and potential

With reservations for changes; our products undergo continuous development

External devices	Lund Imaging System, SAS LOG
Memory Capacity	More than 1 500 000 readings
Power	Optional Clip-on rechargeable power pack or external 12V DC through SAS-EBA
Dimensions (W x L x H)	105 x 325 x 270 mm with SAS-EBA
Weight	5.1 kg
Ambient Temperature Range	- 5ºC to + 50 ºC operating

Accessories

Multi-electrode Survey Systems for 2D & 3D

LUND Resistivity & IP Imaging
A centrally switched system for automatic resistivity, IP profiling and vertical imaging.
See LUND brochure for more information

Borehole logging (SAS LOG 300 logging unit)

Cable length	300 m
Cable markings	Every meter
Probe diameter	40 mm
Weight (200 m)	15 kg
Dimensions (W x L x H)	330 x 750 x 225 mm
Survey modes and ranges:	
16" short normal	0.05 - 100 000 ohmm
64" long normal	0.5 - 100 000 ohmm
18 feet lateral	0.5 - 100 000 ohmm
Fluid resistivity cell	0.05 - 100 000 ohmm
Self Potential	0.05 - 1000 mV
Temperature	0ºC to + 60ºC
Temperature precision	+/- 0.01ºC (0 - 20ºC) +/- 0.1ºC (20 - 60ºC)
Temperature accuracy	+/- 1ºC
Water level indication	

Standard field equipment

1	ABEM Terrameter SAS 1000 includes: One SAS 1000 Receiver / Transmitter unit One RS232 Cable (9 pin D-sub) One SAS-EBA External Battery Adapter One SAS 1000 Software kit One SAS 1000 Documentation kit	33 0021 30
2	S & W sounding cable set includes: 2 x 250 m cable on reel 2 x 750 m cable on reel 4 x interconnect cable 4 x crocodile clip Transport plywood box	33 0012 40
3	Stainless steel electrode	33 0012 61
4	Non-polarizable electrode	33 0015 79

Terrameter SAS – VES system description

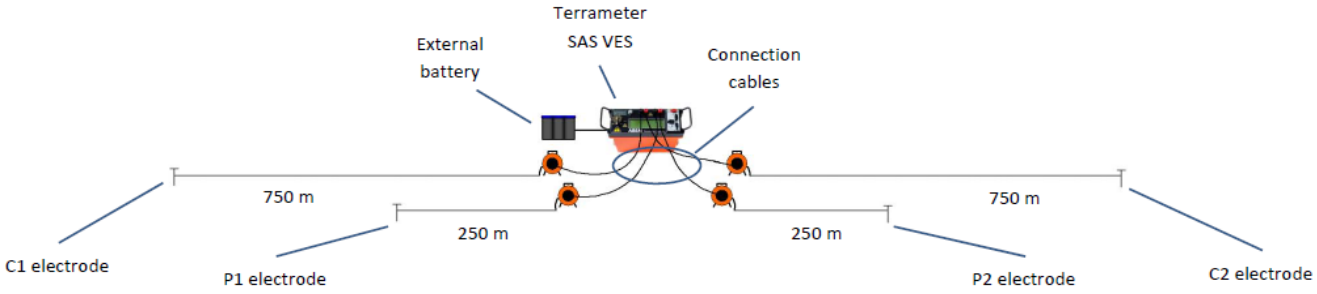

Picture of the ABEM SAS 1000 Terrameter showing layout of the square array measurement equipment in the field (source ABEM website).

Figure A-2. Typical configuration of how the resistivity meter, power source, and current and potential electrodes are connected.

Photos

Carbonate bedrock outcrops used to estimate secondary porosity in the Spring Creek watershed study area.

Photo A-1. Outcrop 1 located on Hamilton Avenue (Lat/long of 40°47'12.23"N/77°51'24.11"W).

Photo A-2. Outcrop 2 along Branch Road (lat/long of 40°45'45.12"N/ 77°50'30.64"W).

Photo A-3. Outcrop 3 at the PSU “Sheep Farm” Fence Row (lat/long of 40°49'24.85"N/77°49'58.13"W).

Photo A-4. Outcrop 4 at Big Hollow (lat/long of 40°48'30.82"N/ 77°52'33.04"W).

Photo A-5. Outcrop 5 near East College Avenue and Walker Drive (lat/long of 40°48'49.66"N/77°49'31.48"W).

Photo A-6. Outcrop 6 along Route 322 near Branch Road (lat/long of 40°48'32.82"N/40°48'32.82"N).

Photo A-7. Outcrop 7 along Route 322 near Warner Blvd (lat/long of 40°47'24.05"N/ 77°48'18.25"W).

Calculations

Outcrop fracture dimensions and associated secondary porosity estimates

Location: OC-1 Hamilton Ave.	Outcrop face dimensions (m)	Cumulative fracture width (cm)	Fracture type and dimensions (m x m)	Fracture volume (cubic meters)
Length	7.6	3.8	Joint (3.05 x 4.57)	0.5
Height	3.0	2.5	Bedding plane (7.62 x 4.57)	0.9
Depth	4.6	10.2	Joint (3.05 x 7.62)	2.4
Total volume (cubic meters)	106.3		Fracture volume (cubic m)	3.8
			Percent void	3.6%

Location: OC-2 Branch Road	Outcrop face dimensions (m)	Cumulative fracture width (cm)	Fracture type and dimensions (m x m)	Fracture volume (cubic meters)
Length	3.0	6.4	Bedding plane (3.05 x 1.2)	0.24
Height	1.5	6.1	Joint (1.5 x 0.6)	0.05
Depth	1.2	0.9	Joint (1.5 x 1.2)	0.02
Total volume (cubic meters)	5.7		Fracture volume (cubic m)	0.30
			Percent void	5.3%

Location: OC-3 PSU Sheep Farm Fence Row	Outcrop face dimensions (m)	Cumulative fracture width (cm)	Fracture type and dimensions (m x m)	Fracture volume (cubic meters)
Length	2.1	7.6	Joint (0.15 x 0.6)	0.01
Height	0.2	0.0		
Depth	0.8	0.0		
Total volume (cubic meters)	0.2		Fracture volume (cubic m)	0.01
			Percent void	3.6%

Location OC-4 Big Hollow Outcrop	Outcrop face dimensions (m)	Cumulative fracture width (cm)	Fracture type and dimensions (m x m)	Fracture volume (cubic meters)
Length	2.1	0.3	Joint (0.25 x 1.8)	0.00
Height	0.9	0.3	Joint (0.25 x 1.8)	0.00
Depth	1.8	0.2	Joint (0.3 x 1.8)	0.00
		0.1	Joint (0.25 x 1.8)	0.00
		1.3	Joint (0.3 x 1.8)	0.01
		1.5	Joint (0.6 x 1.8)	0.02
		1.3	Joint (0.3 x 2.1)	0.01
Total volume (cubic meters)	3.6		Fracture volume (cubic m)	0.04
			Percent void	1.0%

Location: OC-5 East College/Walker Dr.	Outcrop face dimensions (m)	Cumulative fracture width (cm)	Fracture type and dimensions (m x m)	Fracture volume (cubic meters)
Length	1.2	2.5	Joint (0.4 x 0.3)	0.0031
Height	0.6	0.3	Bedding plane (0.3 x 0.6)	0.0001
Depth	0.3	0.0		
Total volume (cubic meters)	0.2		Fracture volume (cubic m)	0.0032
			Percent void	1.4%

Location: OC-6 Rt 322 W near Elmwood Ave	Outcrop face dimensions (m)	Cumulative fracture width (cm)	Fracture type and dimensions (m x m)	Fracture volume (cubic meters)
Length	3.0	1.3	Bedding plane (3 x 0.6)	0.024
Height	1.5	1.9	Bedding plane (3 x 0.6)	0.035
Depth	0.6	0.0		
Total volume (cubic meters)	2.8		Fracture volume (cubic m)	0.059
			Percent void	2.1%

Location: OC-7 Rt 322 E near Warner Rd	Outcrop face dimensions (m)	Cumulative fracture width (cm)	Fracture type and dimensions (m x m)	Fracture volume (cubic meters)
Length	0.6	1.0	Joint (0.45 x 0.6)	0.00
Height	0.5	0.5	Bedding plane (0.6 x 0.4)	0.00
Depth	0.4	0.0		
Total volume (cubic meters)	0.1		Fracture volume (cubic m)	0.00
			Percent void	4.4%

Outcrop-based average porosity	3.04%

Parameters for calculating secondary porosity from square array data.

	Site 1 a-spacing		Site 2 a-spacing		Site 3 a-spacing		Site 4 a-spacing		Site 5 a-spacing		Site 6 a-spacing	
Parameters*	**40 m**	**50 m**	**40 m**	**50 m**	**40 m**	**50 m**	**40m**	**50m**	**40 m**	**50 m**	**40 m**	**50 m**
r1	231.51	225.89	375.18	431.13	321.32	233.17	253.95	281.04	176.89	190.61	259.50	279.00
r2	73.54	72.95	290.14	305.75	330.84	401.11	279.68	276.81	162.40	164.99	440.45	464.74
r3	71.51	71.73	224.10	326.34	425.87	502.21	330.97	304.41	141.94	139.26	641.31	535.28
r4	214.11	210.50	419.86	453.21	460.90	494.65	249.75	318.03	149.27	156.57	466.90	426.15
ρmin	67.07	55.00	224.10	305.75	278.48	233.17	237.23	239.07	141.94	139.26	259.50	257.62
ρmax	231.51	225.89	419.86	458.47	495.42	512.23	341.90	318.62	176.89	190.61	641.31	573.18
A	2002.13	1963.62	4018.10	4597.34	4284.03	4214.10	3143.71	3395.03	1900.65	1990.24	4614.35	4493.46
B	1455.91	1437.29	3502.33	4239.58	4640.95	5132.59	3406.64	3474.82	1781.34	1814.93	5917.84	5368.40
C	1473.72	1451.50	3649.45	4168.24	4285.01	4673.99	3270.80	3373.94	1856.24	1908.65	5227.47	5073.38
D	1953.62	1921.08	4092.32	4671.68	4729.04	4993.33	3168.61	3514.66	1811.44	1879.91	5317.80	4941.62
T	1.44E-06	1.49E-06	2.78E-07	2.06E-07	2.00E-07	1.80E-07	3.80E-07	3.38E-07	1.19E-06	1.11E-06	1.47E-07	1.64E-07
S	5.96E-07	6.07E-07	4.98E-08	2.88E-08	2.53E-08	3.84E-08	3.24E-08	1.59E-08	8.20E-08	1.04E-07	3.69E-08	3.00E-08
N	1.55	1.54	1.20	1.15	1.14	1.24	1.09	1.05	1.07	1.10	1.29	1.20
porosity	0.267	0.250	0.042	0.033	0.019	0.042	0.018	0.007	0.036	0.044	0.042	0.027

*Parameters defined by equations 4-11 in Chapter 2 to calculate secondary porosity per Taylor and Fleming (1984).

Groundwater and streamflow recession data for estimating effective porosity.

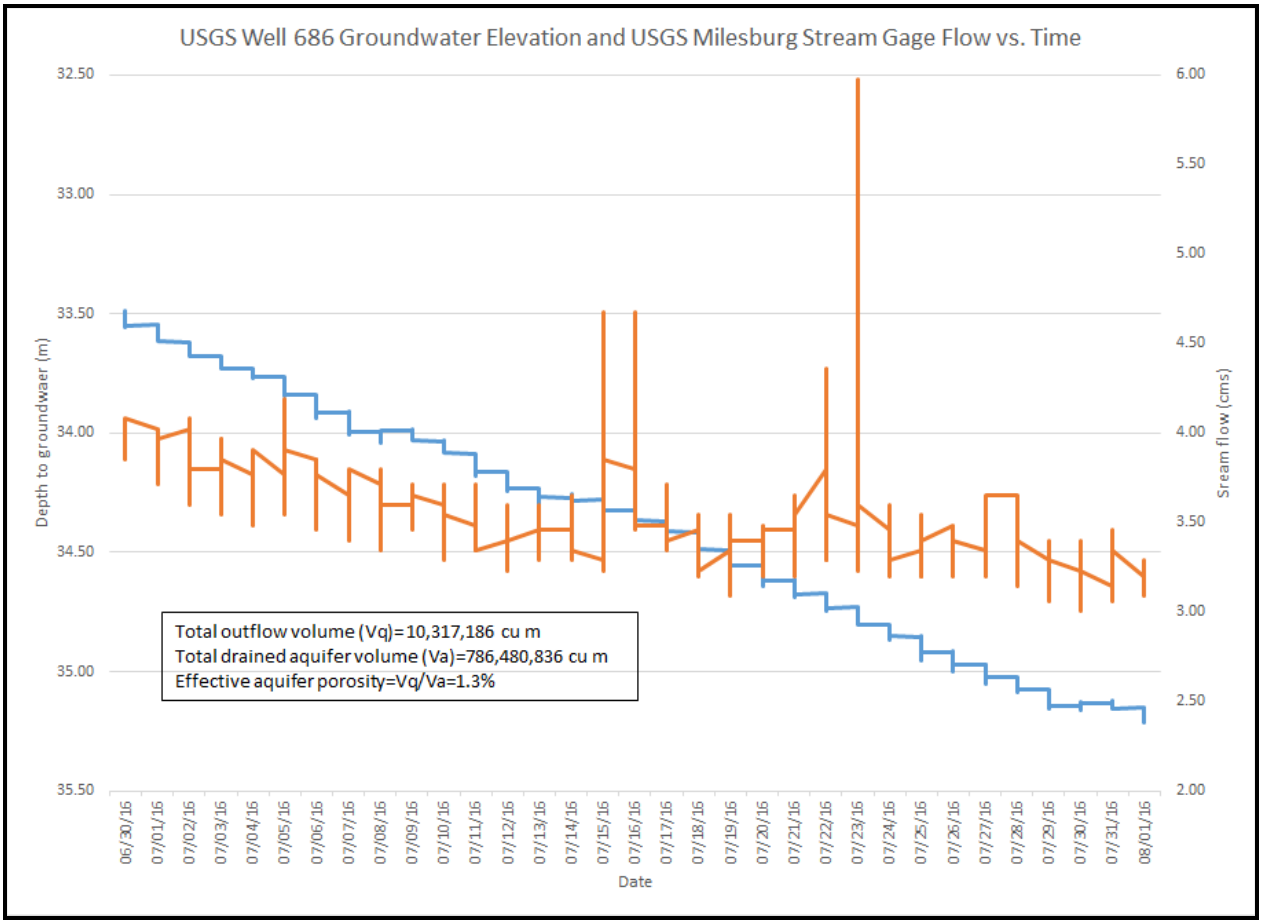

Figure A-4. Groundwater and streamflow recession for estimating secondary porosity

Appendix B

Supplementary Material for Chapter 3

Photos

Photo B-1. SSHCZO site highly-fractured bedrock (photo credit: Andy Nyblade).

Calculations

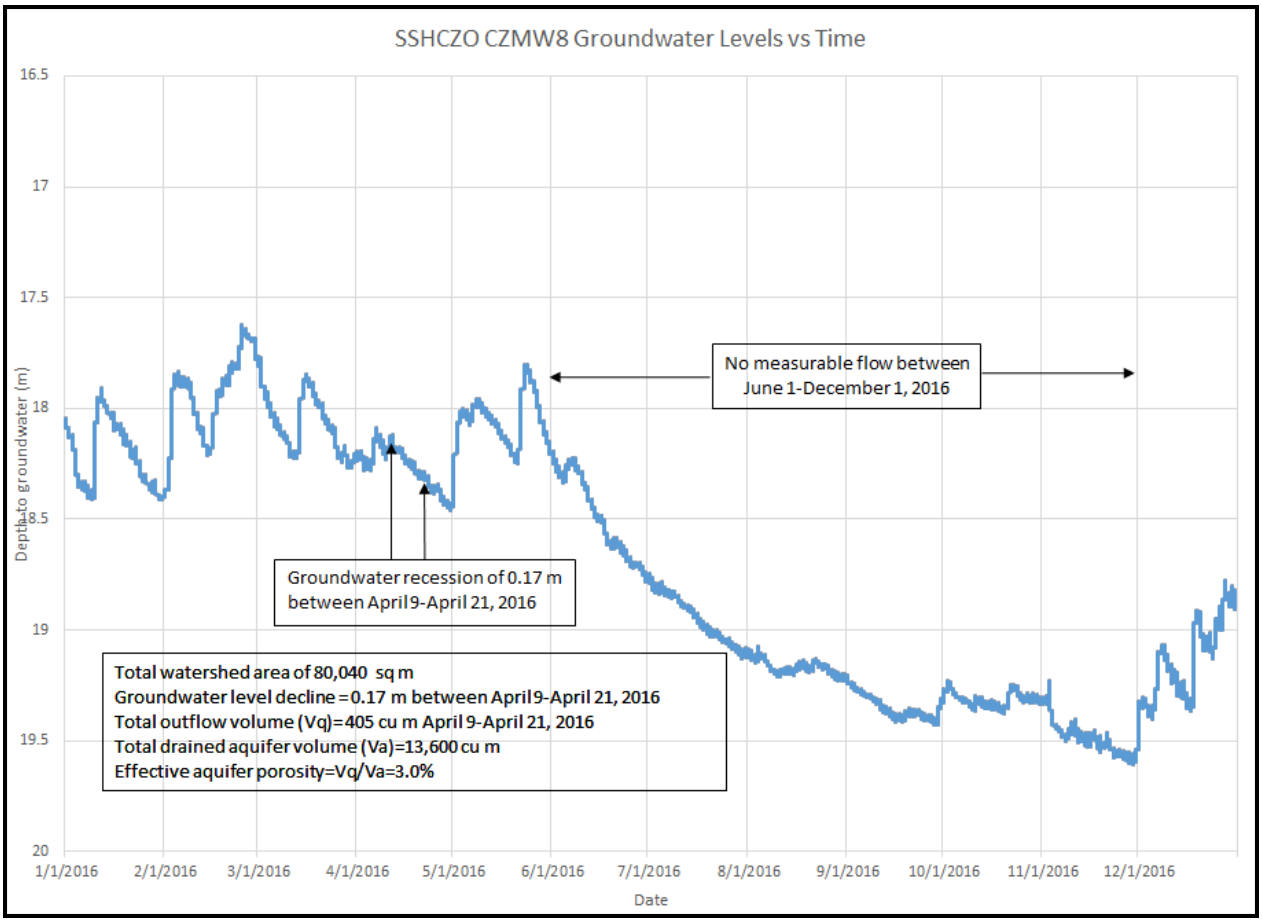

Chart of SSHCZO CZMW8 groundwater levels vs time with estimate of effective porosity based on drained aquifer volume and stream flow volume.

Additional SSHCZO Model Runs

Delisser (2018) previously conducted Wenner array resistivity surveys at the SSHCZO, which indicated the presence of low resistivity pods, but the data had not been corrected for the paradox of anisotropy, which had not been realized at that time. The map below shows the locations of the previous arrays, where two of these arrays, RN4 (oriented northwest/southeast) and RW6 (oriented east-west), intersect one another approximately 150 meters southeast of the square array center point (see map below). The original data and models for both RN-4 and RW-6 display the paradox of anisotropy when compared to the square array data, which were then re-inverted once the apparent resistivity data had been corrected. Array RN4's resistivity values were lower than RN6's at their crossover point, which was opposite of the trend for square array resistivity values with similar orientation and depth. The square array's coefficient of anisotropy was then used to correct the apparent resistivity data and re-invert the data. Uncorrected and corrected models for each array are below for comparison, displaying the low resistivity pods which appear to be common at the SSHCZO. The original RN4 resistivity model shows a zone of vertical low resistivity that emanates from the updgradient pod near the center of the model, while the corrected model has higher resistivity in this zone. The original RN6 model shows several low resistivity pods in the interflow zone, which are further enhanced in the corrected model, especially near the center of the model which is coincident with a narrow channel that runs from south to north and thus expected to have more soil moisture and interflow. In each case, the low resistivity pods extend from approximately 5 to 10 mbls and laterally span upwards of 10 meters, thus appear to be significant hydrologic features. These resistivity models provide investigators insights on the location and geometry of the pods for installation of piezometers or similar monitoring points to further characterize their significance on the catchment's hydrology.

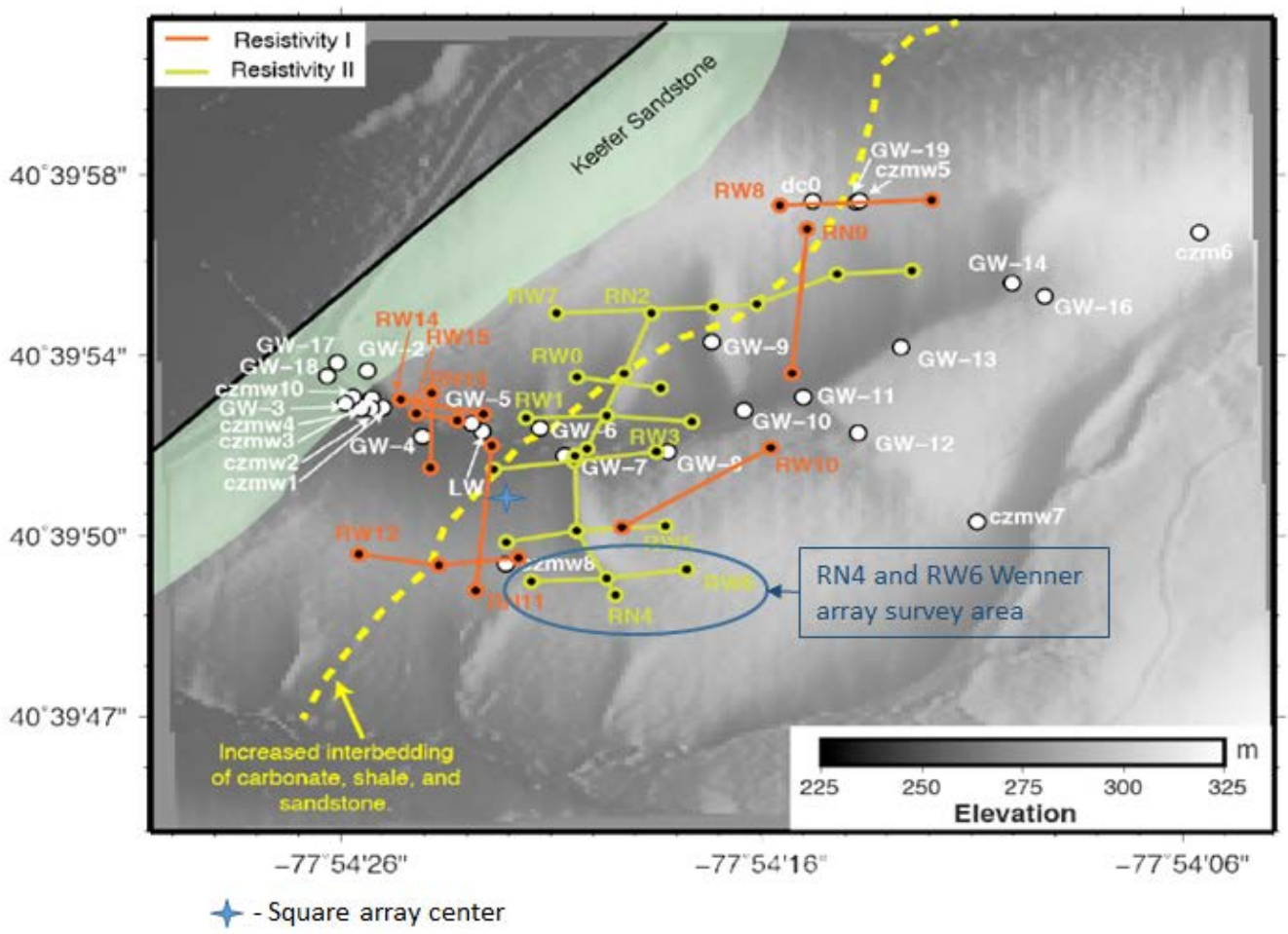

Figure B-1. Map of previous SSHCZO resistivity arrays (modified from Delisser, 2018).

NW SE

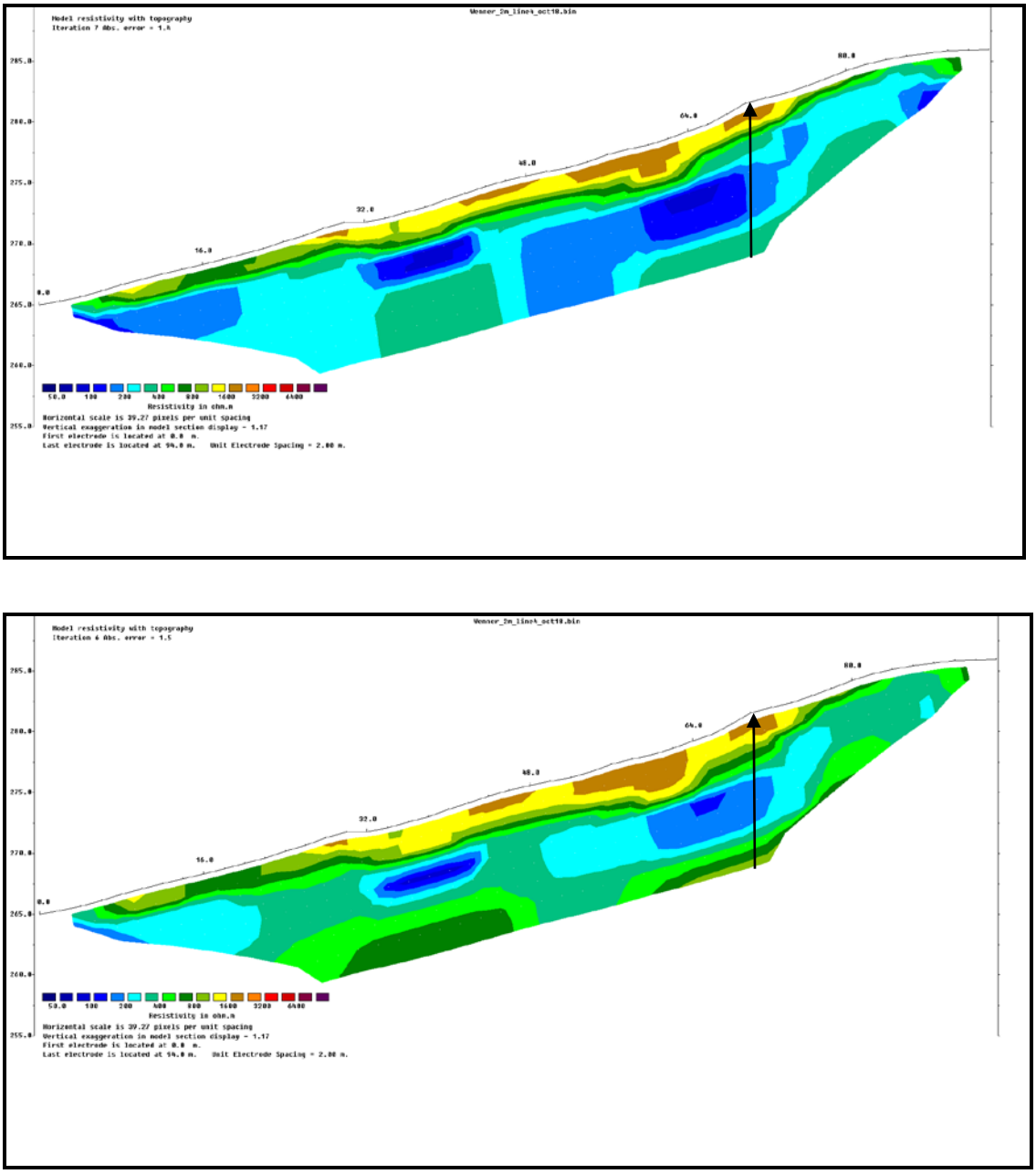

Figure B-2. Wenner array Line RN4 (Delisser, 2018) showing uncorrected (upper) and corrected (lower) model inversions based on paradox of anisotropy adjustments with each displaying low resistivity pods in the interflow zone. Arrows show the approximate cross-over point with Line RN6.

W E

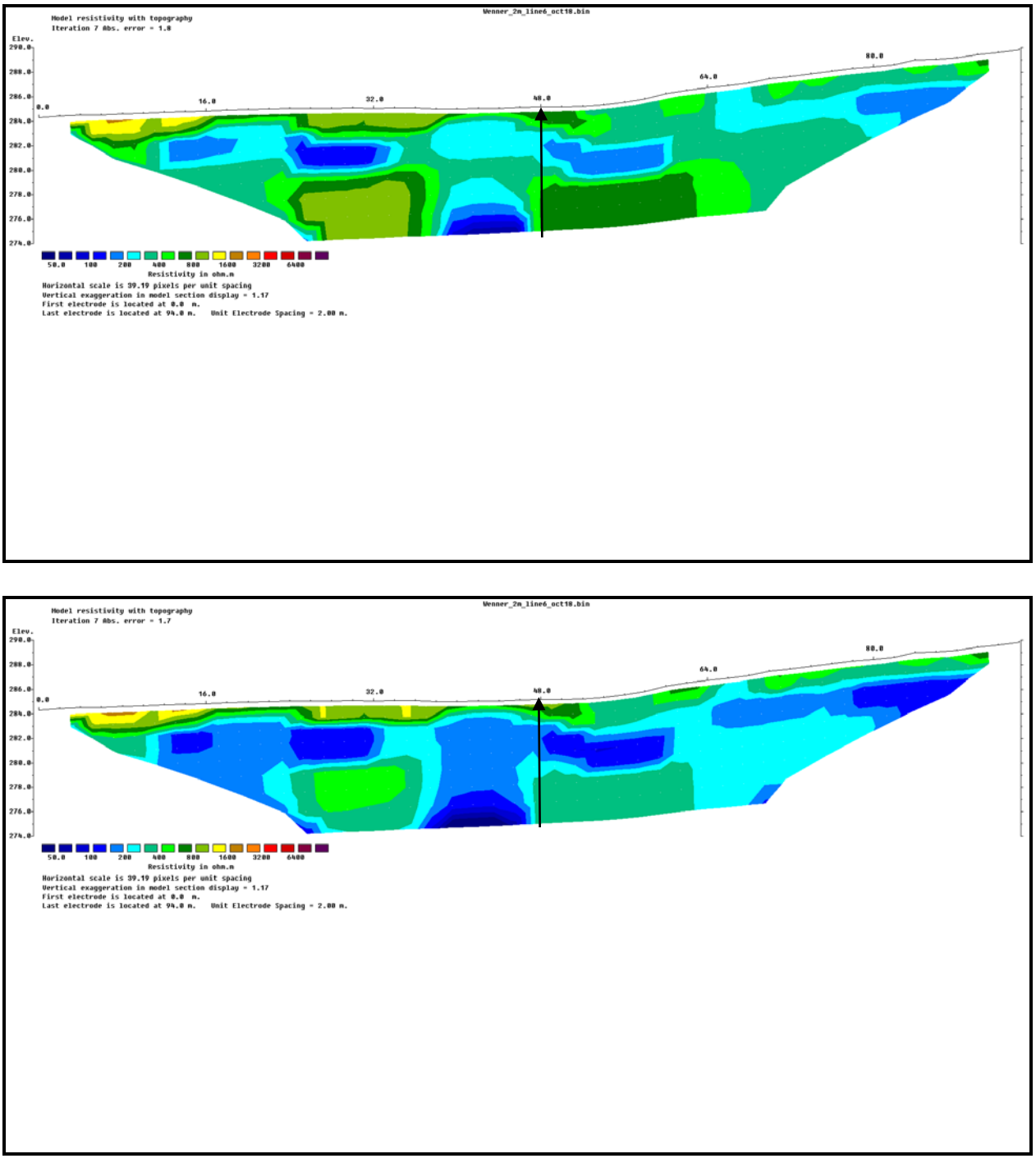

Figure B-3. Wenner array Line RN6 (Delisser, 2018) showing uncorrected (upper) and corrected (lower) model inversions based on paradox of anisotropy adjustments with each displaying low resistivity pods in the interflow zone. Arrows show the approximate cross-over point with Line RN4.

David A. Yoxtheimer, P.G.

Education

The Pennsylvania State University	B.S., Earth Science, Dept. Marshal	1992
The Pennsylvania State University	Ph.D., Geosciences	2019

Appointments

July 2010-present	Extension Associate, Penn State's Marcellus Center for Outreach and Research
July 2017-present	Assistant Research Professor, Penn State's College of Earth and Mineral Sciences

Professional Experience

1992–1998	Hydrogeologist, Nittany Geoscience, Inc., State College, PA
1998–2007	Senior Hydrogeologist, USFilter/Veolia Water, State College, PA
2007–2010	Director of Operations, ARM Oil & Gas Solutions, State College, PA
2011-Current	Owner and Principal Hydrogeologist, AquaLith Technologies LLC

Research and Work Interests

Mr. Yoxtheimer is a research hydrogeologist and extension associate with The Pennsylvania State University's *Marcellus Center for Outreach and Research*. His areas of expertise include: water supply development, geophysical surveying, environmental permitting, karst hydrogeology, shale energy geology, and integrated water resource management. Mr. Yoxtheimer's current research interests include water resource management associated with shale energy development, including methane migration in aquifers, water sourcing, flowback/produced water management, and underground injection waste disposal. In his current position he conducts water-related research and promoting use of best available technologies to minimize environmental impacts, as well as public education and outreach associated with shale energy development. As a consulting hydrogeologist he has conducted large-scale water supply development and environmental projects for large corporate and government clients in both the US and abroad. Mr. Yoxtheimer's long-term professional goals include development of environmentally sustainable practices that balance energy development and economic stability for future generations. Mr. Yoxtheimer current serves as a Technical Advisory Board member for the Pennsylvania Department of Environmental Protection's Bureau of Oil and Gas and recently completed work as an appointed member of the Colombian Interdisciplinary Independent Commission on Hydraulic Fracturing.